THESIS
2004
5698[illegible]

This is to certify that the
dissertation entitled

Shape and Laminate Optimization of Fiber-Reinforced-
Polymer Structures

presented by

Jun Wu

has been accepted towards fulfillment
of the requirements for the

Ph.D. degree in Department of Civil and Environmental Engineering

Major Professor's Signature

5/7/04

Date

MSU is an Affirmative Action/Equal Opportunity Institution

LIBRARY
Michigan State
University

PLACE IN RETURN BOX to remove this checkout from your record.
TO AVOID FINES return on or before date due.
MAY BE RECALLED with earlier due date if requested.

DATE DUE	DATE DUE	DATE DUE

6/01 c:/CIRC/DateDue.p65-p.15

Shape and Laminate Optimization of Fiber-Reinforced-Polymer Structures

By

Jun Wu

A DISSERTATION

Submitted to
Michigan State University
in partial fulfillment of the requirements
for the degree of

DOCTOR OF PHILOSOPHY

Department of Civil and Environmental Engineering

2004

ABSTRACT

Shape and Laminate Optimization of Fiber-Reinforced-Polymer Structures

By

Jun Wu

Fiber Reinforced polymer (FRP) composites, or advanced composite materials, which have shown outstanding mechanical characteristics, such as high strength-to-weight and high stiffness-to-weight, and high chemical and environmental endurance compared to conventional materials, have been adapted from aerospace and defense industries to civil infrastructure applications. The nature of FRP composites makes them strong and stiff in planes along fiber orientations but rather weak through their thickness. Thus, they are most efficient when used under global in-plane stress demands. Due to their high material costs, a way to employ their high material stiffness and strength is to use them in structural forms in which the structural efficiency is maximized by shaping the structural geometry to achieve mainly in-plane behavior under the applied loads. Therefore, an approach is needed to develop the structural forms where the in-plane properties of FRP composites can be used efficiently.

An integrated approach is developed for the shape and laminate optimization of FRP structures. The integrated approach is implemented in a two-level uncoupled procedure: shape and laminate-property optimization followed by laminate design optimization, where structural shape and laminate design are optimized simultaneously with the aim of maximizing structural stiffness.

Examples of optimizing laminated FRP shell structures are provided to validate the procedure. The performance of the integrated approach is evaluated by comparing a shape-and-material optimized FRP shell with two shape-only optimized FRP shells. The numerical results show that the proposed integrated approach is reliable and provides a useful tool for designing optimized laminated FRP structures.

The integrated approach is also used to aid the rational implementation of FRP composites in civil infrastructure by developing innovative bridge design concepts. Innovative FRP composite membrane-based bridge systems were explored through analytical studies of the integrated approach. Two types of bridge systems are developed, FRP membrane beam bridges and FRP membrane suspension bridges. Both bridge systems consist of a shape-and-laminate optimized FRP membrane/shell carrying the in-plane tensile and shear forces together with a conventional reinforced concrete deck providing the live load transfer. The analytical studies of optimizing the FRP membrane bridges provide the initial development of innovative systems that use FRP composites in their inherent behavioral characteristics for new high-performance structures.

Results from this work demonstrate that FRP composites can be used with higher efficiency in new structural systems as long as their advantageous properties of directional strength, lightweight, and tailored properties are properly considered in the design process. The work further discusses the feasible implementation of the optimum design for composite membrane-based bridges in practical engineering construction. The work also provides insight to further development and applications of the integrated optimization approach.

ACKNOWLEDGMENTS

I would like to thank my advisor, Professor Rigoberto Burgueño for his excellent academic guidance, continuous encouragement, and patient support throughout this work. It has been a very enlightening and fruitful experience to work with Dr. Burgueño. My sincere thanks are also extended to the other members of my Ph.D. committee, Professor Ronald S. Harichandran, Professor Charles R. MacCluer, and Professor Amit H. Varma. I have my deep gratitude for Mr. Graig Gunn's selfless help and tremendous assistance during my studies at Michigan State University. I am also grateful for all the help granted to me throughout the course of my work by the faculty and staff members, colleagues and many friends.

I would like to acknowledge the financial support by Michigan State University through the Department of Civil and Environmental Engineering and an Intramural Research Grant Program award from the Office of the Vice President for Research and Graduate Studies.

Grateful thanks should also go to my parents. Their love, encouragement and confidence in my abilities are the backbone of my persistence in the endeavor. Most of all I would like to thank my wife, Yue. Her endless love is the source of my dedication through the completion of this research.

TABLE OF CONTENTS

LIST OF FIGURES .... **viii**

LIST OF TABLES .... **xii**

Shape and Laminate Optimization of Fiber-Reinforced-Polymer Structures **1**

1 Introduction **1**
- 1.1 General 1
- 1.2 FRP composites for civil infrastructure 1
  - 1.2.1 Introduction to FRP composites 2
  - 1.2.2 Mechanical properties of FRP laminates 2
  - 1.2.3 FRP composites in civil structures 4
- 1.3 Outstanding issues and motivation 6
- 1.4 Shape and material optimized FRP structures 7
  - 1.4.1 Shape resistant structures and optimal shape finding 8
  - 1.4.2 FRP laminates and optimal laminate design 9
  - 1.4.3 Shape and laminate optimization of FRP structures 10
- 1.5 Objective and scope of the dissertation 11
- References 13

2 Laminated Fiber Reinforced Polymer (FRP) Composites **14**
- 2.1 Constitutive relations for FRP laminates 15
- 2.2 Stacking sequence of laminates 22
- 2.3 Constrained relations of lamination parameters 24
  - 2.3.1 Relation between in-plane lamination parameters 24
  - 2.3.2 Relation between out-of-plane lamination parameters 27
  - 2.3.3 Relation between in-plane and out-of-plane lamination parameters 29
- 2.4 Summary 34
- References 35

3 Integrated Optimization Process for Laminated FRP Structures **36**
- 3.1 Form finding and structural shape optimization 37
  - 3.1.1 Form finding of tension membrane structures 37
  - 3.1.2 Form finding of shell structures 41
  - 3.1.3 Structural shape optimization 45
- 3.2 Material optimization of laminated FRP composites 52
- 3.3 Integrated shape and FRP laminate optimization 55
- References 58

4 Shape and Laminate-Property Optimization of FRP Structures **60**
- 4.1 Formulation of the shape and laminate-property optimization problem 60
  - 4.1.1 Design variables 60

4.1.2 Objective function ... 61
4.1.3 Constraints ... 63
4.2 Algorithm of shape and laminate-property optimization ... 64
4.2.1 Linearization of objective and constrain functions ... 64
4.2.2 Definition and determination of a searching direction ... 65
4.2.3 Definition of the constrained steepest descent function ... 67
4.2.4 Determination of the step size ... 68
4.3 Implementation of shape and laminate-property optimization ... 69
References ... 71

5 FRP Laminates Design Optimization ... 72
5.1 Formulation of laminate design optimization ... 72
5.1.1 Design variables ... 72
5.1.2 Objective function ... 74
5.1.3 Constraints ... 74
5.2 Algorithm for laminate design optimization ... 74
5.2.1 Design representation by genetic coding ... 75
5.2.2 Definition of a population size ... 76
5.2.3 Definition of fitness values and a selection scheme ... 76
5.2.4 Implementation of genetic operators ... 77
5.3 Implementation of laminate design optimization ... 78
References ... 80

6 Shape and Laminate Optimization of FRP Shells ... 81
6.1 Shape and laminate optimized FRP shell ... 81
6.2 Shape-only optimized laminated FRP shells ... 86
6.3 Comparison of three optimal shells ... 89
6.4 Buckling analyses of optimized laminated FRP shells ... 95
6.5 Summary ... 97
References ... 98

7 FRP Composite Membrane-Based Bridge Systems ... 99
7.1 FRP composite membrane beam (CMB) bridges ... 100
7.1.1 Bridge system description ... 100
7.1.2 Integrated optimization of CMB bridges ... 103
7.1.3 System characteristics of optimal CMB bridges ... 115
7.1.4 Post optimality analyses ... 121
7.2 FRP composite membrane suspension (CMS) bridges ... 127
7.2.1 Bridge system description ... 128
7.2.2 Integrated optimization of CMS bridges ... 130
7.2.3 System characteristics of optimal CMS bridges ... 138
7.2.4 Post optimality analyses ... 142
7.3 Discussion of FRP membrane-based bridge systems ... 150
7.3.1 Comparison of FRP membrane-based bridge systems ... 150
7.3.2 Discussion of the objective function ... 154
7.3.3 Selection of the design variables ... 158

7.4 Summary 159
References 161

8 Conclusions and Future Research Needs 162
8.1 Conclusions 162
8.2 Future research needs 163
8.2.1 About the integrated approach of shape and laminate optimization 163
8.2.2 About applications of the integrated approach 165
8.2.3 About the engineering and construction of optimal FRP composite structures 166

LIST OF FIGURES

Figure 1–1 FRP elastic modulus as a function of fiber orientation 4

Figure 1–2 Applications of FRP composites in civil infrastructures 5

Figure 1–3 Shape resistant structures [Otto, 1969] 8

Figure 2–1 Laminated FRP composites 18

Figure 2–2 Feasible domain of in-plane lamination parameters 27

Figure 2–3 Feasible domain of out-plane lamination parameters 28

Figure 2–4 Boundary determination of V_{1D} for a given $\{V_{1A}, V_{3A}\}$ 31

Figure 2–5 Boundary determination of V_{3D} for a given $\{V_{1A}, V_{3A}, V_{1D}\}$ 32

Figure 2–6 Feasible domain of combining in-plane and out-plane lamination parameters 33

Figure 3–1 Shape resistant structures 36

Figure 3–2 Soap film analogy method and tension membrane structures and [Hildebrandt and Tromba, 1983] 38

Figure 3–3 Hanging method and shell structures and [Isler, 1991, 1994] 43

Figure 3–4 Structural shape optimization [Ramm, 1992] 45

Figure 3–5 Structural shape optimization process 47

Figure 3–6 Two-level approach of shape and laminate optimization 56

Figure 4–1 Shape and laminate-property optimization 69

Figure 5–1 Typical symmetric and balanced laminate 73

Figure 5–2 Design representation by genetic coding 76

Figure 5–3 Crossover operator 77

Figure 5–4 Mutation operator 78

Figure 5–5 Laminate design optimization 79

Figure 6–1 Geometry, loading, and control points for shell structures 82

Figure 6–2 History of objective function – FRP Shell 1 84

Figure 6–3 Histories of partial geometric design variables – FRP Shell 1 84

Figure 6–4 Histories of laminate-property design variables – FRP Shell 1 85

Figure 6–5 Second-level optimization process – FRP Shell 1 86

Figure 6–6 History of objective function – FRP Shell 2: $[45°/-45°/-45°/45°]_{6S}$ 87

Figure 6–7 Histories of geometric design variables – FRP Shell 2: $[45°/-45°/-45°/45°]_{6S}$ 88

Figure 6–8 History of objective function – FRP Shell 3: [0°/90°/90°/0°] 88

Figure 6–9 Histories of geometric design variables – FRP Shell 3: [0°/90°/90°/0°] 89

Figure 6–10 Global and local coordinate systems 91

Figure 6–11 Structural responses of initial and optimal shells 92

Figure 6–12 Membrane force distribution of optimal shells 94

Figure 6–13 Bending moment distribution of optimal shells 94

Figure 7–1 Composite membrane beam (CMB) bridge 100

Figure 7–2 Computational model of the CMB bridge 101

Figure 7–3 Geometric key points for CMB bridge shape optimization 104

Figure 7–4 History of objective function – CMB Model A 106

Figure 7–5 History of geometric design variables – CMB Model A 107

Figure 7–6 History of laminate-property design variables – CMB Model A 107

Figure 7–7 History of objective function – CMB Model B 108

Figure 7–8 History of geometric design variables – CMB Model B 108

Figure 7–9 History of laminate-property design variables – CMB Model B 109

Figure 7–10 History of objective function – CMB Model C 109

Figure 7–11 History of geometric design variables – CMB Model C 110

Figure 7–12 History of laminate-property design variables – CMB Model C 110

Figure 7–13 Laminate design optimization for 8-layer laminates 113

Figure 7–14 Laminate design optimization for 48-layer laminates 114

Figure 7–15 Section force (SF1) distribution 118

Figure 7–16 Section force (SF2) distribution 118

Figure 7–17 Shear section force (SF3) distribution 119

Figure 7–18 Load case for maximum torsion in the strength limit state 126

Figure 7–19 Load case for maximum bending in the strength limit state 126

Figure 7–20 Concept for Composite Membrane Suspension (CMS) Bridges 128

Figure 7–21 Geometry of the CMS bridge 129

Figure 7–22 Loading and geometric key points for the CMS bridge 131

Figure 7–23 Histories of geometric design variables – CMS Model A 133

Figure 7–24 Histories of laminate-property design variables – CMS Model A 133

Figure 7–25 History of objective function – CMS Model A 134

Figure 7–26 Histories of geometric design variables – CMS Model B 134

Figure 7–27 Histories of laminate-property design variables – CMS Model B 135

Figure 7–28 History of objective function – CMS Model B 135

Figure 7–29 Second-level optimization process of Model A 137

Figure 7–30 Second-level optimization process of Model B 138

Figure 7–31 Coordinate systems 139

Figure 7–32 Loading pattern of spaced line loads 145

Figure 7–33 Section force (SF1) distribution in CMS optimal designs 149

Figure 7–34 Section force (SF2) distribution in CMS optimal designs 149

Figure 7–35 Structure material distribution of relative stress index 153

Figure 7–36 Performance of different objective functions for optimal CMB bridge 157

LIST OF TABLES

Table 2–1 A^*, B^*, and D^* matrices in terms of lamina invariants and lamination parameters 21

Table 6–1 Optimal laminate designs of FRP shells 86

Table 6–2 Summary of strain energies and displacements of optimal shells 89

Table 6–3 Summary of structural responses of initial and optimal shells 91

Table 6–4 Buckling analyses of Shell 1 96

Table 6–5 Buckling analyses of Shell 2 96

Table 6–6 Buckling analyses of Shell 3 97

Table 7–1 Load case specification for CMB bridge optimization 101

Table 7–2 Dimensional constraints for geometric design variables 105

Table 7–3 Initial designs of CMB Bridges 106

Table 7–4 Optimum results of shape and material-property optimization 111

Table 7–5 Optimal laminates from laminate design optimization process 115

Table 7–6 Section forces for the optimal CMB bridge 117

Table 7–7 Section moments for the optimal CMB bridge 117

Table 7–8 Buckling eigenvalues and eigenvectors of the optimal CMB bridge 120

Table 7–9 Structural response of optimal CMB bridge with different optimal laminates 122

Table 7–10 Geometric variations of optimal CMB bridges 123

Table 7–11 Laminate stresses of the optimized CMB bridge under different limit states 125

Table 7–12 Stress indices of the optimized CMB bridge under different limit states 125

Table 7–13 Laminate stresses of the optimized CMB due to different extreme effects. 127

Table 7–14 Stress indices of the optimized CMB due to different extreme effects 127

Table 7–15 Load cases specification for CMS bridges 130

Table 7–16 Coordinates constraints for geometric design variables 132

Table 7–17 Initial designs of CMS Bridges... 132

Table 7–18 Optimal results of the first-level optimization for the CMS bridges 136

Table 7–19 Section forces for optimal CMS bridges.. 140

Table 7–20 Section moments for optimal CMS bridges... 140

Table 7–21 Buckling eigenvalues and eigenshapes of the optimal CMS bridges 142

Table 7–22 Structural response of optimized CMS bridges for different limit states 144

Table 7–23 Stress indices of optimized CMS bridges for different limit states 144

Table 7–24 Structural responses of the optimized CMS bridges subject to spaced line loads under the service limits state 146

Table 7–25 Stress indices of the optimized CMS bridges subject to spaced line loads under the service limits state... 146

Table 7–26 Section forces of optimal CMS bridges subject to loading pattern changes 147

Table 7–27 Section moments of optimal CMS bridges subject to loading pattern changes 147

Table 7–28 Stress indices distribution of three bridges 152

Table 7–29 Statistics of relative stress index distribution 153

Table 7–30 Optimal CMB bridge designs with different membrane thickness constraints 155

Table 7–31 Structural response with different membrane thickness 156

Table 7–32 Evaluations of alternative objective functions... 157

1 Introduction

1.1 General

Fiber reinforced polymer (FRP) composites have been adopted from aerospace and defense industries to civil infrastructure due to their unique properties, such as high strength-to-weight and stiffness-to-weight ratios, and high chemical and environmental endurance. However, to date, the use of FRP composites for civil infrastructure is mainly for structural rehabilitation and strengthening. The use of FRP composites to fabricate primary structural components has been limited, primarily due to high material costs and designs based on shapes suitable to conventional materials. The layered and fiber dominated structure of FRP composites makes them most efficient when used under in-plane stress demands. The shape resistance concept that structures carry loads by shaping structural geometries to achieve in-plane or membrane resultants is introduced in this chapter, followed by a brief discussion of shape finding for shape resistant structures. Laminate Optimum designs are then discussed to improve in-plane behavior of shape resistant structures by tailoring the material properties of FRP composites property. The rationale to find material-adapted structural shapes and tailor shape-adapted material properties for efficient use of FRP composites in new construction is thus recognized. The aim of this research is then presented so as to develop an approach that accomplishes these integrated design tasks.

1.2 FRP composites for civil infrastructure

This section provides an overview of the mechanical characteristics of laminated FRP composites and a brief review of current applications in civil infrastructure.

1.2.1 Introduction to FRP composites

Fiber reinforced polymer (FRP) composites are materials in which a reinforcement constituent of fibers is surrounded by a continuous and uniform matrix constituent of polymer. The fibers are generally strong and stiff to provide a primary load-carrying capacity. The polymer matrix holds the fibers together, protects the fibers from damage, and allows loads to be distributed among individual fibers.

FRP composites are typically used in laminates, which consist of thin layers of fiber-reinforced material fully bonded together. Each individual layer, or lamina, contains an arrangement of fibers embedded within a thin layer of polymer matrix material. Depending on the arrangement of the fiber constituent, an individual layer of a laminated composite may be constructed by a number of forms. A typical form is to align unidirectional continuous fibers in a given direction. As it will be discussed in Section 1.2, this arrangement provides a unique feature of the material properties of FRP laminates, which can be altered by varying the percentage of layers in the laminate with different orientations. Therefore, FRP laminates composed of unidirectional continuous-fiber composite layers are commonly used in designs of high-performance structures and are thus primarily considered in this research.

1.2.2 Mechanical properties of FRP laminates

The properties of FRP composite layers, such as stiffness and strength, strongly depend on the directional nature of the fibers. The fibers used in FRP composites usually have much higher stiffness than the polymer matrix. Consequently, unidirectional FRP composites have different stiffness properties along the fiber direction and perpendicular to the fiber direction. The stiffness of FRP composites in the fiber direction is governed by the fibers and the stiffness perpendicular to the fiber direction is mostly dominated by the polymer matrix. Such materials, in which material properties have two mutually perpendicular planes of symmetry, are referred to as orthotropic.

The stiffness of Orthotropic FRP laminates can be fully described by four elastic stiffness properties, which are referred to as the engineering constants, i.e., two Young's moduli, E_1 and E_2, along the fiber and transverse to the fiber directions respectively, and the shear modulus G_{12} and Poisson ratio ν_{12} in the plane of the layer. Typical stiffness properties of various unidirectional FRP composites are given in Table 1.1.

Table 1.1 Properties of various fiber-reinforced composite layers

Material	Constituents	E_1 (GPa)	E_2 (GPa)	G_{12} (GPa)	ν_{12}
300/5208	Graphite/Epoxy	181	10.3	7.17	0.28
AS4/3501	Graphite/Epoxy	138	8.96	7.10	0.30
B(4)/5505	Boron/Epoxy	204	18.5	5.59	0.23
Kevlar49/Ep	Aramid/Epoxy	76	5.50	2.30	0.34
Scotchply 1003	Glass/Epoxy	38.6	8.27	4.14	0.26

It needs to be pointed out that FRP layers are highly dependent on the fiber orientation as shown in Figure 1–1, which demonstrates how the elastic moduli are strongly influenced by deviation of the fiber orientation. In addition, FRP laminates, which are constructed of unidirectional-fiber layers stacked at different orientations, inherit the properties of the individual layers and thus lead to high in-plane but rather low through-thickness properties. However, material properties of an entire laminate in different directions along the plane of fibers can be adjusted to maximize the utility of the directional nature of the material properties by varying the number, orientation, and stacking sequence of the layers.

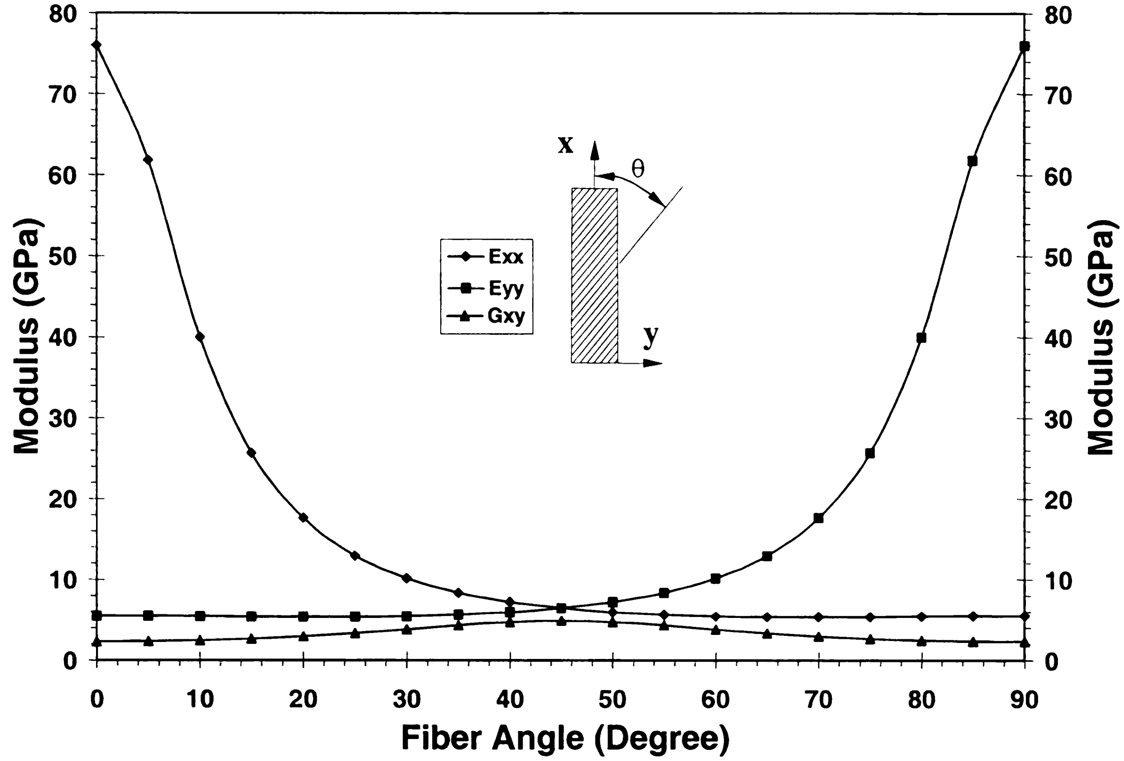

Figure 1–1 FRP elastic modulus as a function of fiber orientation

1.2.3 FRP composites in civil structures

Traditionally, FRP composites have been used extensively in aerospace and consumer sporting goods where their high stiffness and strength-to-weight characteristics were first exploited. These properties, together with their high chemical and environmental endurance and non-magnetic properties compared to conventional materials, have increased interests in the use of FRP composites for civil infrastructure applications [Bakis et al., 2002].

Particularly in the rehabilitation of existing structural systems, advanced composites have shown significant promise in recent laboratory and field applications. The seismic retrofitting of bridge columns (Figure 1–2a) with carbon fiber wraps or pre-formed jackets has been demonstrated to be technically just as effective, and in some circumstances more economical, as conventional steel jacketing. The benefits of light weight and high strength also make FRP composites attractive for the flexural and shear strengthening of existing concrete structures (Figure 1–2b) [Teng et al., 2002; Hollaway and Leeming, 1999].

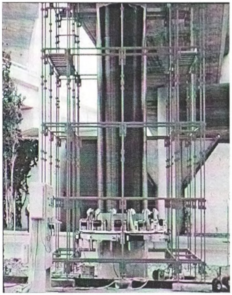

(a) Seismic retrofitting

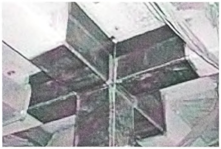

(b) Strengthening

(c) Rehabilitation

Figure 1–2 Applications of FRP composites in civil infrastructures

Structural rehabilitation with FRP composites includes not only repairing and strengthening of aging infrastructure but also replacement of substandard structural components such as new bridge decks [Black, 2000] (Figure 1–2c). The advantages of employing FRPs in new bridge decks include its corrosion resistance, their reduced weight, and ease of installation. Decks made from composite materials can be customized to dimensions of traditional decks and can avoid modifications or replacement to the existing substructure.

Another application of using FRPs in structural components is reinforcing bars (rebars) fabricated from either glass-fiber or carbon-fiber reinforced plastic composites

[Chaallal and Benmokrane, 1996]. Due to corrosion of steel reinforcement in concrete structures, deterioration of concrete results in costly maintenance, repairs and shortening of the structure's service life. FRP rebars have thus shown to be a viable alternative to steel reinforcement and prestressing tendons in areas where the use of steel can lead to a limited life span due to the effects of corrosion.

Finally, the use of all-FRP composite designs for major structural components in new construction has also become of great interest. Two design and construction systems for short- and medium-span bridges consisting of tubular FRP members in combination with conventional materials have been developed and applied to two vehicular bridges in California [Burgueño, 1999].

1.3 Outstanding issues and motivation

In spite of the many applications of FRP composites in civil infrastructure cited above, their use is predominantly in structural rehabilitation and strengthening [Bakis et al., 2002, Karbhari and Seible, 2000]. Construction of new structures composed in their majority by FRP composite materials is still limited to a few highly subsidized demonstration projects. Most of the projects are unique and wide acceptance by the civil engineering community and commercialization has not yet occurred. The limited use is partially due to a high cost of FRP composites compared to the conventional materials such as concrete and steel. Another reason is using FRP composites for primary structural members in shapes copied from those used for conventional materials (i.e., linear shapes such as I-section) does not take advantage of the predominant in-plane stiffness and strength of laminated FRP composites [Burgueño, 1999; Keller, 2002].

In order to make composite structures competitive with metallic counterparts, the overall cost of producing FRP composites needs to be reduced. Advances in manufacturing techniques, such as pultrusion, resin transfer molding, filament winding and the automated or semi-automated manufacturing of large components, has significantly reduced costs. A more efficient way to use FRP composites is in conjunction with conventional structural materials rather than for individual component replacement or complete FRP composite designs [Burgueño, 1999]. This requires new structural concepts and systems that combine the dominant characteristics of concrete in compression and steel in inelastic deformation capacity with the superior mechanical characteristics of directional strength and stiffness in the direction of the composite fibers. Therefore, efficient use of laminated FRP composites requires developing structural concepts and systems that employ them under in-plane stress demands [Burgueño and Wu, 2002].

1.4 Shape and material optimized FRP structures

The development of FRP structures working under in-plane structural demands requires combining shape finding methods and material-property tailoring. The concepts of shape resistant structures and material tailoring are thus introduced next, followed by a brief discussion of the integrated optimization approach for laminated FRP structures presented in this dissertation.

1.4.1 Shape resistant structures and optimal shape finding

A genre of structural systems that can be used to improve the efficiency of laminated FRP composites is called shape-resistant structures (Figure 1–1), which carry design loads in large spans mainly through in-plane or membrane resultants acquired by shaping the material according to the applied loads. Membrane structures and thin-shells are two types of shape resistant structures in which the material is efficiently used under in-plane stress demands developed by the structural shapes.

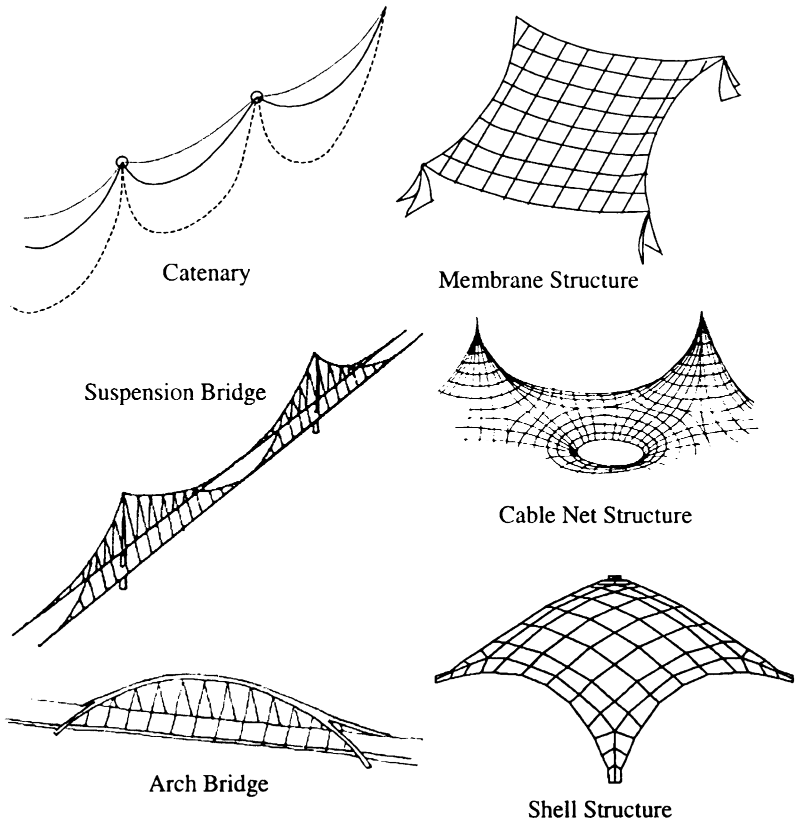
Catenary
Membrane Structure
Suspension Bridge
Cable Net Structure
Arch Bridge
Shell Structure

Figure 1–3 Shape resistant structures [Otto, 1969]

Traditional design methods using trial-and-error are not applicable for the design shape-resistant structures. The methods typically used for the design of shape-resistant structures are called *form-finding* or *shape optimization*. These methods, which range from experimental to diverse numerical approaches, have been successfully developed for determining the optimal shapes and form finding of shell/membrane structures. However, they can not be readily applied to the optimal shape design of laminated FRP composite structures since they apply primarily to structures made from isotropic materials, maintaining the same material properties during the form finding process. Designs for FRP structures obtained through these methods are thus often far from optimal because other competitive material properties cannot be explored.

1.4.2 FRP laminates and optimal laminate design

As previously mentioned in Section 1.2.2, the material properties of FRP laminates can be altered by varying the number, fiber orientations, and the stacking sequence of layers in a laminate. This advantage of tailoring the material properties provides the possibility of improving the structural performance of a shape resistant structure by adjusting the properties of FRP laminates to strengthen the in-plane behavior of the shape resistant design. Evolutionary design optimization methods have been successfully developed and applied for optimal laminate designs requiring discrete changes of fiber orientations and the stacking sequence. However, these methods cannot be directly incorporated with shape optimization procedures, which depend on continuous changes of the structural geometry. Material optimum designs are thus isolated from the shape-finding process of structural resistant designs. Therefore, development of efficient designs for FRP structures in infrastructure requires a general approach accomplishing simultaneous shape and material optimization.

1.4.3 Shape and laminate optimization of FRP structures

From the previous discussion it is understood that finding an efficient structural design of a laminated FRP structure that meets all the requirements for a specific application should be achieved not only by shaping the geometric configuration of the structure, but also by tailoring the material properties, It is thus considerably more complex to find efficient designs for laminated FRP structures than for those made of isotropic materials.

Several researchers have investigated the optimum structural design of FRP structural components. For example, Aref [2001] investigated an approach using genetic algorithms to minimize the weight of structural components by simultaneously changing the cross-sectional shape and ply orientations of the FRP laminates. In another effort, Qiao et al. [1998] developed a global approximation method to optimize material architecture by volume fractions of cross-plies and the cross-sectional area of laminated FRP beams. In spite of these and other developments, the methods developed thus far for the optimization of FRP laminate structures are only applied to what can be termed as *sizing* optimization of standard linear shapes with limited laminate optimization of thickness and/or orientation of limited number of plies.

Although research on the optimum design of FRP laminates and components has been under continued investigation, it is much less developed than shape optimization algorithms for conventional structures. The optimum design of an FRP laminate structure involves both the shape optimization of the structure and the material optimizations of the laminate. Thus, a general approach is required to simultaneously solve for structural shape and material properties thus improve the performance of laminated FRP structures.

1.5 Objective and scope of the dissertation

The main objective of the research reported in this dissertation was to develop an implement a general analytical approach for the development and optimal design c material-adopted shapes for laminated FRP composites in civil structures. The propose analytical approach was evaluated and validated by optimizing FRP shell structures an applied to develop innovative bridge systems using FRP membrane/shell elements.

The dissertation outlines the developed analytical procedure for simultaneousl finding the optimal shape and optimal laminate design of FRP structures. The integrate approach serves as an analytical tool to aid in the design of laminated FRP composit bridge systems and provides insight to the concept of efficiently using FRP laminates b taking advantage of their directional strength and material tailorability.

Chapter 1 provides with an introduction to FRP composites, particularly laminate FRP composites and their mechanical properties. Current applications of FRP composite in civil structures are briefly reviewed. The research motivation is discussed, followed b the research scope.

Chapter 2 presents the fundamental relations that govern the linear elastic propertie of FRP laminates. The chapter then discusses the computation of elastic properties a functions of variables that can be changed during the design process, followed by th formulation of constraints between these variables.

Chapter 3 reviews the existing techniques and their limits for form finding c membrane structures and shape optimization of shell structures. The concept of structura shape optimization is then introduced with a brief discussion of requirements for materia optimization of FRP laminates. Finally, an uncoupled integrated approach is proposed for shape and material optimization.

Chapter 4 and Chapter 5, respectively, describe the optimization problem formulation, the chosen algorithm and its corresponding implementation for each optimization level in the integrated approach.

Chapter 6 focuses on the investigation of the performance and stability of the integrated approach by investigating the optimization of FRP shells. The proposed approach is evaluated by studying and comparing the structural behavior between a shape-and-material optimized shell and two shape-only optimized shells.

Chapter 7 proposes two types of FRP composite membrane-based bridge systems that effectively employ laminated FRP composites. The developed integrated approach is implemented and evaluated through analytical studies on these two bridges.

Chapter 8 summarizes and concludes the current research efforts for the integrated shape and laminate optimization and provides recommendations for future research.

References

Aref, A.J. (2001). A genetic algorithm-based approach for design optimization of fibe reinforced polymer structural components. Mechanics and Materials Summer Conferenc 2001 sponsored by ASME, ASCE, SES, San Diego, CA.

Bakis, C.E., Bank, L.C., Brown, V.L., Cosenza, E., Davalos, Lesko, J.F., A., Machid J.J., Rizkalla, S.H. and Triantafillou, T.C. (2002). Fiber-Reinforced Polymer Composite for Construction – Sate-of-the-Art Review, Journal of Composites for Construction: 6(2 73-87.

Black, S., (2000). A survey of composite bridges, Composites Technology: 6(2), 14-18.

Burgueño, R. (1999). System characteristics and design of modular fiber reinforce polymer (FRP) short- and medium-span bridges, Doctoral Dissertation, Univ. o California, San Diego, California.

Burgueño, R. and Wu, J. (2002, September). Development of an FRP Membrane Bridg System. IABSE Symposium: Towards a Better Built Environment – Innovatior Sustainability, Information Technology, Melbourne, Australia.

Chaallal, O. and Benmokrane, B. (1996). Fiber-Reinforced Plastic Rebars for Concret Applications. Composites: Part B 27B, 245-252.

Hollaway, L.C. and Leeming, M.B., (1999). Strengthening of reinforced concret structures: using externally-bonded FRP composites in structural and civil engineerin Boca Raton, FL: CRC Press.

Otto, F, (1969). Tensile structures: design, structure, and calculation of buildings o cables, nets, and membranes. Cambridge, Mass.: M.I.T. Press.

Karbhari, V.M. and Seible, F. (2000). Fiber Reinforced Composites – Advance Materials for the Renewal of Civil Infrastructure. Applied Composite Materials: 7, 95 124.

Keller, T. (2002). Overview of Fiber-Reinforced Polymers in Bridge Constructior Structural Engineering International: Journal of the International Association for Bridg and Structural Engineering: 2, 66-70.

Qiao, P., Davalos, J.F. and Barbero, E.J. (1998). Design optimization of fiber-reinforce plastic composite shapes, Journal of Composite Materials: 32(2) 177-196.

Teng, J.G., Chen, J.F., Smith, S.T. and Lam, L., (2002). FRP strengthened RC structure New York: Wiley.

2 Laminated Fiber Reinforced Polymer (FRP) Composites

Laminated FRP composites are a class of composite materials where the layers of unidirectional fiber-reinforced composites are staked at different orientations. By varying volume fractions and the fiber orientations of layers in a laminate, material properties of the entire laminate can be adjusted to meet the requirements of a design. FRP laminates have a wide range of application in structural design, especially for high-performance structures that have stringent requirements of specific (property divided by weight) stiffness and strength. In this research, FRP laminates are the only type of FRP composite considered in the composite structures.

Applicable structural designs require meeting certain response quantities such as displacements, stresses, buckling loads and natural frequencies. These response quantities depend on the constitutive behavior of materials, which are determined by the elastic properties such as Young's modulus, shear modulus, and Poisson's ratio. For laminated FRP composites, the constitutive behavior is determined not only by the these elastic properties but also by the parameters of fiber orientations and stacking sequence that can be altered in order to improve structural performance.

The objective of this chapter is to discuss how the *sectional stiffness* calculations of FRP laminates depend on the parameters that can be changed during a design process. The chapter begins by presenting the stress-strain relation that governs linear elastic responses of an orthotropic lamina. The section stiffness of FRP laminates composed of orthotropic laminas oriented at angles is then formulated based on the constitutive relations and the lamination stacking sequence. In addition, the formulation of the section stiffness is given in mathematical terms of *lamina invariants* and *lamination parameters*.

This alternative formulation of the section stiffness requires establishing the relationships between lamination parameters when altering fiber orientations in a stacking sequence. Thus, the feasible domain of out-plane lamination parameters is explored with respect to the in-plane lamination parameters at the end of this Chapter.

2.1 Constitutive relations for FRP laminates

The stress-strain relation for a three-dimensional anisotropic linear material, also known as Hooke's law, is expressed in the following tensor form:

$$\sigma_{ij}=C_{ijmn}\varepsilon_{mn} \tag{2.1}$$

Because of symmetry, $\sigma_{ij}=\sigma_{ji}$ and $\varepsilon_{mn}=\varepsilon_{nm}$, there are only 21 independent material constants in the $\boldsymbol{C}$ matrix, in which $C_{ijmn}=C_{jimn}=C_{ijnm}$. So, Eq. (2.1) can be rewritten in the matrix form:

$$\begin{Bmatrix} \sigma_{11} \\ \sigma_{22} \\ \sigma_{33} \\ \sigma_{23} \\ \sigma_{31} \\ \sigma_{12} \end{Bmatrix} = \begin{bmatrix} C_{11} & C_{12} & C_{13} & C_{14} & C_{15} & C_{16} \\ & C_{22} & C_{23} & C_{24} & C_{25} & C_{26} \\ & & C_{33} & C_{34} & C_{35} & C_{36} \\ & & & C_{44} & C_{45} & C_{46} \\ & & & & C_{55} & C_{56} \\ sym & & & & & C_{66} \end{bmatrix} \begin{Bmatrix} \varepsilon_{11} \\ \varepsilon_{22} \\ \varepsilon_{33} \\ \varepsilon_{23} \\ \varepsilon_{31} \\ \varepsilon_{12} \end{Bmatrix}. \tag{2.2}$$

In the case of a three-dimensional orthotropic material, such as a unidirectional fiber-reinforced lamina, there are two perpendicular planes of symmetry that define two principal axes of material properties. These principal axes correspond to the direction of the fibers and the directions perpendicular to the fibers, denoted by subscripts 1, 2 and 3, respectively. The stress-strain relation in the principal material directions of an orthotropic lamina is given by Eq. (2.3)

$$\begin{Bmatrix} \sigma_{11} \\ \sigma_{22} \\ \sigma_{33} \\ \sigma_{23} \\ \sigma_{31} \\ \sigma_{12} \end{Bmatrix} = \begin{bmatrix} C_{11} & C_{12} & C_{13} & 0 & 0 & 0 \\ & C_{22} & C_{23} & 0 & 0 & 0 \\ & & C_{33} & 0 & 0 & 0 \\ & & & C_{44} & 0 & 0 \\ & & & & C_{55} & 0 \\ sym & & & & & C_{66} \end{bmatrix} \begin{Bmatrix} \varepsilon_{11} \\ \varepsilon_{22} \\ \varepsilon_{33} \\ \varepsilon_{23} \\ \varepsilon_{31} \\ \varepsilon_{12} \end{Bmatrix}. \tag{2.3}$$

Due to the thinness of typical lamina, all layers of the FRP laminates are assumed to behave in a plane stress state in the 1-2 principal material plane so that $\sigma_{33} = 0$, $\sigma_{23} = 0$ and $\sigma_{13} = 0$. The strain-stress relation is then simplified to Eq. (2.4)

$$\begin{Bmatrix} \sigma_{11} \\ \sigma_{22} \\ \sigma_{12} \end{Bmatrix} = \begin{bmatrix} Q_{11} & Q_{12} & 0 \\ Q_{12} & Q_{22} & 0 \\ 0 & 0 & Q_{66} \end{bmatrix} \begin{Bmatrix} \varepsilon_{11} \\ \varepsilon_{22} \\ \varepsilon_{12} \end{Bmatrix}, \tag{2.4}$$

where the Q_{ij} are the reduced material stiffness coefficients which are given in terms of four independent engineering material constants in principal material directions as:

$$\begin{gathered} Q_{11} = \frac{E_1}{1-\nu_{12}\nu_{21}}, \quad Q_{22} = \frac{E_2}{1-\nu_{12}\nu_{21}}, \\ Q_{12} = \frac{\nu_{12}E_2}{1-\nu_{12}\nu_{21}} = \frac{\nu_{21}E_1}{1-\nu_{12}\nu_{21}}, \\ Q_{66} = G_{12}. \end{gathered} \tag{2.5}$$

Since an orthotropic FRP layer can be generally oriented at a certain angle with respect to a structural coordinate system of x-y-z, the stress-strain relations (Eq. (2.4)) in the material coordinate system must be transformed to the structural coordinate system. The transformation of stresses and strains can be accomplished by

$$\begin{Bmatrix} \sigma_{11} \\ \sigma_{22} \\ \sigma_{12} \end{Bmatrix} = \mathbf{T} \begin{Bmatrix} \sigma_{xx} \\ \sigma_{yy} \\ \sigma_{xy} \end{Bmatrix} \text{ and } \begin{Bmatrix} \varepsilon_{11} \\ \varepsilon_{22} \\ \varepsilon_{12} \end{Bmatrix} = \mathbf{T} \begin{Bmatrix} \varepsilon_{xx} \\ \varepsilon_{yy} \\ \varepsilon_{xy} \end{Bmatrix}, \tag{2.6}$$

where T is a transformation matrix. Assuming that the 1-2-3 axis originally coincides with the x-y-z axis and considering a rotation θ about the 3 (or z) axis, the transformation matrix is given by:

$$T = \begin{bmatrix} \cos^2\theta & \sin^2\theta & 2\cos\theta\sin\theta \\ \sin^2\theta & \cos^2\theta & -2\cos\theta\sin\theta \\ -\cos\theta\sin\theta & \cos\theta\sin\theta & \cos^2\theta - \sin^2\theta \end{bmatrix}. \tag{2.7}$$

With Eq. (2.6) and Eq. (2.7) substituted into Eq. (2.4), the strain-stress relation in the structural coordinate system is transformed to:

$$\begin{Bmatrix} \sigma_{xx} \\ \sigma_{yy} \\ \sigma_{xy} \end{Bmatrix} = T^{-1}QT \begin{Bmatrix} \varepsilon_{xx} \\ \varepsilon_{yy} \\ \varepsilon_{xy} \end{Bmatrix} = \begin{bmatrix} \overline{Q}_{11} & \overline{Q}_{12} & \overline{Q}_{16} \\ \overline{Q}_{12} & \overline{Q}_{22} & \overline{Q}_{26} \\ \overline{Q}_{16} & \overline{Q}_{26} & \overline{Q}_{66} \end{bmatrix} \begin{Bmatrix} \varepsilon_{xx} \\ \varepsilon_{yy} \\ \varepsilon_{xy} \end{Bmatrix}. \tag{2.8}$$

$\overline{Q}_{ij}$ are called the transformed reduced stiffness coefficients, which can be expressed in a simpler form by introducing the lamina invariants [Tsai and Hahn, 1980] as:

$$\overline{Q}_{11} = U_1 + U_2 \cos 2\theta + U_3 \cos 4\theta \tag{2.9a}$$

$$\overline{Q}_{12} = U_4 - U_3 \cos 4\theta \tag{2.9b}$$

$$\overline{Q}_{22} = U_1 - U_2 \cos 2\theta + U_3 \cos 4\theta \tag{2.9c}$$

$$\overline{Q}_{16} = \frac{1}{2} U_2 \sin 2\theta + U_3 \sin 4\theta \tag{2.9d}$$

$$\overline{Q}_{26} = \frac{1}{2} U_2 Sin 2\theta - U_3 Sin 4\theta \tag{2.9e}$$

$$\overline{Q}_{66} = U_5 - U_3 \cos 4\theta \tag{2.9f}$$

where the U's are the lamina invariants defined as [Tsai and Hahn, 1980]:

$$U_1 = \frac{1}{8}(3Q_{11} + 3Q_{22} + 2Q_{12} + 4Q_{66}) \tag{2.10a}$$

$$U_2 = \frac{1}{2}(Q_{11} - Q_{22}) \tag{2.10b}$$

$$U_3 = \frac{1}{8}(Q_{11} + Q_{22} - 2Q_{12} - 4Q_{66}) \tag{2.10c}$$

$$U_4 = \frac{1}{8}(Q_{11} + Q_{22} + 6Q_{12} - 4Q_{66}) \tag{2.10d}$$

$$U_5 = \frac{1}{8}(Q_{11} + Q_{22} - 2Q_{12} + 4Q_{66}) \tag{2.10e}$$

When *n* orthotropic layers oriented at different angles are stacked together, a set of additional assumptions are needed in order to derive the equations that govern the constitutive behavior of the laminate. Each layer is assumed to be perfectly bonded to the adjacent layers so that the laminated layers deform in unison without experiencing any discontinuity in displacements. Furthermore, Classical Kirchhoff plate theory is assumed for the bending behavior of the laminate so that the strains in the out-of-plane direction z are neglected and the w displacement in direction z is constant through the thickness of the laminate. These two assumptions, along with the assumption of the layers being in a state of plane stress, define what is known as *classical lamination theory* (CLT), which will be applied herein to formulate the constitutive behavior of the laminates.

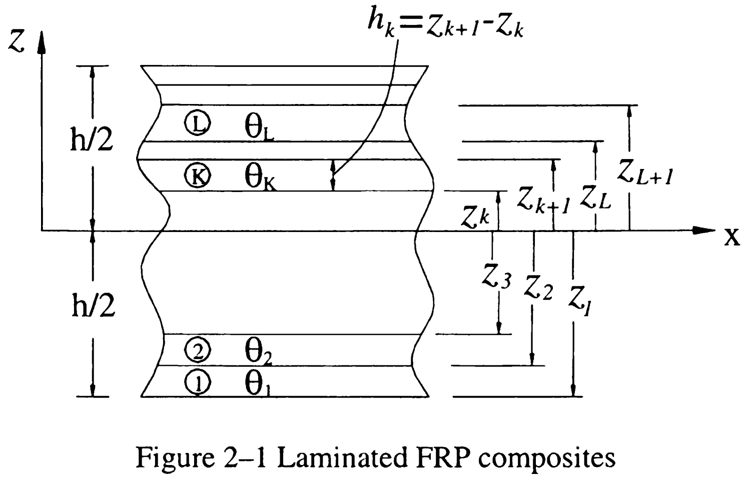

Figure 2–1 Laminated FRP composites

According to CLT, the strains in a plate under a state of stress can be defined by the addition of the constant mid-plane strain $\{\varepsilon^o\}$ and the linear variation due to the bending curvatures $\{\kappa\}$ as:

$$\begin{Bmatrix} \varepsilon_{xx} \\ \varepsilon_{yy} \\ \varepsilon_{xy} \end{Bmatrix} = \begin{Bmatrix} \varepsilon^o_{xx} \\ \varepsilon^o_{yy} \\ \varepsilon^o_{xy} \end{Bmatrix} + z \begin{Bmatrix} \kappa_{xx} \\ \kappa_{yy} \\ \kappa_{xy} \end{Bmatrix}. \tag{2.11}$$

The stresses in the k^{th} ply expressed by the material reduced stiffness of that particular ply are:

$$\begin{Bmatrix} \sigma_{xx} \\ \sigma_{yy} \\ \sigma_{xy} \end{Bmatrix}^{(k)} = \begin{bmatrix} \overline{Q}_{11} & \overline{Q}_{12} & \overline{Q}_{16} \\ \overline{Q}_{12} & \overline{Q}_{22} & \overline{Q}_{26} \\ \overline{Q}_{16} & \overline{Q}_{26} & \overline{Q}_{66} \end{bmatrix}^{(k)} \left(\begin{Bmatrix} \varepsilon^o_{xx} \\ \varepsilon^o_{yy} \\ \varepsilon^o_{xy} \end{Bmatrix} + z^{(k)} \begin{Bmatrix} \kappa_{xx} \\ \kappa_{yy} \\ \kappa_{xy} \end{Bmatrix} \right). \tag{2.12}$$

The stress resultants and moment resultants for unit width of the cross section are obtained by integrating the stresses of all plies through the laminate thickness:

$$\begin{Bmatrix} N_x \\ N_y \\ N_{xy} \end{Bmatrix} = \int_{-h/2}^{h/2} \begin{Bmatrix} \sigma_{xx} \\ \sigma_{yy} \\ \sigma_{xy} \end{Bmatrix}^{(k)} dz = \sum_{k=1}^{n} \int_{z_{k-1}}^{z_k} \begin{Bmatrix} \sigma_{xx} \\ \sigma_{yy} \\ \sigma_{xy} \end{Bmatrix} dz, \tag{2.13a}$$

$$\begin{Bmatrix} M_x \\ M_y \\ M_{xy} \end{Bmatrix} = \int_{-h/2}^{h/2} \begin{Bmatrix} \sigma_{xx} \\ \sigma_{yy} \\ \sigma_{xy} \end{Bmatrix}^{(k)} z dz = \sum_{k=1}^{n} \int_{z_{k-1}}^{z_k} \begin{Bmatrix} \sigma_{xx} \\ \sigma_{yy} \\ \sigma_{xy} \end{Bmatrix} z dz. \tag{2.13b}$$

Substituting the stress-strain relations of Eq. (2.12) into Eq. (2.13), the following section stiffness of the laminate is obtained:

$$\begin{Bmatrix} N_x \\ N_y \\ N_{xy} \\ M_x \\ M_y \\ M_{xy} \end{Bmatrix} = \begin{bmatrix} A_{11} & A_{12} & A_{16} & B_{11} & B_{12} & B_{16} \\ & A_{22} & A_{26} & B_{12} & B_{22} & B_{26} \\ & & A_{66} & B_{16} & B_{26} & B_{66} \\ & & & D_{11} & D_{12} & D_{16} \\ & & & & D_{22} & D_{26} \\ sym & & & & & D_{66} \end{bmatrix} \begin{Bmatrix} \varepsilon_x^o \\ \varepsilon_y^o \\ \varepsilon_{xy}^o \\ \kappa_x \\ \kappa_y \\ \kappa_{xy} \end{Bmatrix} \tag{2.14}$$

where, $[A]_{3\times3}$ is the extensional (in-plane) stiffness matrix; $[B]_{3\times3}$ is the bending-extension coupling stiffness matrix; and $[D]_{3\times3}$ is the flexural (out-plane) stiffness matrix. The components of the ***A-B-D*** matrix can be expressed in terms of the reduced stiffness $\overline{Q}_{ij}^{(k)}$'s of each layer by

$$A_{ij} = \sum_{k=1}^{n} \overline{Q}_{ij}^{(k)} \left(z_k - z_{k-1} \right) \tag{2.15a}$$

$$B_{ij} = \frac{1}{2} \sum_{k=1}^{n} \overline{Q}_{ij}^{(k)} \cdot \left(z_k^2 - z_{k-1}^2 \right) \tag{2.15b}$$

$$D_{ij} = \frac{1}{3} \sum_{k=1}^{n} \overline{Q}_{ij}^{(k)} \left(z_k^3 - z_{k-1}^3 \right) \tag{2.15c}$$

If all layers are of the same material, the components of the stiffness matrix can be further simplified by substituting (2.9) into (2.15) obtaining:

$$A_{ij} = h \cdot A_{ij}^{*} \left(U, V \right) \tag{2.16a}$$

$$B_{ij} = \frac{h^2}{2} \cdot B_{ij}^{*} \left(U, V \right) \tag{2.16b}$$

$$D_{ij} = \frac{h^3}{12} \cdot D_{ij}^{*} \left(U, V \right) \tag{2.16c}$$

where the V's are termed lamination parameters. The use of lamination parameters was first proposed by Tsai and Hahn [1980]. However, it should be noted that the notation used in Eq. (2.16) uses a non-dimensional formulation of the lamination parameters, which deviates from the classical definition from Tsai and Hahn [1980] by the multipliers h, $h^2/2$, and $h^3/12$, respectively. The non-dimensional formulation has been found to be more convenient for use in optimization problems [Miki, 1982; 1985], and is defined by the following expressions.

$$V_{0\{A,B,D\}} = \{1, 0, 1\}, \tag{2.17a}$$

$$V_{1\{A,B,D\}} = \sum_{k=1}^{n} \cos 2\theta^{(k)} \left\{ \frac{1}{h}\left(z_k - z_{k-1}\right), \frac{2}{h^2}\left(z_k^2 - z_{k-1}^2\right), \frac{12}{h^3}\left(z_k^3 - z_{k-1}^3\right) \right\}, \tag{2.17b}$$

$$V_{2\{A,B,D\}} = \sum_{k=1}^{n} \sin 2\theta^{(k)} \left\{ \frac{1}{h}\left(z_k - z_{k-1}\right), \frac{2}{h^2}\left(z_k^2 - z_{k-1}^2\right), \frac{12}{h^3}\left(z_k^3 - z_{k-1}^3\right) \right\}, \tag{2.17c}$$

$$V_{3\{A,B,D\}} = \sum_{k=1}^{n} \cos 4\theta^{(k)} \left\{ \frac{1}{h}\left(z_k - z_{k-1}\right), \frac{2}{h^2}\left(z_k^2 - z_{k-1}^2\right), \frac{12}{h^3}\left(z_k^3 - z_{k-1}^3\right) \right\}, \tag{2.17d}$$

$$V_{4\{A,B,D\}} = \sum_{k=1}^{n} \sin 4\theta^{(k)} \left\{ \frac{1}{h}\left(z_k - z_{k-1}\right), \frac{2}{h^2}\left(z_k^2 - z_{k-1}^2\right), \frac{12}{h^3}\left(z_k^3 - z_{k-1}^3\right) \right\}. \tag{2.17e}$$

The A_{ij}^*, B_{ij}^*, D_{ij}^* coefficients in terms of the lamina invariants U's and the lamination parameters V's are summarized in Table 2–1.

Table 2–1 A*, B*, and D* matrices in terms of lamina invariants and lamination parameters

	$V_{0\{A,B,D\}}$	$V_{1\{A,B,D\}}$	$V_{2\{A,B,D\}}$	$V_{3\{A,B,D\}}$	$V_{4\{A,B,D\}}$
$\{A_{11}^*, B_{11}^*, D_{11}^*\}$	U_1	U_2	0	U_1	0
$\{A_{22}^*, B_{22}^*, D_{22}^*\}$	U_1	$-U_2$	0	U_1	0
$\{A_{12}^*, B_{12}^*, D_{12}^*\}$	U_4	0	0	U_1	0
$\{A_{66}^*, B_{66}^*, D_{66}^*\}$	U_5	0	0	U_1	0
$\{A_{16}^*, B_{16}^*, D_{16}^*\}$	0	0	U_2	0	$2U_3$
$\{A_{26}^*, B_{26}^*, D_{26}^*\}$	0	0	U_2	0	$-2U_3$

The lamina invariants U's are independent of the ply orientation and are determined only by the property of a single layer with respect to the material coordinate system. The lamination parameters V's are related to the fiber orientations and stacking sequence of the layers with respect to the structural coordinate system. Thus, as long as the properties of the FRP lamina are known, the section stiffness of an FRP laminate can be determined by lamination parameters representing the fiber orientations and the stacking sequence.

2.2 Stacking sequence of laminates

In the previous section, the section stiffness matrix describing the elastic responses of a laminate was presented. According to the section stiffness matrix, it should be noted that coupling effects may exist. These coupling effects are easily introduced by random stacking sequences. However, these coupling effects can hamper the effective use of FRP laminates, and their source and effect should be clearly understood.

The **[B]** matrix represents the coupling effects between in-plane and out-of-plane deformations. Then, according to Eq. (2.17), the **[B]** matrix vanishes when the stacking sequence of a laminate is restricted to be symmetric with respect to the laminate mid-plane. According to Eq. (2.14), for symmetric laminates, the in-plane responses and out-of-plane responses can be solved independently. The in-plane resultants are only related to the mid-plane strains and the moment resultants are only related to the section curvatures.

The stiffness terms A_{16} and A_{26} in the in-plane stiffness matrix creates a shear-and-extension coupling effect. This coupling effect will result in in-plane normal stress resultants by shear deformations. The shear-and-extension coupling can be eliminated by balancing layers of off-axis fiber orientations. Balanced laminates require that for each layer with a negative orientation angle θ there is a layer with a positive orientation angle θ. Although the layers in a balanced pair do not need to be placed adjacent to each other, the distance of two balanced layers will determine the value of the bending-twisting coupling terms of D_{16} and D_{26}.

The bending-twisting coupling terms D_{16} and D_{26} exist for all laminates that have off-axis fiber orientations. The out-of-plane bending-twisting coupling effect can not be eliminated even when balanced laminates are used. However, balanced laminates in which layers of positive and negative off-axis angles are placed adjacent to one another will reduce the effect of out-of-plane bending-twisting coupling. Furthermore, for a certain laminate thickness, the bending-twisting terms, D_{16} and D_{26}, vanish with an increasing number of the layers. This behavior will be proved in the following section dealing with constrained relations between lamination parameters.

Designs with consideration of coupling effects are generally avoided in the use of FRP laminates, unless the coupling behavior is sought for pseudo-active structures. Thus, only balanced and symmetric laminates, which have the least-pronounced coupling characteristics, were investigated in the current research. Coupling of the in-plane and out-of-plane responses, denoted by the **[B]** matrix, vanishes for symmetric laminates. According to the Eq. (2.17), the in-plane shear-extension coupling defined by A_{16} and A_{26} vanishes when the laminates are balanced. The out-of-plane bending-twist coupling is considered zero on condition that the number of layers is large enough. Based on the above-mentioned assumptions of the staking sequences, the section stiffness of laminates can be simplified to:

$$\begin{Bmatrix} N_x \\ N_y \\ N_{xy} \\ M_x \\ M_y \\ M_{xy} \end{Bmatrix} = \begin{bmatrix} A_{11} & A_{12} & 0 & 0 & 0 & 0 \\ A_{12} & A_{22} & 0 & 0 & 0 & 0 \\ 0 & 0 & A_{66} & 0 & 0 & 0 \\ 0 & 0 & 0 & D_{11} & D_{12} & 0 \\ 0 & 0 & 0 & D_{12} & D_{22} & 0 \\ 0 & 0 & 0 & 0 & 0 & D_{66} \end{bmatrix} \begin{Bmatrix} \varepsilon_x^o \\ \varepsilon_y^o \\ \varepsilon_{xy}^o \\ \kappa_x \\ \kappa_y \\ \kappa_{xy} \end{Bmatrix}. \qquad (2.18)$$

2.3 Constrained relations of lamination parameters

Use of the lamination parameters to define the section stiffness of laminates requires the definition of an allowable domain for each lamination parameter so that they meet the coupled constraints in relation with other lamination parameters. The constrained relationship between the lamination parameters V_{1A}, V_{3A}, V_{1D}, V_{2D}, V_{3D} and V_{4D} and their feasible domain are established in the following sections.

2.3.1 Relation between in-plane lamination parameters

As discussed previously, in-plane shear-extension coupling effects vanish for balanced and symmetric laminates. Then, according to Eq. (2.18), the in-plane section stiffness is determined by:

$$\mathbf{A} = \begin{bmatrix} A_{11} & A_{12} & 0 \\ A_{12} & A_{22} & 0 \\ 0 & 0 & A_{66} \end{bmatrix}. \qquad (2.19)$$

Recalling Table 2.1and Eq. (16), the components of the stiffness matrix ***A*** can be determined in terms of lamination parameters and lamina invariants by:

$$\begin{Bmatrix} A_{11} \\ A_{22} \\ A_{12} \\ A_{66} \end{Bmatrix} = h \begin{Bmatrix} A_{11}^* \\ A_{22}^* \\ A_{12}^* \\ A_{66}^* \end{Bmatrix} = h \begin{bmatrix} U_1 & V_{1A} & V_{3A} \\ U_1 & -V_{1A} & V_{3A} \\ U_4 & 0 & -V_{3A} \\ U_5 & 0 & -V_{3A} \end{bmatrix} \begin{Bmatrix} 1 \\ U_2 \\ U_3 \end{Bmatrix}. \tag{2.20}$$

According to Eq. (2.20), when the properties of the lamina are known (i.e., U_1, U_2, and U_5), the in-plane stiffness is fully determined by the axial lamination parameters V_{1A} and V_{3A}, which are defined as follows:

$$V_{1A} = \sum_{r=1}^{n} v_r \cos 2\theta_r \, , \tag{2.21a}$$

$$V_{3A} = \sum_{r=1}^{n} v_r \cos 4\theta_r \, , \tag{2.11b}$$

where n is the number of different $\pm\theta$ groups, and v_r is the volume fraction of the layer with $\pm\theta_i$ orientation angle

$$v_r = \frac{2z_r}{h} - \frac{2z_{r-1}}{h}, \tag{2.22}$$

and satisfies:

$$\sum_{r=1}^{n} v_r = 1 . \tag{2.23}$$

where z_r in Eq. (2.22) is defined with respect to Figure 2–1.

From Eq. (2.21) and Eq. (2.23), it can be noted that the lamination parameters V_{1A} and V_{3A}, respectively, have the boundary:

$$-1 \le V_{1A}, V_{3A} \le 1 \tag{2.24}$$

Obviously, the allowable value of lamination parameters of V_{1A} and V_{3A} should satisfy the inequality equation (2.24). Furthermore, the possible in-plane elastic properties are constrained by an allowable combination of V_{1A} and V_{3A} . Using the trigonometric relation, $\cos 4\theta = 2\cos^2 2\theta + 1$, the allowable region of V_{1A} and V_{3A} should satisfy:

$$\begin{aligned} V_{3A} - \left(2V_{1A}^2 - 1\right) &= \sum_{r=1}^{n} v_r \cos 4\theta - \left(2\left(\sum_{r=1}^{n} v_r \cos 2\theta \right)^2 - 1 \right) \\ &= 2\sum_{r=1}^{n} v_r \left(\cos 2\theta_r - \sum_{r=1}^{n} v_r \cos 2\theta_r \right)^2 . \end{aligned} \tag{2.25}$$

The term $V_{3A} - \left(2V_{1A}^2 - 1\right)$ is non-negative, and achieves zero only on the condition of n = 1, that is, when the laminate has only one layer. Therefore, the relation stated by Eq. (2.25) can be expressed as:

$$V_{3A} \geq 2{V_{1A}}^2 - 1 . \tag{2.26}$$

Consequently, the allowable combination domain of in-plane lamination parameters specified by Eq. (2.24) and Eq. (2.26) can be depicted in a diagram (Figure 2–2). The diagram has been effectively used to design laminates with prescribed in-plane stiffness properties in a general graphical procedure introduced by Miki [1982].

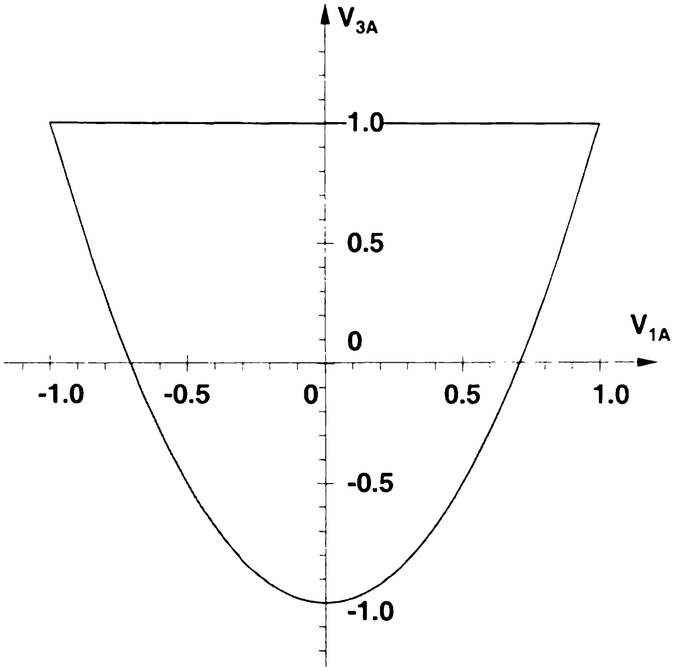

Figure 2–2 Feasible domain of in-plane lamination parameters

2.3.2 Relation between out-of-plane lamination parameters

For symmetric and balanced symmetric laminates, the flexural lamination parameters V_{1D} and V_{3D} are defined as:

$$V_{1D} = \sum_{r=1}^{n} s_r \cos 2\theta_r \,, \tag{2.27a}$$

$$V_{3D} = \sum_{r=1}^{n} s_r \cos 4\theta_r \,, \tag{2.27b}$$

where n is the number of different $\pm\theta$ groups, and s_r is defined as:

$$s_r = \left(\frac{2z_r}{h}\right)^3 - \left(\frac{2z_{r-1}}{h}\right)^3 . \tag{2.28}$$

As before, both lamination parameters must satisfy the boundary defined by $-1 \le V_{1D}, V_{3D} \le 1$. In addition, in a procedure similar to that presented previously, it can be shown that the allowable region (Figure 2–3) of combining V_{1D} and V_{3D} satisfies [Miki, 1985]:

$$V_{3D} \geq 2V_{1D}^2 - 1 . \tag{2.29}$$

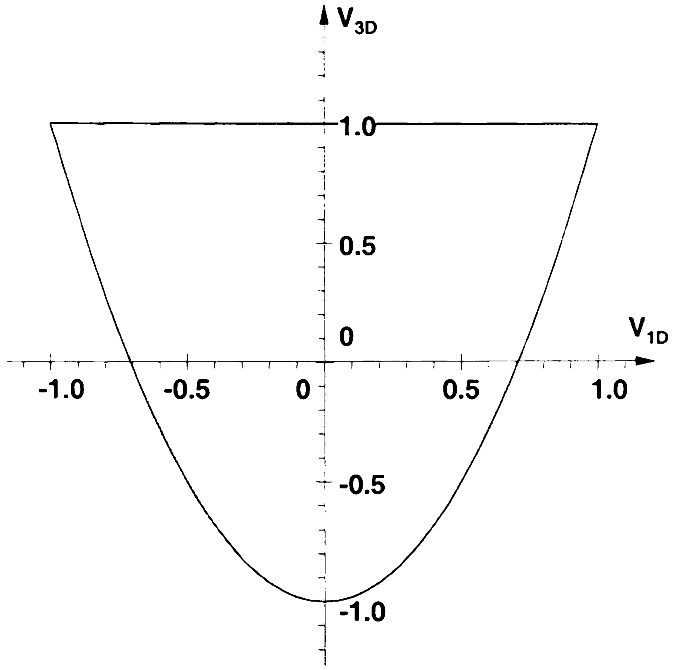

Figure 2–3 Feasible domain of out-plane lamination parameters

As previously discussed, the bending-twisting coupling terms D_{16} and D_{26}, which are caused by any off-axis fiber orientation layer, exist even for balanced and symmetric laminates. The bending-twisting coupling terms D_{16} and D_{26} are determined by the V_{2D} and V_{4D} lamination parameters, where:

$$V_{2D} = \sum_{r=1}^{n} s_r \sin 2\theta_r , \tag{2.30a}$$

$$V_{4D} = \sum_{r=1}^{n} s_r \sin 4\theta_r . \tag{2.30b}$$

Considering symmetric and balanced laminates in which each layer has constant thickness and the balanced layers are placed adjacent with each other, s_r can be expressed by:

$$\begin{aligned} s_r &= \left(\frac{2z_r}{h}\right)^3 - 2\left(\frac{z_r + z_{r-1}}{h}\right)^3 + \left(\frac{2z_{r-1}}{h}\right)^3 \\ &= \left(\frac{r}{n}\right)^3 - 2\left(\frac{r+r-1}{2n}\right)^3 + \left(\frac{r-1}{n}\right)^3 \\ &= \frac{1}{4n^3}\left[4r^3 + 4(r-1)^3 - (2r-1)^3\right] \\ &= \frac{6r-3}{4n^3}. \end{aligned} \tag{2.31}$$

Then, V_{2D} and V_{4D} satisfy

$$V_{2D} = \sum_{r=1}^{n} \frac{6r-3}{4n^3} \sin 2\theta_r \le \sum_{r=1}^{n} \frac{6r-3}{4n^3} = \frac{3}{4n}, \tag{2.32a}$$

$$V_{4D} = \sum_{r=1}^{n} \frac{6r-3}{4n^3} \sin 4\theta_r \le \sum_{r=1}^{n} \frac{6r-3}{4n^3} = \frac{3}{4n}. \tag{2.32b}$$

According to Eq. (2.32), as the number of layers increases, the lamination parameters of V_{2D} and V_{4D} that define the bending-twisting coupling tend to vanish.

2.3.3 Relation between in-plane and out-of-plane lamination parameters

In optimization practices that use lamination parameters to design FRP laminates, it has been observed that the in-plane lamination parameters (V_{1A}, V_{3A}) and out-of-plane lamination parameters (V_{1D}, V_{3D}) are not independent of each other when altering fiber orientations and the stacking sequence of a laminate. This implies that determination of laminate properties by in-plane and out-of-plane lamination parameters is constrained by an allowable combination domain.

Considering symmetric and balanced laminates, in which each layer has a constant thickness and the balanced layers are placed adjacent to each other, the in-plane and out-of-plane lamination parameters can be expressed as:

$$V_{1A} = \sum_{r=1}^{n} \cos 2\theta_r \frac{1}{n}, \tag{2.33a}$$

$$V_{3A} = \sum_{r=1}^{n} \cos 4\theta_r \frac{1}{n}, \tag{2.33b}$$

$$V_{1D} = \sum_{r=1}^{n} \cos 2\theta_r \frac{1}{n} \frac{3r^2 - 3r + 1}{n^2}, \tag{2.33c}$$

$$V_{3D} = \sum_{r=1}^{n} \cos 4\theta_r \frac{1}{n} \frac{3r^2 - 3r + 1}{n^2}. \tag{2.33d}$$

The allowable combination domain is defined as a feasible region of (V_{1D}, V_{3D}) with respect to a given in-plane feasible design (V_{1A}, V_{3A}). The mathematical equivalence can be alternatively implemented to find out the feasible region bound of (V_{1D}, V_{3D}) in terms of functions of (V_{1A}, V_{3A}) throughout whole feasible domain previously defined for the in-plane lamination parameters (Eq. (2.26)) and Figure 2–2.

The region boundaries of (V_{1D}, V_{3D}) with respect to (V_{1A}, V_{3A}) can be implemented by a two-step procedure. The first step is to define the bounds of V_{1D} with respect to a given feasible design (V_{1A}, V_{3A}). This step can be formulated by the optimization problem stated in Eq. (2.34). Figure 2–4 shows an example of determining the feasible boundary of V_{1D} for a given point of $\{V_{1A}, V_{3A}\} = \{-0.4, -0.4\}$;

Objective:

$$Max/Min\ V_{1D} - V_{1A} = \sum_{r=1}^{n} \cos 2\theta_r \frac{1}{n}\left(\frac{3r^2 - 3r + 1}{n^2} - 1\right) \tag{2.34a}$$

Constraints given by:

$$V_{1A} = \sum_{r=1}^{n} \cos 2\theta_r \frac{1}{n} \tag{2.34b}$$

$$V_{3A} = \sum_{r=1}^{n} \cos 4\theta_r \frac{1}{n}, \tag{2.34c}$$

where the θ_k's are chosen as design variables, and $\theta_k \in \left[-90^\circ, 90^\circ\right]$.

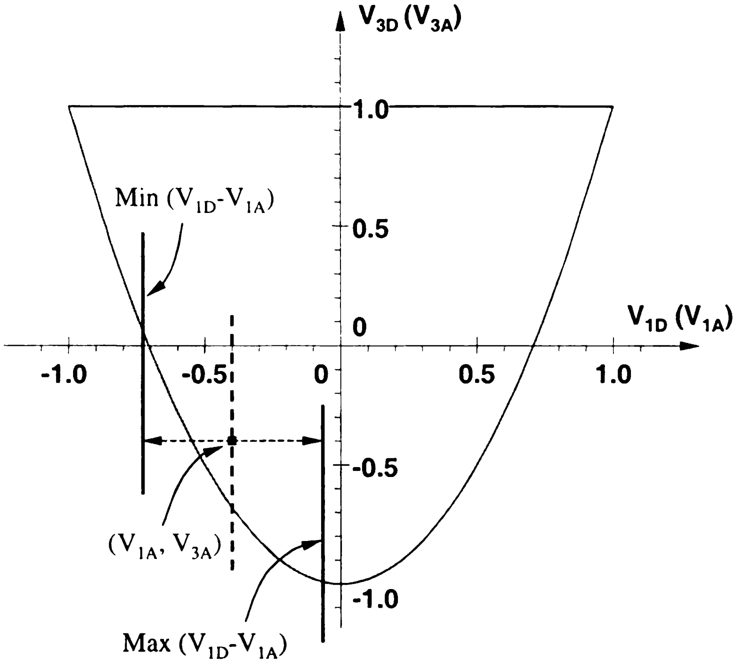
V3D (V3A)
1.0
0.5
0
-0.5
-1.0
V1D (V1A)
-1.0
-0.5
0
0.5
1.0
Min (V1D-V1A)
(V1A, V3A)
Max (V1D-V1A)

Figure 2–4 Boundary determination of V_{1D} for a given $\{V_{1A}, V_{3A}\}$

The second step is then to define the bounds of V_{3D} for a given value within the domain of V_{1D} found in the first step with respect to the given design of (V_{1A}, V_{3A}). The procedure can be accomplished by solving another optimization problem as stated in Eq.

(2.35) below. Figure 2–5 shows an example of determining the feasible boundary of V_{3D} for a given point of $\{V_{1A}, V_{3A}, V_{1D}\} = \{-0.4, -0.4, V_{1D}\}$ for $V_{1D} \in$ [max V_{1D}, min V_{3D}].

Objective:

$$Max/Min\ V_{3D} - V_{3A} = \sum_{r=1}^{n} \cos 4\theta_r \frac{1}{n}\left(\frac{3r^2 - 3r + 1}{n^2} - 1\right) \tag{2.35a}$$

Constraints given by:

$$V_{1D} = V \in \left[V_{1D,\min}, V_{1D,\max}\right] \tag{2.35b}$$

$$V_{1A} = \sum_{r=1}^{n} \cos 2\theta_r \frac{1}{n} \tag{2.35c}$$

$$V_{3A} = \sum_{r=1}^{n} \cos 4\theta_r \frac{1}{n}, \tag{2.35d}$$

where the θ_k's are chosen as design variables, and $\theta_k \in \left[-90^\circ, 90^\circ\right]$.

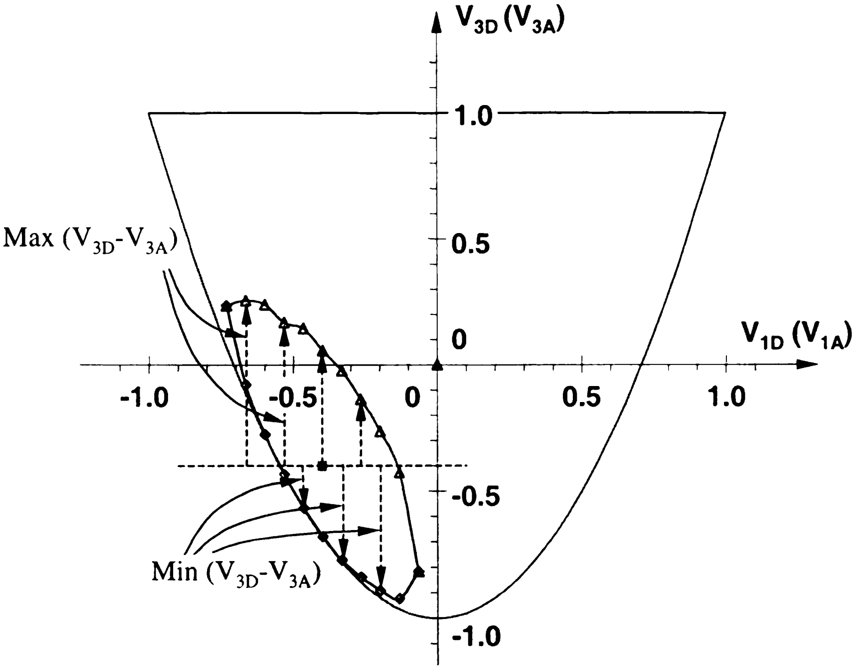

Figure 2–5 Boundary determination of V_{3D} for a given $\{V_{1A}, V_{3A}, V_{1D}\}$

Due to the highly non-linear objective functions, numerical methods are best suited for use in the optimization process. Given a pair of (V_{1A}, V_{3A}), a set of θ_k was searched to achieve the maximum/minimum objective. The optimization search is performed for the different feasible sets of (V_{1A}, V_{3A}) throughout the feasible design domain. Thus, the bound for any given point (V_{1D}, V_{3D}) can be constructed by interpolating between discrete points within the (V_{1A}, V_{3A}) space.

The numerical solution was implemented with the optimization toolbox provided in Matlab [MathWorks, 2000]. Figure 2–6 illustrates the allowable regions of out-of-plane lamination parameters (V_{1D}, V_{3D}) for three in-plane lamination parameter sets {V_{1A}, V_{3A}}: {-0.4, -0.4}, {0,0} and {0.7, 0.8}.

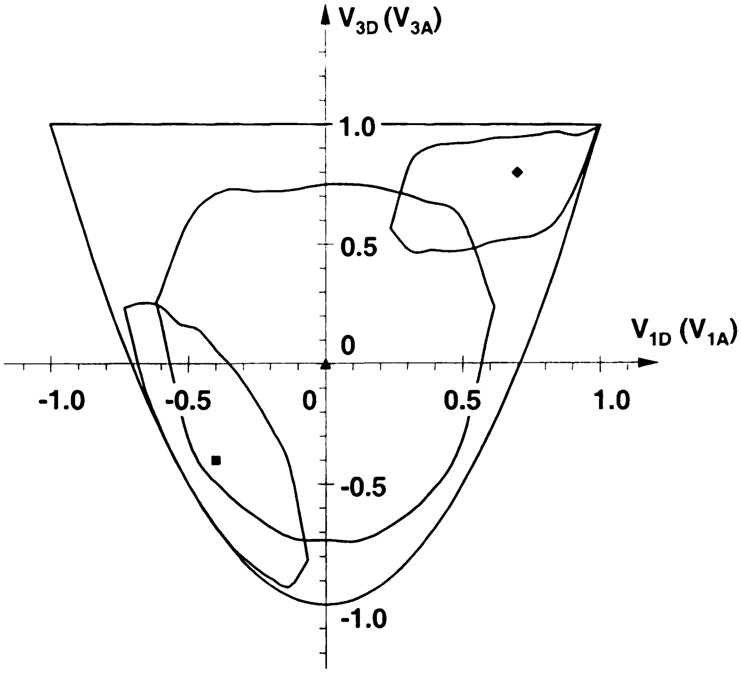

Figure 2–6 Feasible domain of combining in-plane and out-plane lamination parameters

As shown in Figure 2–6, the feasible domain for a pair of out-plane lamination parameters can not achieve the feasible region illustrated in Figure 2–3 in combination with a given pair of in-plane lamination parameters. Moreover, its feasible region will depend on the given pair of in-plane lamination parameters.

2.4 Summary

In this chapter, the *section stiffness* matrix of FRP laminates based on *classical lamination theory* were derived in terms of *lamina invariants* and *lamination parameters*. The elastic properties and coupling effects were discussed, followed by the assumptions about the stacking sequences of laminates considered in this work. The section stiffness matrix of the laminates that will be used throughout the research was derived based on these assumptions. Finally, constrained relations of lamination parameters were established for laminate designs.

References

MathWorks, Inc. (2001). Matlab – Using Matlab Version 6.

Miki, M. (1982). Material design of composite laminates with required in-plane elastic properties, Progress in Science and Engineering of Composites Vol. 2, 1725-1731. Hayashi, T., Kawata, K., and Umekawa, S. (eds) ICCM-IV, Tokyo.

Miki, M. (1985). Design of laminated fibrous composite plates with required flexural thickness. Recent advances in composites in the United States and Japan, ASTM 864. Vinson, J.R. and Taya, M. (eds) American Society for testing and materials, Philadelphia: 387-400.

Tsai, S.W. and Hahn, H.T. (1980). Introduction to composite materials. Lancaster: Technomic.

3 Integrated Optimization Process for Laminated FRP Structures

The nature of laminated FRP composites makes them strong and stiff in-plane, along the fiber orientation, but rather weak through their thickness. Thus, they are most efficient when used under global in-plane stress demands. Therefore, the efficient use of laminated FRP composites in civil infrastructure requires finding structural forms that can maximize the in-plane carrying capacity of laminated FRP composites.

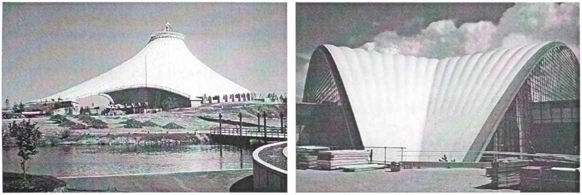
(a) Membrane structure (b) Shell Structure

Figure 3–1 Shape resistant structures

Tension membrane structures (Figure 3–1 (a)) and thin-shells (Figure 3–1 (b)) are two structural form types for lightweight structures that carry loads in large spans mainly through in-plane, or membrane resultants. These two types of lightweight structures belong to the genre of shape resistant structures in which structural strength is obtained primarily by shaping the material to achieve membrane behavior under the applied loads. The shape-resistant nature of in-plane structural response makes structures highly efficient since only a minimal amount of material is used. Therefore, the form finding of lightweight structures is to determine the layout, or shape, in which the material is optimally used so that the structure is subjected primarily to membrane forces rather than bending.

This chapter presents an overview of the capabilities and limitations of different approaches to the optimization of laminated FRP structures. An integrated approach accomplishing the combined tasks of shape and FRP laminate optimization is conceptually presented. The algorithms for each level of optimization are identified, followed by a discussion of the proposed integrated approach.

3.1 Form finding and structural shape optimization

Different experimental methods and computational methods have been developed for the form finding of lightweight structures. Methods for form finding of tension membrane structures and compression thin-shell structures, which depend on different types of membrane action, are introduced in this chapter. The computational methods derived from the experimental methods are also presented. A general computational method for form finding of lightweight structures is then discussed.

3.1.1 Form finding of tension membrane structures

Tension membrane structures, which may consist of prestressed cable nets or fabric membranes, are very attractive alternatives to span large distances. They are very light, elegant, and structurally efficient. The material is optimally used since membranes are subjected to constant surface stresses. Therefore, the form finding of a membrane structure implies finding a shape that results in a constant surface stress distribution under prestressing and externally applied loads.

A membrane that exhibits a constant surface stress is described as a stable minimal surface. Naturally, stable minimal surfaces are achieved by soap films, which have zero mean curvature at every point on the surface and maintain a minimum surface area when in stable equilibrium. The *soap film analogy* (Figure 3–2) [Hildebrandt and Tromba, 1983] is an experimental method that mimics the characteristics of soap films to determine an optimal shape for a tension membrane structure, which is to act in a similar state to that of a soap film.

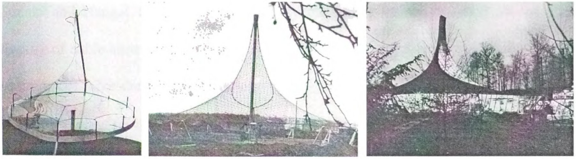

(a) (b) (c)

Figure 3–2 Soap film analogy method and tension membrane structures and [Hildebrandt and Tromba, 1983]

The inherent basis of the soap film analogy method for form finding is to find an optimal membrane shape due to a uniform stress distributed on a deformed structure. Mathematically, this procedure leads to minimal surfaces sustained in a stable equilibrium state. The mathematical principle of the soap film analogy was used to develop several numerical methods, such as the force density method [Schek, 1974; Linkwitz, 1999], the dynamic relaxation method [Barnes, 1994; Lewis and Lewis, 1996], and the updated reference strategy method [Bletzinger, 1997; Bonet and Mahaney, 2001].

The *force density method* [Schek, 1974; Linkwitz, 1999] is primarily used for cable structures. A cable net structure is discretized into branches. The force-length ratios, or force densities, of the branches are defined as structural degrees of freedom. Each node, or the intersection of the branches, is subject to external loads and internal forces from the connecting branches. The optimal shape is the deformed shape of the cable structure that achieves an equilibrium state with the prescribed cable forces. Equilibrium of the structure is obtained by shaping the structure to achieve force balance at every node. The problem can be solved by a set of linear equations in terms of nodal coordinates and force-densities at the branches. However, based on special discretization and linearization techniques, such as modified Newton-Raphson iterations [Haug and Powell, 1972; Suzuki and Hangai 1991], the force density method is mainly intended for the form finding of cable structures, for which equilibrium can be enforced by linear equilibrium equations of force-density parameters.

The *dynamic relaxation method* [Barnes, 1994; Lewis and Lewis, 1996] finds optimal shapes of tension membranes by the principle of minimum potential energy of surface tension, which governs the formation of soap films. This method solves a static problem by non-linear equilibrium equations simulating a pseudo-dynamic process in time. Initially, the membrane surface is discretized by finite elements. The mass of the structure is equivalently distributed to the nodes of the elements. Initially, the nodal velocities and displacements of the structure are set to zero. The residual forces, which are calculated as a difference of external and internal loads, excite an oscillation of the structure. The nodes of the structure start to vibrate with increasing velocities and accumulating displacements. The kinetic energy of the structure is monitored during this process. At the peak of the kinetic energy, the oscillation is interrupted. The nodal velocities are reset to zero and the residual forces are recomputed for the current deflected structure. The iteration process is restarted from the current deformed geometry and continued until the residual forces are reduced to a minimum. The dynamic relaxation method is particularly suitable for structural analyses involving large displacements. However, this technique has no reliable means of controlling the in-plane distortion of finite element meshes [Bonet and Mahaney, 2001]. Therefore, the method can produce unreliable results or, in some cases, result in unstableperformance procedures.

The *updated reference strategy* (URS) method [Bletzinger, 1997; Bonet and Mahaney, 2001] is another form-finding approach to solve minimal surfaces. This method is consistently derived from continuum mechanics of elastic bodies with respect to large deflections and small strains. The fundamental concept of the method is to supplement the stiffness matrix in terms of Cauchy stress tensors in the actual deformed configuration with an additional stiffness matrix. The additional stiffness matrix is derived in terms of the second Piola-Kirchhoff stress tensor in a reference configuration. According to the URS, the reference configuration is chosen as the previous deformed shape of the last iteration. The additional stiffness matrix is known as a geometrical stiffness matrix, which measures the amount of shear distortion of the deformed structures between two continuous steps. The reference configuration is iteratively adapted and the optimization process is terminated when the differences of shear distortion in subsequent reference configurations are within an acceptable tolerance. The structural shape leads to the minimum surface area of a membrane. This method can be applied to cable net structures and membrane structures. If applied to one-dimensional elastic bodies such as cable structures, it will reduce to the force density method. However, update of the reference configuration requires nodal movements normal to the structural surface. This enforcement reduces the nodal degrees of freedom to a 1D direction, which is in conflict with the generation of a free-form surface in 3D space.

Also, the additional stiffness matrix will be singular for the special cases in which nodal displacements are tangential to the surface. This main deficiency exists for all the procedures previously presented for minimal surface. From a mathematical point of view, this deficiency is inherited for all numerical solutions of minimal surfaces. Furthermore the stress filed of a deformed structure is prescribed and not related to structural deformations.

Other computational approaches that involve non-finite element analyses have been developed for the form finding of tension membrane structures [Brew and Lewis, 2003]. However, all of these methods are limited to special applications due to their inherent simulation of the soap film analogy. The soap film analogy, which can physically only be implemented in isotropic films, leads to uniform membrane stresses by minimizing the surface area of the membrane. The computational methods inherent the limitations of the physical approach that they simulate. These computational methods solve an optimal shape by achieving either a minimum area of a stable surface or uniform membrane stresses, which can be only implemented in tension membrane structures.

3.1.2 Form finding of shell structures

Shell structures are another type of shape resistant structures that use materials efficiently. Their excellent structural performance for high load resistance over large spans results from their double-arching behavior that allows them to carry loads by membrane resultants rather than bending. Hanging chains are the simplest structures to carry external loadings by tangent tension resultants obtained through catenary shapes. Several experimental methods have been developed for the form finding of shell structures on the basis of the mechanical principle of bending-free hanging chains, or catenaries.

The *hanging method* (Figure 3–3) is an experimental approach that directly employs the mechanical principle of hanging chains. The models obtained by the hanging method are free of bending and only subject to tension. Therefore, the inverse of the hanging shapes can be considered as the optimal shapes for masonry arches and vaults in pure compression. Applying this principle to three-dimensional structures, Heinz Isler [1991, 1994] successfully implemented optimal shapes of shell structures defined by physical hanging experiments. In the experimental manipulation, shell structures are simulated by similar-dimension membrane materials such as textile cloths that are not able to resist bending and shear. The membranes are hanged according to the boundary conditions of the real structure. The optimal shape of a shell is obtained by taking the inverse shape of the deflected structure subject to a variety of forces, preferably self-weight. In addition to the hanging method, other physical handling techniques are also used in form-finding experimental methods for shell structures, such as the *pneumatic method* and the *flow method* [Isler, 1991].

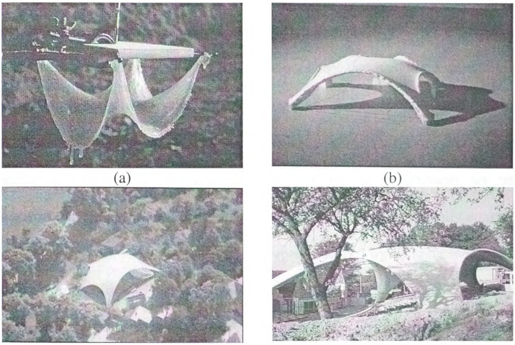

(a) (b)

(c) (d)

Figure 3–3 Hanging method and shell structures and [Isler, 1991, 1994]

The inherent nature of the hanging method generates an optimal shape that is the deflected shape of a structure made of "membrane materials" or materials with negligible bending stiffness. This process can be numerically simulated by *finite element analyses* based on *geometrical nonlinear* theory that allows finite deformations. The structure is discretized into a finite element model using membrane elements. A geometric nonlinear analysis starts with a plane structural geometry. Two approaches are used to achieve optimal shapes. The first approach is to fasten the membrane on the final supports and to load the structure until it reaches its equilibrium state. The second one is to define a membrane with oversize dimensions and to allow the boundary points to slip into their final positions by large rigid body motions. In the numerical simulation of hanging models, in-plane shear stiffness needs to be a fraction of the modulus of elasticity in order to avoid a singular structural stiffness matrix and obtain a fold-free deformed shape.

Additionally, the critical stresses and deflections measured on controlling points are used to control the deformation states in the form finding process.

A variety of concrete shell structures designed by the hanging method or other physical experiments have shown good structural performance and also have good aesthetical qualities. However, shape optimum designs by the hanging method are limited to specific applications. Membrane materials used in the experiments are usually isotropic and thus do not relate even to the actual materials used for actually constructing the shells. In addition, because the optimal shapes achieved by hanging methods result from mechanical deformations, design factors that alter the optimal results can not be considered simultaneously in the optimization processes. For example, the anisotropic property of laminated FRP composites can be tailored by fiber orientations and stacking sequences. However, these factors, in which material alterations may change the optimal shape from a positive to a negative curved surface, can not be taken into account by hanging methods. Stability effects such as buckling also can not be considered by hanging models since the hanging model is only subjected to tension [Isler, 1991]. A sophisticated analysis or a test on a stiff and slender real model is needed to clarify instability issues. The cutting pattern for initial flat membranes, which are critical to avoid developing wrinkles and folds in the deformed shapes, has to be determined by trial and error in a variety of possible solutions. Therefore, a more general approach, which can take into account more design freedom and constraints that are not implemented in physical experiments and their corresponding numerical simulation has become of growing research interest for the form finding of lightweight structures (Figure 3–4) [Ramm et al., 1991; 1993].

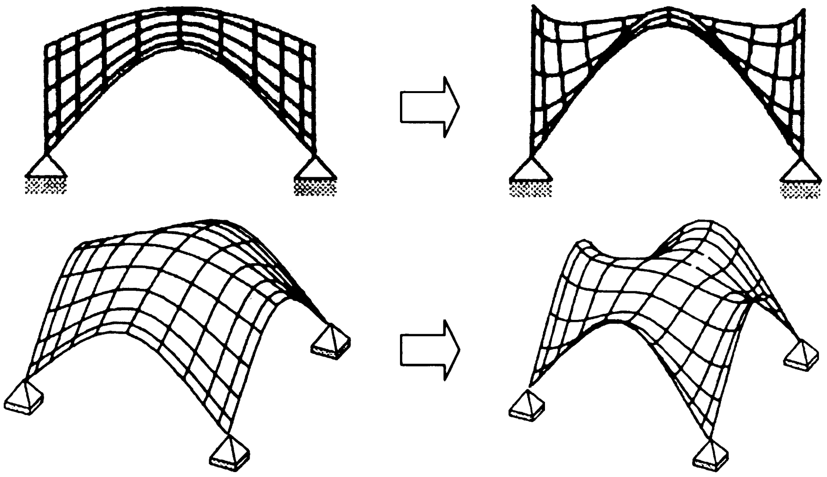

Figure 3–4 Structural shape optimization [Ramm, 1992]

3.1.3 Structural shape optimization

The experimental form-finding methods previously presented rely on the selection of experimental materials and are limited to specific structural forms. The numerical methods used inherit the limitations of the physical approaches that they simulate. A better approach to form finding is *structural shape optimization*, which solves the form finding problem by defining an optimization problem through an *objective function* that measures the “goodness” or “efficiency” of a structural shape design. The objective function is defined by *design variables*, which are parameters that change during the design process. Design variables can be *continuous* or *discrete* depending on whether they can take values from a continuum or are limited to a set of discrete values. The process of shape optimization is then to improve the goodness of the design. Optimization processes are generally performed with some limits that constrain the choice of a design. Such limits are called *constraints* and usually include performance criteria. Structural shape optimization is thus a general and versatile technique for structural form finding.

Shape optimization problems are typically defined in standard mathematical terms as:

Objective: $\text{Min } f(\boldsymbol{x})$

Subject to: $g_i(\boldsymbol{x}) \leq 0 \qquad i = 1 \text{ to } m$

$h_j(\boldsymbol{x}) = 0 \qquad j = 1 \text{ to } p$

$\boldsymbol{X}^L \leq \boldsymbol{x} \leq \boldsymbol{X}^U$

where $\boldsymbol{x}$ is the design variables vector, $\boldsymbol{X}^L$ and $\boldsymbol{X}^U$, are the lower and upper bound vectors of the design variables, $f(\boldsymbol{x})$ is the objective function, and $g_i(\boldsymbol{x})$ and $h_i(\boldsymbol{x})$ are the equality and inequality constraints, respectively.

As far as structural shapes is concerned, the design variables are obviously chosen as the coordinates of points that govern the geometry of a structure. The selection of the objective function depends on the application. For example, the objective for the shape optimization of shell structures consists in the form finding of membrane structures such as to obtain a minimal area of stable surfaces while maximizing the structural stiffness. The constraints are used to implement design limits such as maximum stresses and displacements for the achievement of an optimum objective.

Structural shape optimization combines highly specialized techniques from different disciplines including computer aided geometrical design (CAGD) [Bohm et al., 1984], structural finite element analyses [Cook et al., 2001], structural sensitivity analyses [Arora and Haug, 1979; Haftka and Adelman, 1989], and mathematical algorithms [Arora, 1989].

The classical approach employed in structural shape optimization is based on the following steps:

1. A finite element model is generated by computer aided geometric design;
2. Structural responses, such as displacements and stresses, are evaluated through structural analyses;
3. Sensitivities are computed to formulate the optimization problem in mathematical terms;
4. A mathematical algorithm is chosen to solve the optimization problem and a new design of the structure is generated until an optimum is achieved.

The above-mentioned procedure is structural depicted by an optimization procedure of a shell structure in Figure 3–5.

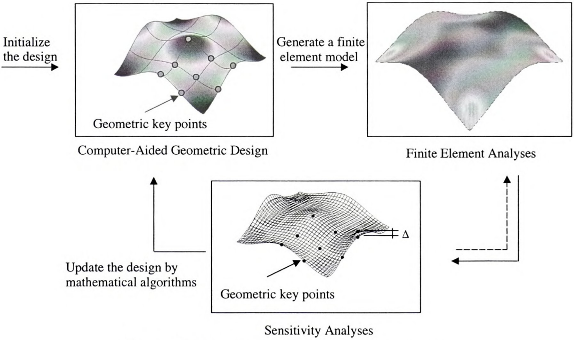
Initialize the design
Geometric key points
Computer-Aided Geometric Design
Generate a finite element model
Finite Element Analyses
Δ
Update the design by mathematical algorithms
Geometric key points
Sensitivity Analyses

Figure 3–5 Structural shape optimization process

3.1.3.1 Computer aided geometric design

In a shape optimization problem, the design variables are geometric parameters defining a structural shape. The generality of a structural shape requires as many geometric design variables as possible. However, considering the efficiency of computational approaches, the number of design variables should be restricted as far as possible. CAGD techniques [Bohm et al., 1984] can assure the generality of a structural shape defined by fewer design variables. The coordinates of the key nodes governing the structural shape are thus typically chosen as the design variables. The shape of an entire structure can then be generated by appropriate shape functions in terms of the coordinates of the key nodes. A finite element mesh is then defined discretize the resulting shape for conducting the finite element analyses.

3.1.3.2 Finite element analysis

Finite element analyses used in structural optimization provide the evaluation of structural responses required by the objective and constraint functions, and also by the design sensitivity analyses. The finite element method provides a numerical procedure for analyzing continua and structures that are too complicated to be solved satisfactorily by analytical methods. In most of practical optimization problems, structures are modeled by the finite element method to calculate their response to applied loads.

3.1.3.3 Design sensitivity analysis

The design sensitivity analysis (DSA) is a fundamental requirement for structural shape optimization. Design sensitivity analysis supplies gradient information on objective and constraint funcions with respect to the design variables for formulating the optimization problem. Considering that finite element analyses are used, two major techniques, numerical and analytical, can be used to calculate structural sensitivity derivatives for finite element modeled structures [Adelman and Haftka, 1986].

Numerical techniques using finite difference methods are straightforward methods in which derivatives are calculated by a finite difference approximation. The accuracy of the derivatives obtained by this technique is depended on the selection of the perturbation step size for the finite difference. Analytical techniques, such as direct differentiation methods and adjoint variable methods, are reliable methods for most kinds of applications at the cost of a higher programming and computational effort. They can be more efficient than numerical techniques if only parts of the structure are affected by shape variants. However, especially for the sensitivity analyses in general shape optimization, analytical techniques will not be able to calculate structural sensitivity derivatives when structural responses implicitly depend on the design variables. In general, the techniques employed for design sensitivity analyses rely on the algorithm to be chosen to solve the optimization problem.

3.1.3.4 Mathematical algorithm

Given a *constrained* optimization problem, design updates and the convergence to an optimum design rely on a mathematical algorithm. Most of mathematical algorithms are based on the general iteration:

$$\mathbf{x}^{(k+1)} = \mathbf{x}^{(k)} + \alpha_k \mathbf{d}^{(k)}$$

where $\boldsymbol{x}^{(k)}$ is the design variables vector of the kth iteration, $\boldsymbol{x}^{(k+1)}$ is the design estimate of the (k+1)th iteration, α_k is a step size, and $\boldsymbol{d}^{(k)}$ is a search direction.

Depending on techniques used to update the designs, mathematical algorithms for solving constrained optimization problems are broadly classified as transformation methods and direct methods [Belegundu and Arora, 1985]. Transformation methods were developed to solve a constrained optimization problem by transforming it into an unconstrained problem whose solution converges to a solution of the original problem. The basic concept of transformation methods is to construct a transformed function by adding a *penalty* for constraint violations to the objective function. Transformation methods include the penalty (exterior) and barrier (interior) function methods as well as multiplier (augmented Lagragian) methods.

Due to the limitation inherited from the transformed functions, direct methods, also known as primal methods, were developed to directly solve the original constrained optimization problem. Many methods such as the method of *feasible directions*, the *gradient projection method* and the *constrained steepest descent method* have been developed and successfully used for engineering design problems. Compared to other methods, the constrained steepest descent (CSD) method is robust and effective for solving nonlinear constrained optimization problems. Direct methods are generally based on the following four basic steps:

1. *Linearize* the objective and constraint functions about the current desing estimate;
2. Define a subproblem formulated by the linearized objective and constraint functions to determine a *searching direction*;
3. Solve the subproblem to give a search direction in the design space;
4. Calculate a step size to minimize a *descent function* in the search direction.

The objective and constraint functions are linearized by the design sensitivity analyses previously discussed. The searching direction is determined by a subproblem based on the linearized objective and constraint functions of the current design. In numerical practices, the subproblems using nonlinear programming have a better algorithm performance and optimum convergence rate than those using linear programming.

The descent function plays a very important role in CSD methods for constrained problems. The basic concept is to compute a step size along the search direction such that the descent function is reduced. Therefore, the descent function is used to monitor the progress of the algorithm towards an optimum point. For constrained problems, the descent function is generally constructed by adding a penalty for constraint violations to the current value of the objective function. Several descent functions have been proposed and applied successfully in practical optimization designs [Han, 1971; Powell, 1978; Schittkowski, 1981].

Based on a descent function, a step size is determined by searching for a minimum of the descent function along the desirable direction in the design space. The step size determination is also known as a one-dimensional search, or line search, problem. Several numerical techniques have been employed for the step size calculation, such as equal interval search, golden section search and polynomial interpolation. However, such exact line search techniques can be inefficient for constrained optimization methods. Therefore, an inexact line search is preferred to determine a step size for practical implementation of constrained problems.

All of these classical mathematical algorithms make use of derivatives of the objective function and constraint functions with respect to the design variables to construct an approximate model of the initial optimization problem. These algorithms rely on the gradients derived by linearizing the original functions to perform the optimization processes. Such gradient-based algorithms can not be generally applied on the optimization of FRP laminates, which typically involve discrete design variables in the objective function and constraints. The rationale behind this limitation brings about the concept and technique presented here for material optimization of laminated FRP composites as discussed in the next section.

3.2 Material optimization of laminated FRP composites

Laminated FRP composites consist of thin layers of fiber-reinforced material fully bonded together. Each individual layer, or lamina, contains an arrangement of unidirectional fibers embedded within a thin layer of polymer matrix material. The material properties of the entire laminate can be adjusted to meet the requirements of a design by varying the percentage of layers in the laminate, their individual orientations and the stacking sequence of the layers. Therefore, finding an efficient structure design can be achieved by tailoring the material properties. FRP laminates are thus the most commonly used type of composite material in the design of high-performance structures.

From the above statements, and as presented in Chapter 3, it follows that the design space for the material optimization of laminated FRP composites is typically a set of discrete parameters that define the material elastic properties. Such optimization problems in which design variables are restricted to take only discrete/integer value are referred to as *integer programming* (IP) problems. Classical gradient-based algorithms for structural optimizations requiring the gradient information of objective and constraint functions can not generally be employed to solve IP optimization problems. In recent years, there has been considerable interest in exploring new optimization methods that do not rely on derivatives of the objective function and constraints to solve this type of problems. For example, the branch-and-bound algorithm [Lawler and wood, 1966; Tomlin, 1970] was advanced to solve linear integer programming problems. Due to the robustness and reliability to achieve global optimums in nonlinear integer programming problems, *genetic algorithms* [Holland, 1975] and *simulated annealing* methods [Kirkpatrick et al., 1983] have emerged as strong contenders against classical gradient-based algorithms. These methods belong to a genetic category of stochastic search techniques. Such *evolution-based algorithms* rely on the selection of fittest “individuals” in a “population” to obtain an optimum design by implementing the operations based on the principles of natural genetics. Unlike classical gradient-based algorithms that move from one point to another in the design space, such algorithms work with a population of designs. By keeping the solutions that have the potential of being the optimum in the population, such algorithms generally result in a global or near-global optimum rather than converging to a local optimum.

The evolution-based algorithms, such as genetic algorithms have been successfully applied to the material design of FRP composites [Gürdal et al., 2000; Liu el al., 2000]. However, most of the research on FRP optimum design for use in high-performance structures has focused only on material optimization, that is, altering material properties by arranging the stacking sequence and fiber orientations. Such optimization is isolated from the structural shape, which also influences the mechanical behavior of a structure. This approach may thus lead to designs that make limited use of the dominant in-plane strength and stiffness of FRP laminates. On the other hand, the structural shape optimization procedures discussed in Section 1.4.1 were primarily focused on optimum designs of structures made from isotropic materials. Optimum designs obtained by traditional shape optimization methods maintain the same material properties during the form finding process. These designs are often far from optimal because other competitive material properties cannot be explored. Therefore, efficient structural designs can be best obtained through shape efficient structures constructed with tailored laminated FRP composites.

Finding an efficient structure design that meets all the requirements for a specific application can then be achieved not only by shaping the geometric configuration of the structure but also by tailoring the material properties. It follows that not only continuous parameters (defining the shape of the structure) but also discrete parameters of lay-up and angles (defining the elastic properties of the material) should be taken into account in an optimization procedure. For the optimal design of FRP composite structures, the design space is thus a mixed set of discrete and continuous design variables.

Gradient-based algorithms, which depend upon sensitivity analyses requiring continuity and derivative existence, are thus not applicable. Although genetic algorithms have been used with some success in problems where a mixed set of integer, discrete, and continuous variables are presented, they generally require more iteration steps to arrive at an optimum design. The random search in genetic algorithms requires more finite element analyses for evaluation of the objective and constraint functions, which decreases computational efficiency and may result in a slower convergence compared to gradient-based algorithms. Therefore, an efficient optimization process needs to be explored for the combined shape and laminate optimization of FRP composite structures.

3.3 Integrated shape and FRP laminate optimization

From the above discussions, shape optimization problems and FRP laminate optimization problems are generally highly nonlinear. However, gradient-based and genetic-based algorithms, which are robust and reliable to solve shape optimization problems and laminate optimization problems respectively, can not be directly applied to solve optimum designs of shaped-optimized laminated FRP structures. Therefore, an integrated approach that utilizes the computational advantages offered by both algorithms is proposed to accomplish the combined task of shape and material optimization. Due to difficulties to solve the entire problem through a single optimization procedure, the optimization task is thus to be implemented in a two-level uncoupled approach (Figure 3–6):

Level 1: Shape and laminate-property optimization: to achieve an optimal shape with optimal stiffness properties;

Level 2: Laminate design optimization: to design an FRP laminate that has the same stiffness properties as those obtained in the first step.

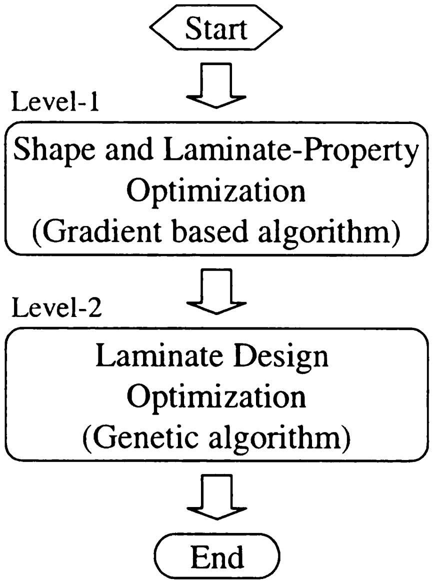
Start
Level-1
Shape and Laminate-Property Optimization (Gradient based algorithm)
Level-2
Laminate Design Optimization (Genetic algorithm)
End

Figure 3–6 Two-level approach of shape and laminate optimization

The alternative formulation of the laminated composite material stiffness derived in terms of lamina invariants and lamination parameters (see Section 2.1) allows implementation of the proposed optimization scheme. First, the lamination parameters ($V_{i(A,\,D)}$) that determine the sectional stiffness of laminates are combined with geometric parameters that define the shape of the structure. The optimum set of continuous design variables (sectional stiffness and geometry) is found so as to maximize the stiffness of the structure. As a second and final step, a set of stacking sequences of variable fiber orientations is then searched to achieve the desired lamination parameters, as obtained from the first step.

The two-level optimization approach combines shape optimization of the structural geometry with material optimization for the FRP laminate design. In addition to the computational efficiency provided by gradient-based algorithms, diverse laminate designs can be achieved by implementing genetic-based algorithms in the proposed integrated approach. The proposed approach takes advantage of decoupling the two different optimization processes and corresponding optimization objectives with respect to their own set of design variables.

According to the two levels employed in the integrated approach, each optimization level involves an independent problem formulation by identifying and defining design variables, objective functions and constraints, and requires the implementation of the corresponding algorithm. The following two chapters describe in detail the procedure for each optimization level.

References

Adelman, H.M. and Haftka, R.T. (1986). Sensitivity analysis of discrete structural systems. AIAA Journal: 24(5), 823-832.

Arora, J.S. (1989). Introduction to Optimum Design. New York: McGraw-Hill.

Arora, J.S. and Haug, E.J. (1979). Methods of design sensitivity analysis in structural optimization. AIAA Journal: 17, 970-974.

Barnes, M. (1994). Form and stress engineering of tension structures. Structural Engineering Review: 6, 175-202.

Bletzinger, K.U. (1997) Form finding of tensile structures by the updated reference strategy. IASS International Colloquium - Towards the new millennium, University of Nottingham

Bohm, W., Farin, G. and Kahmann, J. (1984). A survey of curve and surface methods in CAGD. Computer Aided Geometric Design: 1(1), 1-60.

Bonet, J. and Mahaney, J. (2001). Form finding of membrane structures by the updated reference method with minimum mesh distortion. International Journal of Solids and Structures: 38, 5469-5480.

Booker, L. (1987). Improving search in genetic algorithms. In Genetic algorithms and simulated annealing, Davis, L. (ed.). Los Altos, CA: Morgan Kaufmann Inc., 61-73.

Brew, J.S. and Lewis, W.J. (2003). Computational form finding of tension membrane structures – Non-finite element approaches (part 1-3). International Journal for numerical methods in engineering: 56(3), 651-698.

Cook, R.D., Malkus, D.S. and Plesha, M.E. (2001). Concepts and applications of finite element analysis. NewYorK: Wiley.

Gürdal, Z., Haftka, R.T. and Hajela, P. (1999). Design and optimization of laminated composite materials. New York: Wiley.

Haftka, R.T. and Adelman, H.M. (1989). Recent developments in structural sensitivity analysis. Structural Optimization: 1, 137-151.

Han, S.P. (1979). A globally convergent method for nonlinear programming. Journal of optimization theory and applications: 22, 297-309.

Haug, E. and Powell, G.H. (1972). Finite element analysis of nonlinear membrane structures, Proc 1971 IASS Pacific Symposium Part II on Tension and Space Structures, Tokyo and Kyoto: 165-175.

Hildebrandt, S. and Tromba, A. (1983). Mathematics and optimal form. New York: Scientific American Library.

Isler, H. (1991). Generating shell shapes by physical experiments, IASS Bulletin: 34, 53-63.

Isler, H. (1994). Concrete shells derived from experimental shapes. Structural Engineering international: 3, 142-147.

Lewis, W.J. and Lewis T.S. (1996). Application of formian and dynamic relaxation to the form finding of minimal surfaces, Journal of the International Association for the Shell and Spatial Structures: 37(122) 165-186.

Linkwitz, K. (1999). Formfinding by the "direct approach" and pertinent strategies for the conceptual design of prestressed and hanging structures. International Journal of Space Structures: 14 (2), 73-87.

Liu, B., Haftka, R.T., Akgün, M.A. and Todoroki, A. (2000). Permutation genetic algorithm for stacking sequence design of composite laminates. Computer Methods in Applied Mechanics and Engineering: 186, 357-372.

Powell, M.J.D. (1978). Algorithms for nonlinear functions that use Lagrange functions. Mathematical Programming: 14, 224-248

Ramm, E., (1992). Shape finding methods of shells. IASS Bulletin: 33, 89-99.

Ramm, E., Bletzinger, K. U., and Kimmich, S., (1991). Strategies in shape optimization of free form shells. Nonlinear computational mechanics – state of the art, P. Wriggers, W. Wagner (eds.): 163-192.

Ramm, E., Bletzinger, K.U., and Reitinger, R., (1993). Shape optimization of shell structures. IASS Bulletin: 34, 103-121.

Schek, H.J. (1974). The force density method for form finding and computation of general networks. Computer Methods in Applied Mechanics and Engineering: 3, 115-134.

Suzuki, T. and Hangai, Y. (1991). Shape analysis of minimal surface by the finite element method, Int. IASS Symposium on Spatial Structures at the Turn of the Millenium, Copenhagen: 103-110.

4 Shape and Laminate-Property Optimization of FRP Structures

This optimization level seeks the most efficient structural geometry and laminate sectional stiffness subject to constraints such as structural performance, geometrical dimensions, and laminate failure criteria. This chapter firstly presents the formulation of optimization problem by identifying the design variables and the objective function used for this level of optimization. The algorithm used to solve the optimization problem is given first, followed by its implementation.

4.1 Formulation of the shape and laminate-property optimization problem

Solving optimization problems involves transcribing a verbal description of an optimization problem into a well-defined mathematical statement. Therefore, this optimization level starts by identifying design variables, an objective function and the corresponding constraints, which are presented in the following three sections.

4.1.1 Design variables

The design variables are independent parameters chosen to describe the design of a system in mathematical terms. Proper formulation of an optimization problem always starts by identifying the design variables for the system. In this optimization level, the design variables are the continuous geometric parameters defining the structural shape and the continuous lamination parameters defining the section stiffness properties of the FRP laminate.

The generality of an optimal shape requires as many geometric design variables as possible. However, in order to maximize the efficiency of the computational algorithm, only key dimensional points that define the geometric shape of a structure are chosen as the shape (geometric) design variables. The entire structure is then constructed by CAGD techniques by interpolating the key points.

The laminate coupling effects, which are introduced by random stacking sequences of angle plies (see Section 2.2), are generally avoided for effective use of engineering materials. Therefore, symmetric and balanced laminates, which have the least-pronounced coupling characteristics, are considered in this research. The in-plane and out-of-plane coupling defined by the **[B]** matrix, and the in-plane shear-extension coupling, defined by the A_{16} and A_{26} terms, vanish due to the use of symmetric and balanced laminates. In order to reduce the effects of out-of-plane bend-twist coupling, defined by the D_{16} and D_{26} terms, 48-layer symmetric and balanced laminates are used, in which the lamination parameters V_{2D} and V_{4D} are considered to be equal to zero. Thus, only the lamination parameters V_{1A}, V_{3A}, V_{1D} and V_{3D} (see Section 2.2) [Gürdal et al., 1999], which fully define the in-plane and out-of-plane section stiffness properties, are chosen as the material-property design variables.

4.1.2 Objective function

The objective of the shape optimization procedure to determine the layout of a shape resistant structure is to maximize structural stiffness as measured by the structural stiffness matrix. However, the two-order tensor of the structural stiffness matrix can not be used to evaluate the objective function, which requires a scalar value. Therefore, the structural strain energy, a scalar that quantifies the structural stiffness, is calculated instead in the objective function.

Considering a finite-element-discretized structure without initial strains and stresses, the total strain energy, U, can be stated as

$$U = \frac{1}{2}\int_V \{\varepsilon\}^T [E]\{\varepsilon\} dV = \frac{1}{2}\{D\}^T [K]\{D\} \tag{4.1}$$

where $[E]$ is the material stiffness, $\{D\}$ is the global degree-of-freedom (d.o.f.) vector of the entire structure, and $[K]$ is the structural stiffness matrix.

The global d.o.f. vector $\{D\}$ can be solved by the equilibrium equation as:

$$\{D\} = [K]^{-1}\{R\}, \tag{4.2}$$

where $\{R\}$ is the consistent global nodal load vector.

By substituting Eq. (4.2) into (4.1), the strain energy can be evaluated as:

$$\begin{aligned} U &= \frac{1}{2}\{[K]^{-1}\{R\}\}^T [K]\{[K]^{-1}\{R\}\} \\ &= \frac{1}{2}\{R\}^T [K]^{-1}[K][K]^{-1}\{R\} \\ &= \frac{1}{2}\{R\}^T [K]^{-1}\{R\}. \end{aligned} \tag{4.3}$$

According to Eq. (4.3), for a given statically equivalent load $\{R\}$, the total strain energy U decreases as the structural stiffness $[K]$ increases. Furthermore, the strain energy contribution by different strain types can be determined by recalling Kirchhoff's theory, which is assumed in classical lamination theory. Thus, the strain in a plate under a state of plane stress is defined by the addition of the mid-plane strain $\{\varepsilon^o\}$ and the linear variation due to bending curvatures $\{\kappa\}$ as:

$$\{\varepsilon\} = \{\varepsilon^o\} + z\{\kappa\}. \tag{4.4}$$

Substituting Eq. (4.4) into Eq. (4.1) one obtains:

$$
\begin{aligned}
U &= \frac{1}{2}\int_V \left(\left\{\{\varepsilon^o\} + z\{\kappa\}\right\}^T [Q]\left\{\{\varepsilon^o\} + z\{\kappa\}\right\}\right) dV \\
&= \frac{1}{2}\int_V \left(\{\varepsilon^o\}^T [Q]\{\varepsilon^o\} + 2z\{\varepsilon^o\}^T [Q]\{\kappa\} + z^2\{\kappa\}^T [Q]\{\kappa\}\right) dV.
\end{aligned}
\tag{4.5}
$$

It is thus shown in Eq. (4.5) that, within a unit volume, the strain energy contributed by the bending curvature and axial-bending coupling are quadratically and linearly proportional to the section thickness, respectively. Therefore, minimization of the structural strain energy implies minimizing bending and axial-bending effects, thus maximizing in-plane response and consequently increasing the system stiffness.

4.1.3 Constraints

As previously stated, the objective of the shape and laminate-property optimization is to maximize structural stiffness. However, maximizing the stiffness without restricting material use is meaningless since stiffness can be improved if the amount of material is increased. Thus, the mass of FRP composite used is restricted. Instead of using the equality constraint that the volume of FRP laminates remains the constant during the optimization process, an inequality constraint is chosen to limit the volume of FRP laminates within a certain level. This can be implemented by constraining the thickness of the laminate and the structural geometry.

Among the several function constraints that need to be satisfied for a laminated FRP structure, service and failure constraints are the two most important design criteria for engineering applications. These design criteria can be investigated by the structural responses of maximum structural deflection and maximum section stresses as evaluated by finite element analyses.

4.2 Algorithm of shape and laminate-property optimization

In the shape and laminate-property optimization of laminated FRP structures, the objective function and constraints are nonlinear functions with respect to the design variables. The *constrained steepest descent* (CSD) method is a simple, yet effective, gradient-based algorithm used for solving this type of nonlinear problems [Arora, 1989]. The CSD method is based on four basic steps as presented in the following.

4.2.1 Linearization of objective and constrain functions

For shape and material-property optimization, the objective and constraint functions are implicit functions of the design variables. The solution strategy employed by the CSD method involves solving an approximate problem obtained by linearizing the original objective and constraint functions. The derivatives of objective and constraints functions used to construct the approximate problem are derived by Taylor series expansions. The approximate optimization problem using the first-order Taylor series expansion is formulated as:

Objective:

$$f = \sum_{i=1}^{n} c_i d_i \text{; or } f = \mathbf{c}^T \mathbf{d} \tag{4.6a}$$

Subject to:

$$\sum_{i=1}^{n} a_{ij} d_i \le b_j, \quad j = 1 \text{ to } m\text{; or } \mathbf{A}^T \mathbf{d} \le \mathbf{b} \tag{4.6b}$$

$$\sum_{i=1}^{n} n_{ij} d_i = e_j, \quad j = 1 \text{ to } p\text{; or } \mathbf{N}^T \mathbf{d} = \mathbf{e} \tag{4.6c}$$

where e_j is the negative of the j^{th} equality constraint function value at the current design $\boldsymbol{x}^{(k)}$, $e_j = -h_j\left(x^{(k)}\right)$; b_j is the negative of the j^{th} inequality constraint function value at the current design $\boldsymbol{x}^{(k)}$, $b_j = -g_j\left(x^{(k)}\right)$; c_j is the derivative of the objective function with respect to the i^{th} design variable, $c_j = \partial f\left(x^{(k)}\right)/\partial x_i$; n_{ij} is the derivative of the j^{th} equality constraint with respect to the i^{th} design variable, $n_{ij} = \partial h_j\left(x^{(k)}\right)/\partial x_i$; a_{ij} is the derivative of the j^{th} inequality constraint with respect to the i^{th} design variable, $a_{ij} = \partial g_j\left(x^{(k)}\right)/\partial x_i$.

The derivatives obtained by a linear Taylor series expansion can be numerically evaluated by finite difference approaches. In this optimization level, the forward difference technique is used to evaluate the numerical differentiation of a multi-variable function $f(\boldsymbol{x})$ with respect to variables x_i, which is defined as:

$$\frac{\partial f}{\partial x_i} = \underset{\partial x_i \to 0}{\text{limit}} \frac{f(x_1,\ldots,x_i+\Delta x_i,\ldots,x_n) - f(x_1,\ldots,x_i,\ldots,x_n)}{\Delta x_i} \tag{4.7}$$

where Δx_i is a small perturbation in the variables x_i.

The accuracy of function gradients depend on the selection of the perturbation Δx. Value selection of the perturbation is presented in detail by Gill, Murray and Wright [1981]. In general, a perturbation of 1% of the current value, which works fairly well for most of optimum designs, was chosen for this optimization problem.

4.2.2 Definition and determination of a searching direction

In order to solve the constrained optimization problem, the CSD method requires a desirable *searching direction* towards the optimum design. A searching direction is determined by solving an subproblem. Due to its high efficiency and quadratic convergence rate, a subproblem using a *quadratic programming* (QP) formulation is chosen to determine the searching direction.

The QP subproblem employs a *Hessian matrix* constructed by a quadratic objective function and linear constrains, which are defined in the following:

Minimize:

$$f = \mathbf{c}^T\mathbf{d} + \frac{1}{2} \cdot \mathbf{d}^T\mathbf{H}\mathbf{d}$$

Subject to:

$$\mathbf{N}^T\mathbf{d} = \mathbf{e}$$

$$\mathbf{A}^T\mathbf{d} \leq \mathbf{b} \tag{4.8}$$

where **H** is the Hessian matrix, which represents the second-order derivatives of the objective function with respect to the design variables.

For large-scale optimization problems it is difficult and inefficient to calculate the second-order derivatives matrix. However, due to the usefulness of incorporating the Hessian matrix into the optimization algorithm, the *Quasi-Newton method* was developed to approximate the Hessian matrix by making use of information obtained from previous iterations. In the Quasi-Newton method, an approximate Hessian matrix is updated by using design changes and the gradient vector of the previous iteration. Several updating procedures have been developed [Gill et al., 1981]. The modified BFGS (Broyden-Fletcher-Goldfarb-Shanno) method [Powell, 1978] is implemented to numerically approximate the Hessian matrix in this optimization level.

4.2.3 Definition of the constrained steepest descent function

For shape and laminate-property optimization the objective is to minimize the strain energy of a structure. Achievement of this optimum requires a reduction of the objective function value in each iteration. A descent function is used to ensure the reduction in optimization processes towards the minimum. For constrained optimization problems, the descent function needs to take into account violations of the constraints by adding a penalty for constraint violations to the current value of the objective function.

Several descent functions [Han, 1977; Powell, 1978] have been proposed for constrained optimization problems. *Pshenichny's descent function* [Pshenichny and Danilin, 1978, Arora, 1989, 1997] is chosen as the descent function of the CSD method in the shape and laminate-property optimization due to its wide use in engineering optimization problems.

Pshenichny's descent function Φ at point $\boldsymbol{x}^{(k)}$ is defined as

$$\Phi\left(\mathbf{x}^{(k)}\right) = f\left(\mathbf{x}^{(k)}\right) + RV\left(\mathbf{x}^{(k)}\right), \text{ or } \Phi_k = f_k + RV_k \tag{4.9}$$

where f_k is the kth value of objective function, R is a penalty parameter initially specified by the user, V_k is the k^{th} value of the maximum among all the constraint violations and zero.

The penalty parameter R is a positive number and may be changed during the iterative process. It must be greater than or equal to the sum of all the Lagrange multipliers of the QP subproblem at the point $\boldsymbol{x}^{(k)}$.

$$R \geq \sum_{i=1}^{p} \left| v_i^{(k)} \right| + \sum_{i=1}^{m} u_i^{(k)} \tag{4.10}$$

where $v_i^{(k)}$ and $u_i^{(k)}$ are the values of Lagrange multiplier at the k^{th} iteration for the i^{th} equality and inequality constraint, respectively.

The maximum constraint violation V is nonnegative and is determined at the point $\boldsymbol{x}^{(k)}$ of the k^{th} iteration by

$$V = \max\{0, |h_1|, |h_2|, \dots, |h_p|; g_1, g_2, \dots, g_m\} \tag{4.11}$$

4.2.4 Determination of the step size

Given a descent function, a step size will be searched to minimize the descent function along with the given direction in the design space. The step size determination is often called a one-dimensional search (or line search) problem. Several zero-order methods [Cooper and Steinberg, 1970] are available for one-dimensional search problems, such as the Equal Interval Search and the Gloden Section Search. Other methods using polynomial interpolation can be an efficient technique to solve one-dimensional searches. However, sometimes it is difficult to approximate a function of the step size at the current point $\boldsymbol{x}^{(k)}$ by, e.g., a second-order polynomial interpolation. Thus, in the numerical implementations of this optimization level, the step size determination is solved by an inexact line search using a bisection procedure as described in the following.

At the k^{th} iteration, an acceptable step size α_k is determined as t_j with the smallest integer j to satisfy the descent function:

$$\Phi_{k+1,j} \le \Phi_k - t_j \beta_k \tag{4.12}$$

where $\Phi_{k+1,j}$ is the descent function evaluated at the trial design point $\mathbf{x}^{(k+1,j)}$ that is $\mathbf{x}^{(k+1,j)} = \mathbf{x}^{(k)} + t_j \mathbf{d}^{(k)}$, t_j is the j^{th} trial step determined by using the bisection $t_j = (1/2)^j$, $j = 0,1,2,\ldots$, and β_k is the constant determined by $\beta_k = \gamma \left\| \mathbf{d}^{(k)} \right\|^2, \gamma \in [0,1]$,

4.3 Implementation of shape and laminate-property optimization

The scheme of shape and laminate-property optimization (Figure 4–1) was implemented in a fully automated custom program written in Matlab [MathWorks, Inc., 2000]. An initial reference structure, generated by a custom program for computer-aided-geometric-design (CAGD), is chosen as the starting design for the optimization procedure. The objective strain energy function and constraint values are evaluated by the

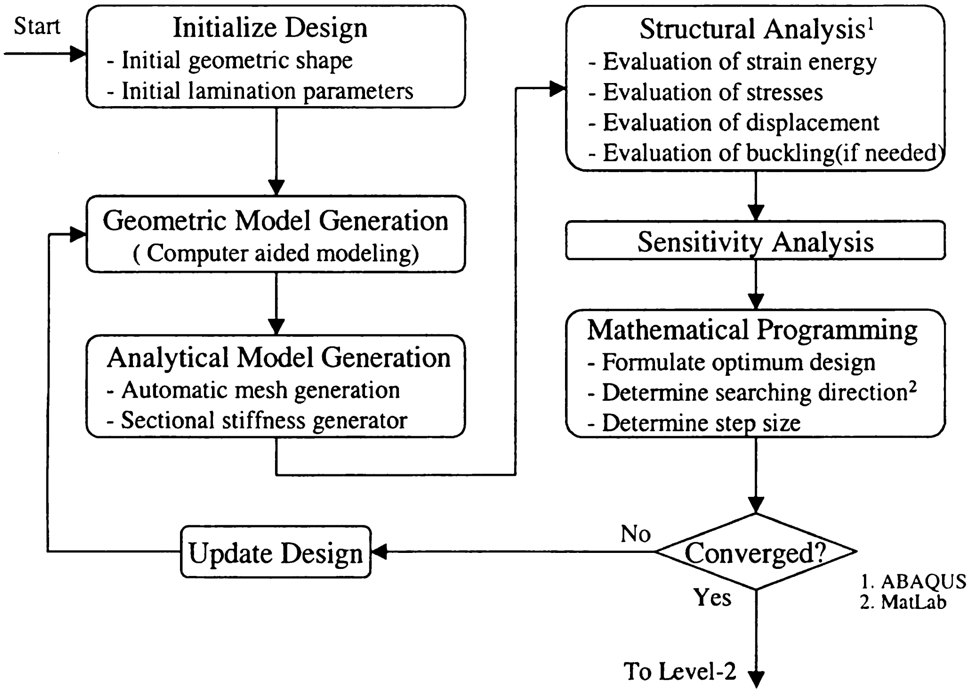
Start
Initialize Design
- Initial geometric shape
- Initial lamination parameters
Geometric Model Generation
(Computer aided modeling)
Analytical Model Generation
- Automatic mesh generation
- Sectional stiffness generator
Structural Analysis¹
- Evaluation of strain energy
- Evaluation of stresses
- Evaluation of displacement
- Evaluation of buckling(if needed)
Sensitivity Analysis
Mathematical Programming
- Formulate optimum design
- Determine searching direction²
- Determine step size
Converged?
No
Yes
Update Design
To Level-2
1. ABAQUS
2. MatLab

Figure 4–1 Shape and laminate-property optimization

finite element software ABAQUS [HKS, 2001]. A numerical searching strategy implemented with Matlab functions determines a search direction and a step size towards an optimal solution. The new geometry and section stiffness properties of the structure are updated and provided as input for the next ABAQUS analysis. The iterative process is continued until no further modifications are required and the optimality conditions are satisfied.

References

Arora, J. S. (1997). Guide to structural optimization. ASCE Manuals and Reports on Engineering Practice No. 90, Reston. VA: American Society of Civil Engineers.

Belegundu, A.D. and Arora, J.S., (1985). A study of mathematical programming methods for structural optimization. International Journal for Numerical Methods in Engineering: 21, 1583-1599.

Cooper, L. and Steinberg, D. (1970). Introduction to methods of optimization. Philadelphia: W. B. Saunders.

Gill, P. E., Murray, W. and Wright, M. H. (1981). Practical Optimization. NY: Academic Press.

Lawler, E.L. and Wood, D.E. (1966). Branch-and-bound methods – A Survey. Operations research: 14, 699-719.

MathWorks, Inc. (2001). Matlab – Using Matlab Version 6.

Miki, M. (1983). A graphical method for designing fibrous laminated composites with required in-plane stiffness. Trans. JSCM: 9, 2, 51-55.

Tomlin, J.A. (1070). Branch-and-bound methods for integer and non-convex programming. In integer and nonlinear programming, Abadie, J. (ed.), 437-450. New York: Elsevier Publishing Co.

Tsai, S. W. and Pagano, N. J. (1968). Invariant properties of composite material. Composite Matreials Workshop: 233-253.

5 FRP Laminates Design Optimization

This optimization level is to design laminates based on the optimal section stiffness, defined by the optimal lamination parameters, which was obtained in the first optimization level. This chapter starts with the formulation of the laminate optimum design problem by identifying the design variables and objective function. The algorithm chosen to solve the optimum design is then presented, followed by a description of its implementation.

5.1 Formulation of laminate design optimization

Similar to the shape-and-material optimization, the process of formulating this optimization level, as described in Section 4.1, involves identifying the design variables, the objective function and the corresponding constraints, which are presented in the following three sections.

5.1.1 Design variables

The goal of the second optimization level is to find stacking sequences of several orthotropic layers with certain fiber orientations that will lead to the lamination parameters obtained in the first optimization level. The fiber orientations for each of a predefined number of plies, which determine the lamination parameters for the section stiffness properties of an FRP laminate, are defined as discrete design variables. Because balanced laminates are used (see Figure 5–1), negative and positive fiber orientations will occur in the laminate designs. Therefore, the definition domain of fiber orientations is from -90° to 90°.

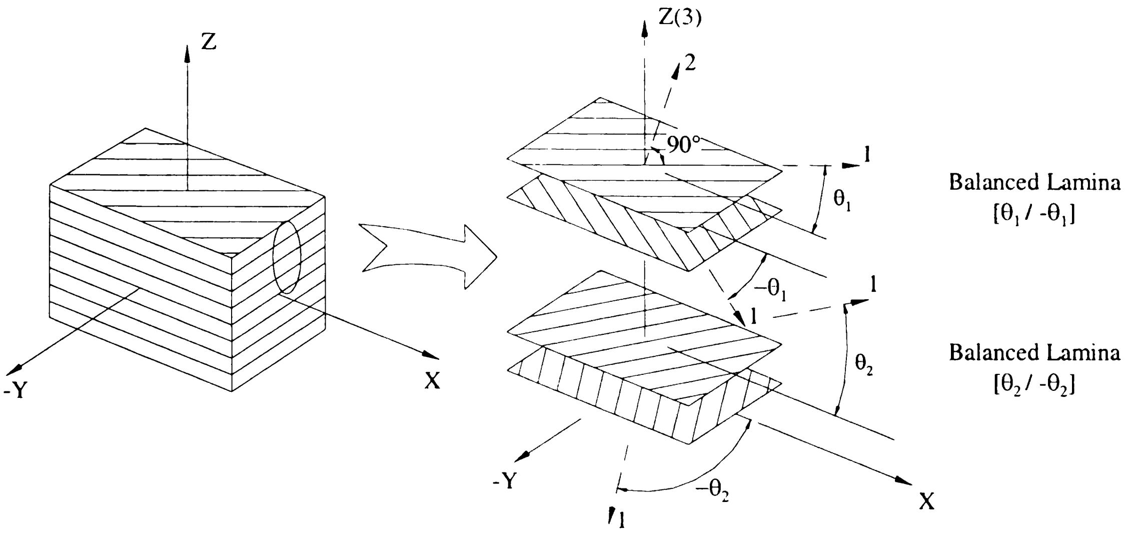

Balanced and Symmetric Laminate
$[\theta_1 / -\theta_1 / \theta_2 / -\theta_2]_S$

Material coordinate system: axis-1,2,3
Structural coordinate system: axis-x,y,z

Figure 5–1 Typical symmetric and balanced laminate

As shown in Section 2.3.2, the lamination parameters of V_{2D} and V_{4D}, which determine the out-plane bend-twist coupling terms of D_{16} and D_{26}, will vanish when the number of plies increases. However, a large number of plies will make the computation inefficient. According to Eq. (2.31), a 48-layer balanced and symmetric laminate has lamination parameters V_{2D} and V_{4D} smaller than 0.0625, which leads to the bend twist terms of D_{16} and D_{26} (see Table 2–1) much smaller than D_{11}, D_{12}, D_{22}, and D_{26} terms. Its out-plane bend-twist coupling effect can thus be neglected compared to the other out-plane stiffness terms. Therefore, 48-layer balanced and symmetric laminates are employed in this research and their optimum designs are to be determined in this optimization level.

5.1.2 Objective function

The objective function is to minimize the discrepancy between the lamination parameters (i.e. V_{1A}, V_{3A}, etc.) evaluated with the design variables from this (2^{nd}) optimization level and the optimal lamination parameters obtained from the first optimization level. The objective function can be expressed as

$$\text{Minimize: } \Delta = \sqrt{\sum_i \left(V_i - \overline{V}_i\right)^2},$$

where V_i are the lamination parameters evaluated by the design variables of fiber orientations, and $\overline{V}_i$ are the lamination parameters of the optimal laminates derived in the first optimization level.

5.1.3 Constraints

The laminate design optimization problem as formulated here is an unconstrained problem. Therefore, no constraints are required in this laminate design optimization problem.

5.2 Algorithm for laminate design optimization

For the laminate design optimization problem, the objective function is not continuous and derivable with respect to the discrete design variables representing the fiber orientations. Gradient-based algorithms, which depend upon the requirements of continuity and derivative existence, are thus not applicable. Conversely, genetic algorithms, which do not rely on derivatives, are suitable to solve this type of problem.

A genetic algorithm is a guided random search technique that works on a population of designs. Each individual in the population represents a design obtained by genetic coding techniques. A fitness value is selected for each individual in order to determine its probability of being chosen as a future "parent design" to create a "children design." Therefore, the application of a genetic algorithm to an optimization problem is based on the steps [Gen and Cheng, 2000] presented in the following sections.

5.2.1 Design representation by genetic coding

In order to reduce the bending-twisting coupling terms D_{16} and D_{26}, balanced laminates pairs of positive ($+\theta$) and negative ($-\theta$) off-axis layers adjacent to each other are assumed for this research. Therefore, a pair of balanced off-axis layers can be represented by the fiber orientation of the top layer in the pair. Considering that the laminates are also symmetric, the 48-layers balanced and symmetric laminates designed in this optimization level can thus be interpreted by 12 integer design variables, which represent 12 different fiber orientations of $\pm\theta$ with a certain stacking sequence.

The optimum achieved by genetic algorithms depends on genetic operators that mimic the principle of natural genetics. The application of genetic operators requires representing the possible combinations of design variables in terms of bit strings that simulate genetic chromosomes. Binary numbers, which are predominantly used for the purpose of computer implementation [Bäck, et. al., 1997], are therefore employed as the technique of genetic coding to represent 12 design variables of different fiber orientations as bit strings. The process of genetic coding for the balanced and symmetric laminate designs, with the reduction mentioned above, is illustrated in Figure 5–2.

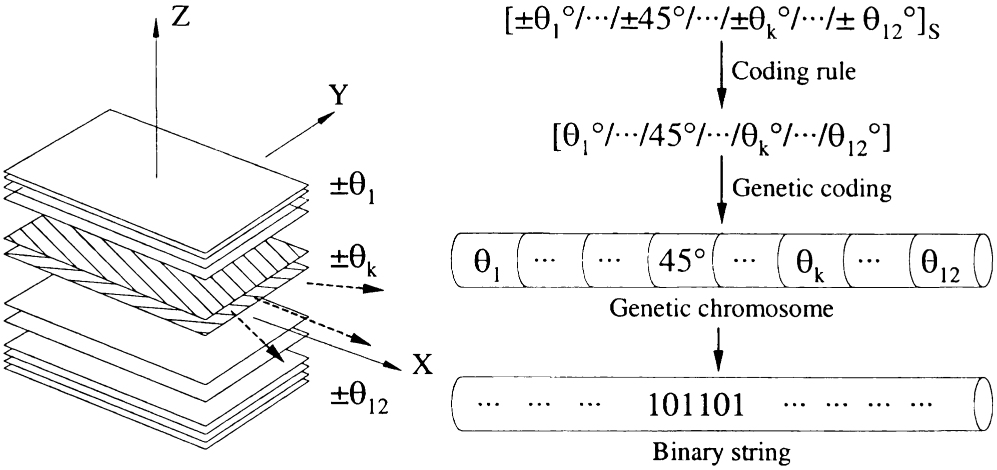

Figure 5–2 Design representation by genetic coding

5.2.2 Definition of a population size

A population in genetic algorithms includes all the designs in a generation. The size of the population is determined by the initial generation and is fixed for all future generations. Currently there are no general rules or solutions for determining the optimal population size for a specific problem. Typically, a population size is chosen at least as large as the chromosome string length in terms of binary bits. The current laminate design problem has 12 integer design variables with values ranging between –90 and 90. Each design variable requires at least 8 bits for binary representation. Therefore, a population size of 100 is chosen for the total 96-bit length of a genetic chromosome.

5.2.3 Definition of fitness values and a selection scheme

The forward movement of genetic algorithms depends on a selection process by giving higher chances for better individual designs to pass their characteristics to future generations. Thus, the selection process requires a value to evaluate the fitness of an individual design in a generation. For unconstrained optimization problems, the value of the objective function can be used as the fitness value of a design.

Once the fitness values of the designs in a generation are determined, the designs with higher fitness values will be selected to create child designs by a selection scheme. Several selection schemes [Goldberg, 1989; Davis, 1991] have been developed for genetic procedure, such as roulette wheel, tournament selection and ranking selection. Due to its small spread about the desired distribution and its freedom from bias, stochastic universal sampling [Baker, 1987] is used in this work as the selection scheme in the laminate design optimization.

5.2.4 Implementation of genetic operators

Crossover (Figure 5–3) is one of two major genetic operators used in genetic algorithms. The task of the crossover operator [Goldberg, 1989; Davis, 1991] is to explore new designs alternatives by combining the existing family traits. The crossover operation generates children designs by exchanging genetic segments of the selected parent designs. The crossover operation is typically to be executed with a probability number. A random number, uniformly distributed between 0 and 1, will determine the implementation of the crossover operator. The crossover operation is performed when the random number is less than the probability of occurrence.

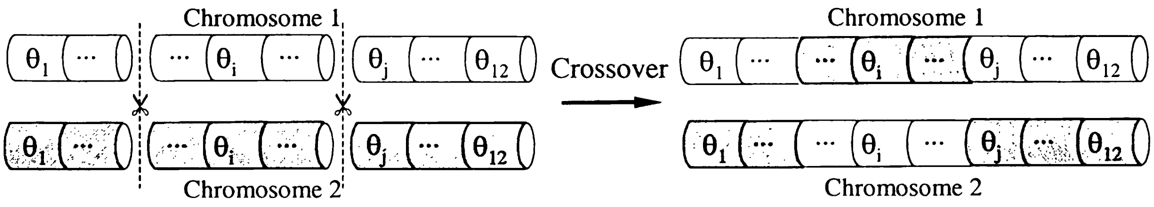

Figure 5–3 Crossover operator

In addition to the crossover, mutation (Figure 5–4) is needed to prevent the premature of the optimization procedure to achieve an optimum design by exploring new traits with the genes that are not represented in the initial population. This function is implemented by the mutation operator [Goldberg, 1989; Davis, 1991], which introduces occasional random alteration of a genetic bit string. Based on the small rates of occurrence of this phenomenon in biological systems and on numerical experiments, mutation is generally performed with a small probability of occurrence.

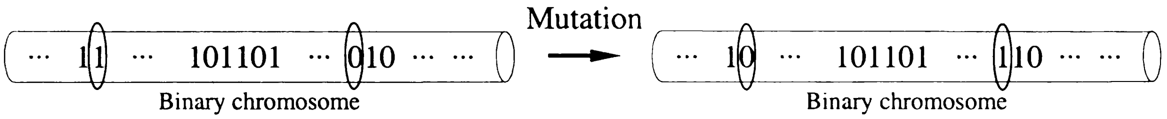

Figure 5–4 Mutation operator

5.3 Implementation of laminate design optimization

The laminate design optimization by a genetic algorithm begins with the random generation of a population of design alternatives. It is processed by means of genetic operators (see Figure 5–5), crossover and mutation create a new population. Among several types of crossover operators, two-point crossover is considered to be superior [Booker, 1987] and is thus employed in this work for the laminate design optimization. The new generation, which combines the most desirable characteristics of the old population with less discrepancy to the optimal lamination parameters, will replace the old population. The process is repeated until a stopping criterion is satisfied. The stopping criterion is implemented in the form of a maximum number of generations without improvement in the best design. The scheme of the genetic algorithm described above was implemented in the program GALOPPS by Goodman [1996]. As part of this work, custom programs were specifically developed to be used together with GALOPPS. The additional programs allow implementation of the genetic representation of design variables and evaluation of the objective function to accomplish the laminate design optimization.

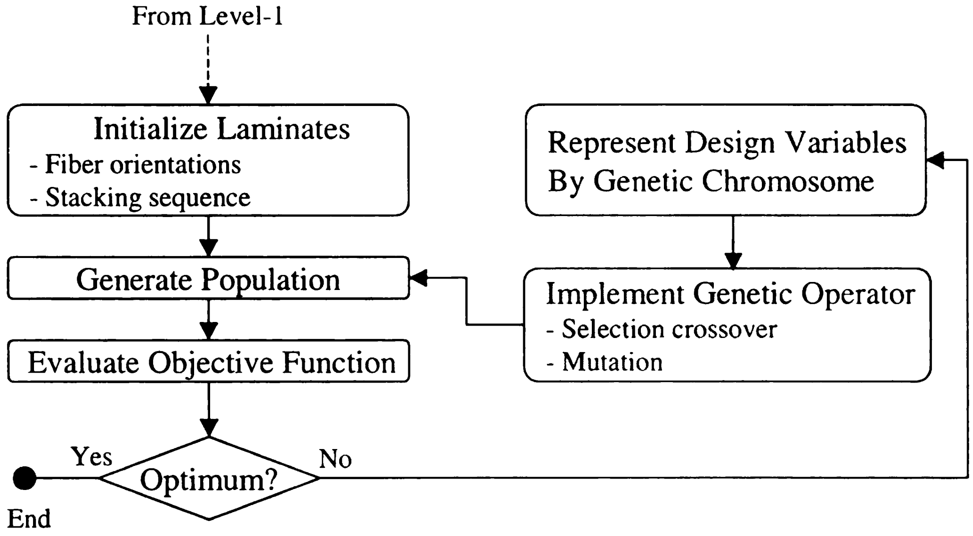
From Level-1
Initialize Laminates
- Fiber orientations
- Stacking sequence
Generate Population
Evaluate Objective Function
Optimum?
Yes
No
End
Represent Design Variables
By Genetic Chromosome
Implement Genetic Operator
- Selection crossover
- Mutation

Figure 5–5 Laminate design optimization

References

Baker, J.E. (1987). Reducing bias and inefficiency in the selection algorithm, In: Proceedings of the Second International Conference on Genetic Algorithms Lawrence Erlbaum Associates Hillsdale: 14-21.

Bäck, T., Hammel, U., and Schwefel, H.P. (1997). Evolutionary computation: Comments on the history and current state. IEEE Transactions on evolutionary Computation: 1, 1.

Davis, L. (1991). Handbook of genetic algorithms. New York: Van Nostrand Reinhold.

Gen, M. and Cheng, R., (2000). Genetic algorithms and engineering optimization. New York: Wiley.

Goldberg, D. (1989). Genetic Algorithms in Search, Optimization, and Machine Learning. Massachusetts: Addison-Wesley, Reading.

Goodman, E.D. (1996). An Introduction to GALOPPS – the Genetic Algorithm Optimized for Portability and Parallelism System, Release 3.2. Technical Report 96-07-01, Intelligent Systems Laboratory and Case Center for Computer-Aided Engineering and Manufacturing. East Lansing, MI: Michigan State University.

6 Shape and Laminate Optimization of FRP Shells

As discussed in Section 3.1.2, shells are shape-resistant structures in which strength and stiffness is obtained by shaping the material to achieve primarily in-plane or membrane compression resultants due to the applied loads. The efficiency of FRP structures can then be enhanced by their use in this type of geometry. Thus, the shape and laminate optimization of FRP shell structures is presented here to evaluate the proposed integrated approach for shape and material optimization. To demonstrate the capability and effectiveness of the integrated optimization approach, the results and performance of a shape-and-material optimized shell are compared to two other shape-only optimized shells. Shape-only optimized shells, optimized only with the shape optimization technique used in the integrated approach utilize laminates with fiber orientations of ±45° and 0°/90. The optimum designs of three FRP shells are compared to similar optimal studies obtained for isotropic materials [Ramm et al., 2000, 1992; Isler, 1991, 1994]. The optimum results for all three FRP shells are also compared with respect to the objective of strain energy and other types of structural performance in terms of displacements and section resultants.

6.1 Shape and laminate optimized FRP shell

The shell selected for studies of integrated optimization, referred later as Shell 1, is of arbitrary dimensions with has a projected area of 4.88 m by 4.88 m and a thickness of 25.4 mm. The shell is taken to be simply supported at the corners and is subjected to a uniform gravity load of 6.89 kN/m^2 (Figure 6–1). The laminates used in the shell studies are based on a typical medium-performance carbon/epoxy material system for use in civil structures. Thus the lamina orthotropic properties are taken as: E_{11} = 155.025 GPa, E_{22} = 10.335 GPa, G_{12} = 6.89 GPa, G_{13} = 6.89 GPa, G_{23} = 0.689 GPa, and ν_{12} = 0.3.

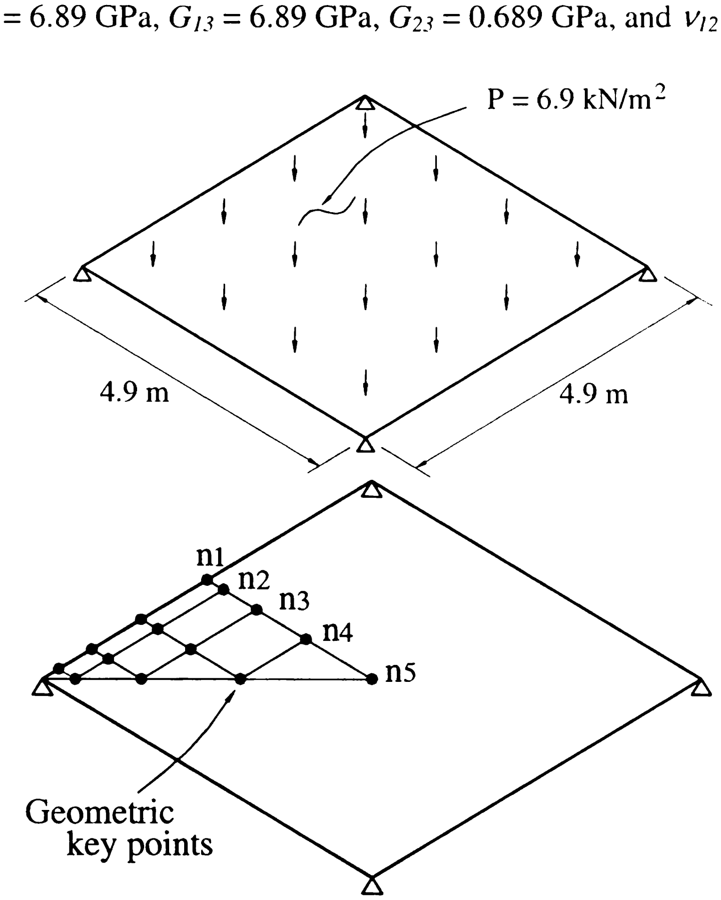

Figure 6–1 Geometry, loading, and control points for shell structures

Taking advantage of symmetry, the geometric shape of the shell can be controlled by 14 design variables that define the vertical coordinates of key points as shown in Figure 6–1. The key points are distributed non-uniformly over 1/8 of the shell area in order to sample geometric details about the free edges of the shell. The shape of the entire shell is then constructed by spline interpolation of the key points. Four-node doubly curved general-purpose shell elements, which use reduced integration with hourglass control [HKS, 2001], are used to discretize the entire shell into a 64×64 finite element mesh.

The first-level optimization histories of the objective, partial geometric design variables and FRP laminate-property design variables are presented in Figure 6–2, Figure 6–3 and Figure 6–4 respectively. The optimization starts with a flat shell with a section stiffness corresponding to a [90°/0°/0°/90°] laminate, which lamination parameters are $\{V_{1A}, V_{3A}, V_{1D}, V_{3D}\}=\{0, 1, -0.75, 1\}$. In the course of the optimization process, the strain energy of the shell, starting at 112.98 kN-m converges stably to 0.0496 kN-m after 66 iterations with the optimal shape shown and the optimal material property defined by lamination parameters $\{V_{1A}, V_{3A}, V_{1D}, V_{3D}\}=\{-0.12654, -0.08372, -0.00498, -0.79898\}$. Stiffness variation is small (Figure 6–2) during the last steps with minor changes in shape and material properties (Figure 6–3 and Figure 6–4). Figure 6–2 also shows a collection of the shell shapes as they evolved during the optimization process. It can be seen that the central point of the shell rises in order to reduce bending moments while a negative curvature appears at the edges of the shell. This featuring shape is clearly illustrated in the elevation view of the shell (see Figure 6–3). These features of the optimal shape have also been observed by other researchers on the shape optimization of concrete shells (see Figure 3–3 (b) and Figure 3–4) [Ramm et al., 2000, 1992; Isler, 1991, 1994; Ramm and Mehlhorn, 1991].

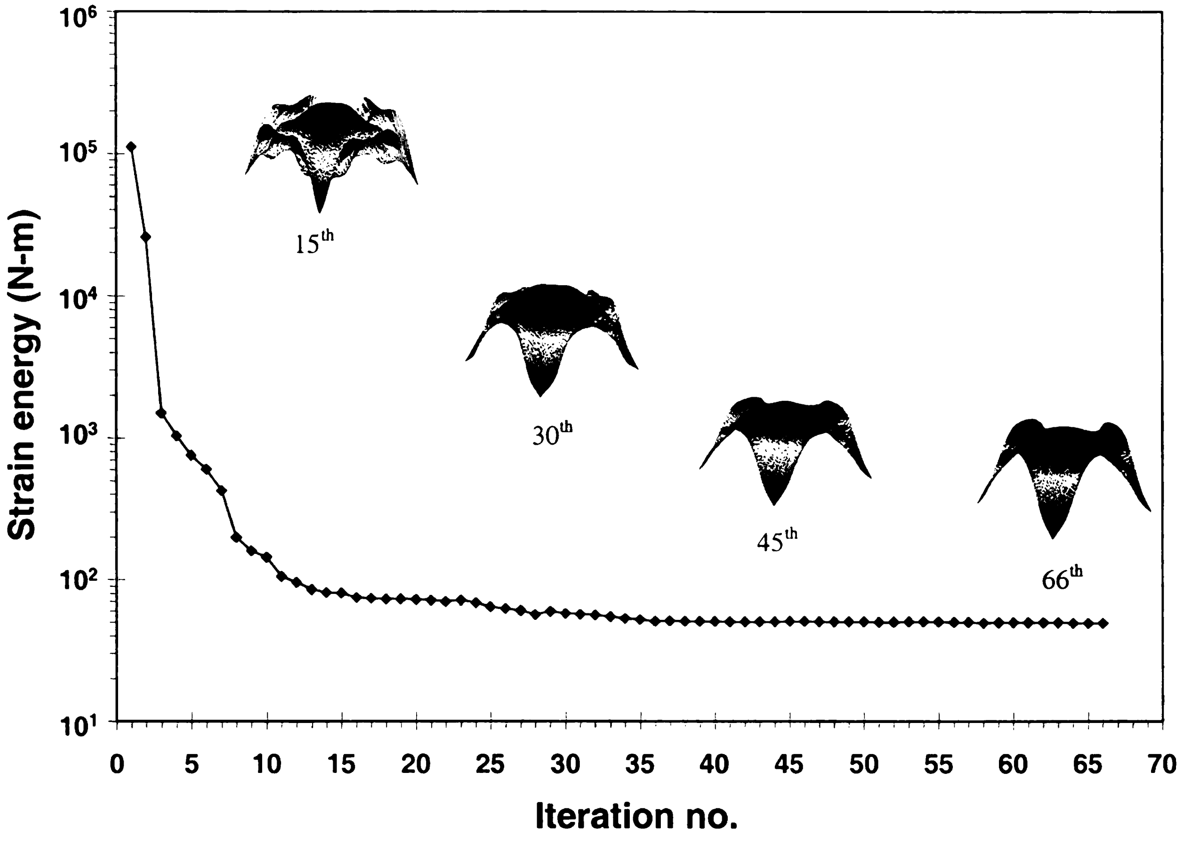

Figure 6–2 History of objective function – FRP Shell 1

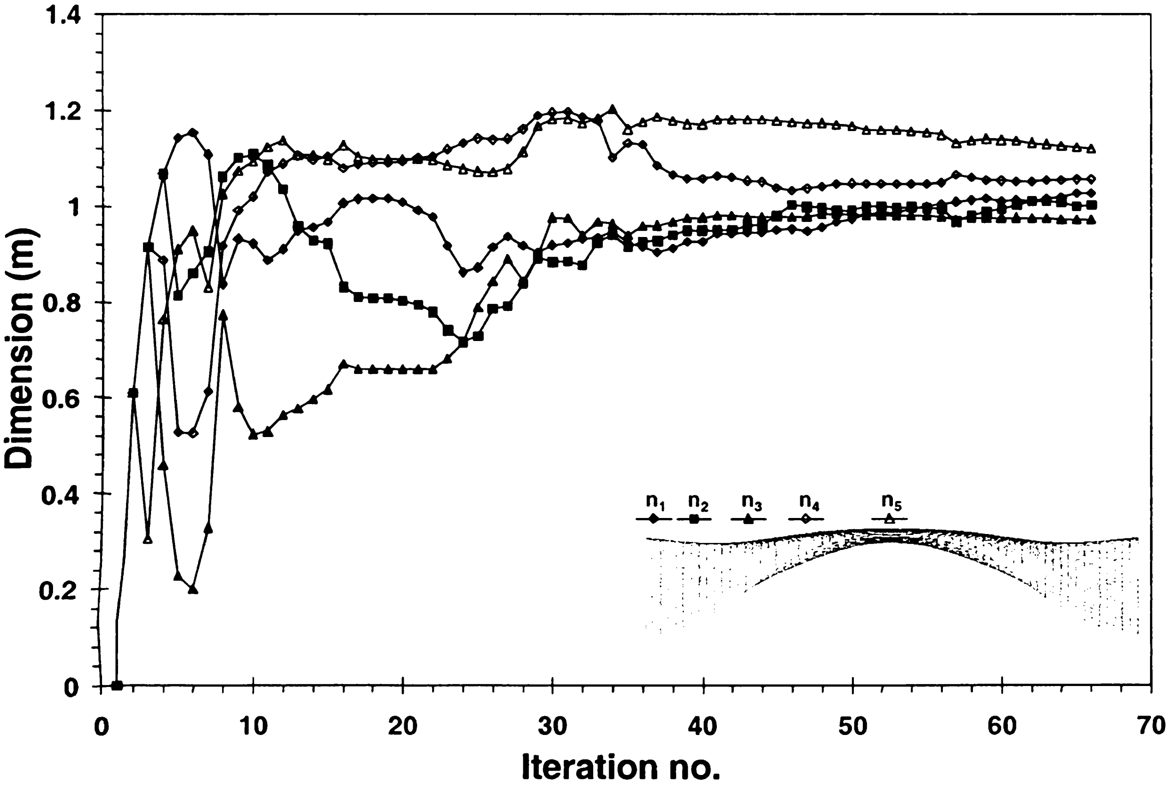

Figure 6–3 Histories of partial geometric design variables – FRP Shell 1

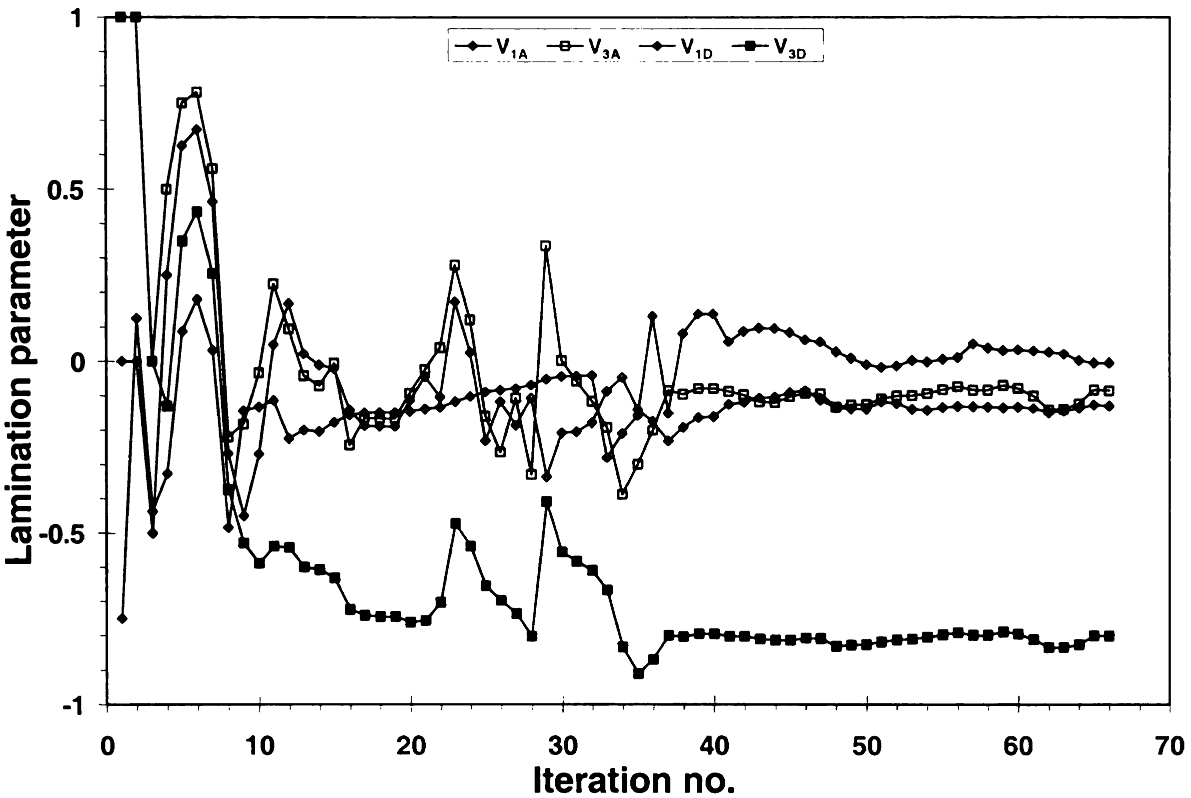

Figure 6–4 Histories of laminate-property design variables – FRP Shell 1

After the optimal laminate properties represented by lamination parameters were achieved, the optimal design of the laminate by fiber orientations and stacking sequence was carried out to achieve the optimal properties. The genetic algorithm optimization process included 10,000 generations and each of them had a population of 50 individuals.

The second-level optimization history is presented in Figure 6–5. Genetic-based optimization algorithms can lead to multiple designs that satisfy the optimization criteria. Thus, multiple optimal designs of laminates were found with the optimal laminate properties derived in the first optimization. The optimal laminate designs, with corresponding lamination parameters within an error of 1% compared to the optimal lamination parameters obtained in the first-level optimization, are listed in Table 6–1. It should be further noted that all optimal laminates have several common laminas with the same fiber orientations arranged in the same stacking sequence.

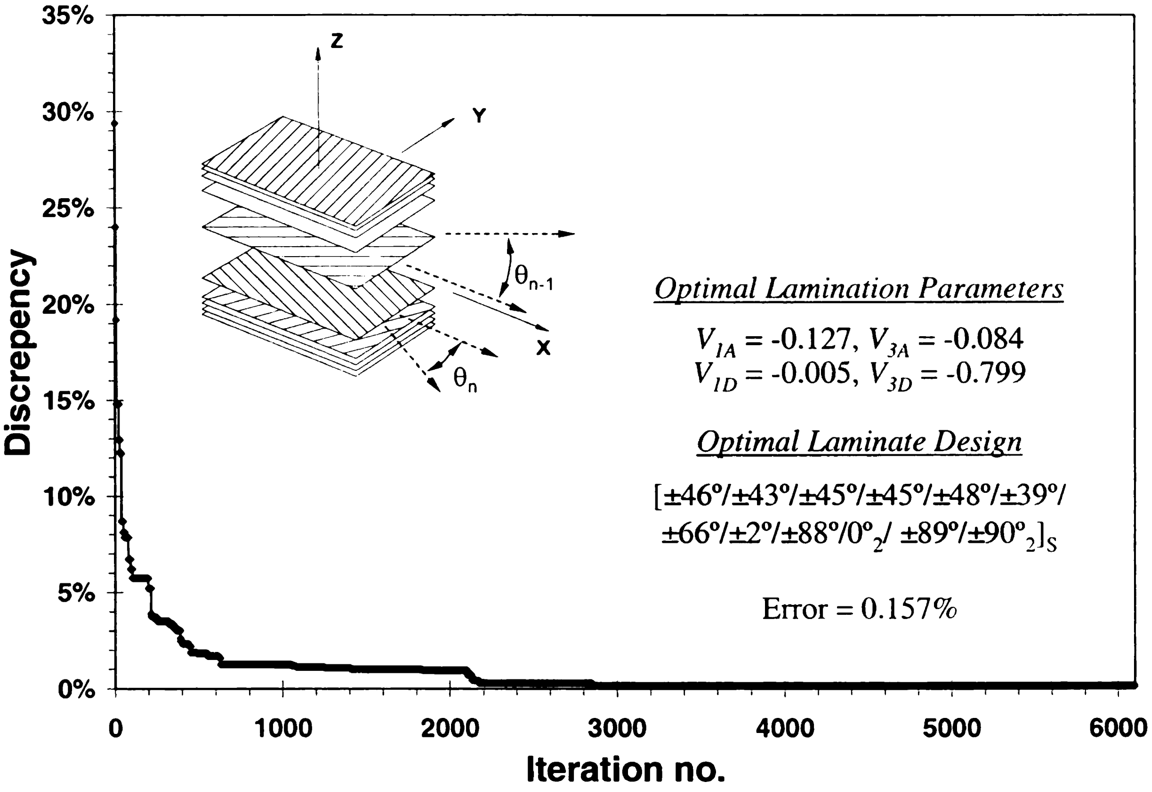

Figure 6–5 Second-level optimization process – FRP Shell 1

Table 6–1 Optimal laminate designs of FRP shells

Laminate designs	Error
$[\pm 46/\pm 43/\pm 46/\pm 45/\pm 39/\pm 47/\pm 66/\pm 2/\pm 88/0_2/90_2/\pm 87]_S$	0.610%
$[\pm 46/\pm 43/\pm 46/\pm 45/\pm 46/\pm 39/\pm 66/\pm 2/\pm 88/0_2/\pm 89/\pm 87]_S$	0.445%
$[\pm 46/\pm 43/\pm 46/\pm 45/\pm 46/\pm 39/\pm 66/\pm 2/\pm 88/0_2/90_2/\pm 87]_S$	0.427%
$[\pm 46/\pm 43/\pm 46/\pm 45/\pm 46/\pm 39/\pm 66/\pm 2/\pm 88/0_2/\pm 89/90_2]_S$	0.300%
$[\pm 46/\pm 43/\pm 46/\pm 45/\pm 46/\pm 39/\pm 66/\pm 2/\pm 88/0_2/90_2/90_2]_S$	0.287%
$[\pm 46/\pm 43/\pm 45/\pm 45/\pm 48/\pm 39/\pm 66/\pm 2/\pm 88/0_2/\pm 89/90_2]_S$	0.157%

6.2 Shape-only optimized laminated FRP shells

The optimum result above (Shell 1) is compared to the shape optimization of two laminated FRP shells (Shell 2 and Shell 3) with constant material properties. These two shells have the same geometry and loading of the shell analyzed in the previous example.

The geometric design variables used here were the same as before, see Figure 6–1. Guided by the experiments of hanging models [Ramm et al., 2000], two laminate designs were chosen. Shell 2 used a $[45°/-45°/-45°/45°]_{6S}$ laminate with the lamination parameters $\{V_{1A}, V_{3A}, V_{1D}, V_{3D}\}=\{0, -1, 0, -1\}$ while Shell 3 used a [0°/90°/90°/0°] laminate with the lamination parameters $\{V_{1A}, V_{3A}, V_{1D}, V_{3D}\}=\{0, 1, 0.75, 1\}$. Therefore, the laminate-property design variables of the lamination parameters determining the stiffness matrix of each shell are constant throughout the optimization procedure. The optimization process histories for Shell 2 and Shell 3 are presented in Figure 6–6 and Figure 6–7, and Figure 6–8 and Figure 6–9, respectively. It should be noted that the obtained optimal shapes for the two shells using different laminate designs are different (see Table 6–2), although the initial shapes were the same.

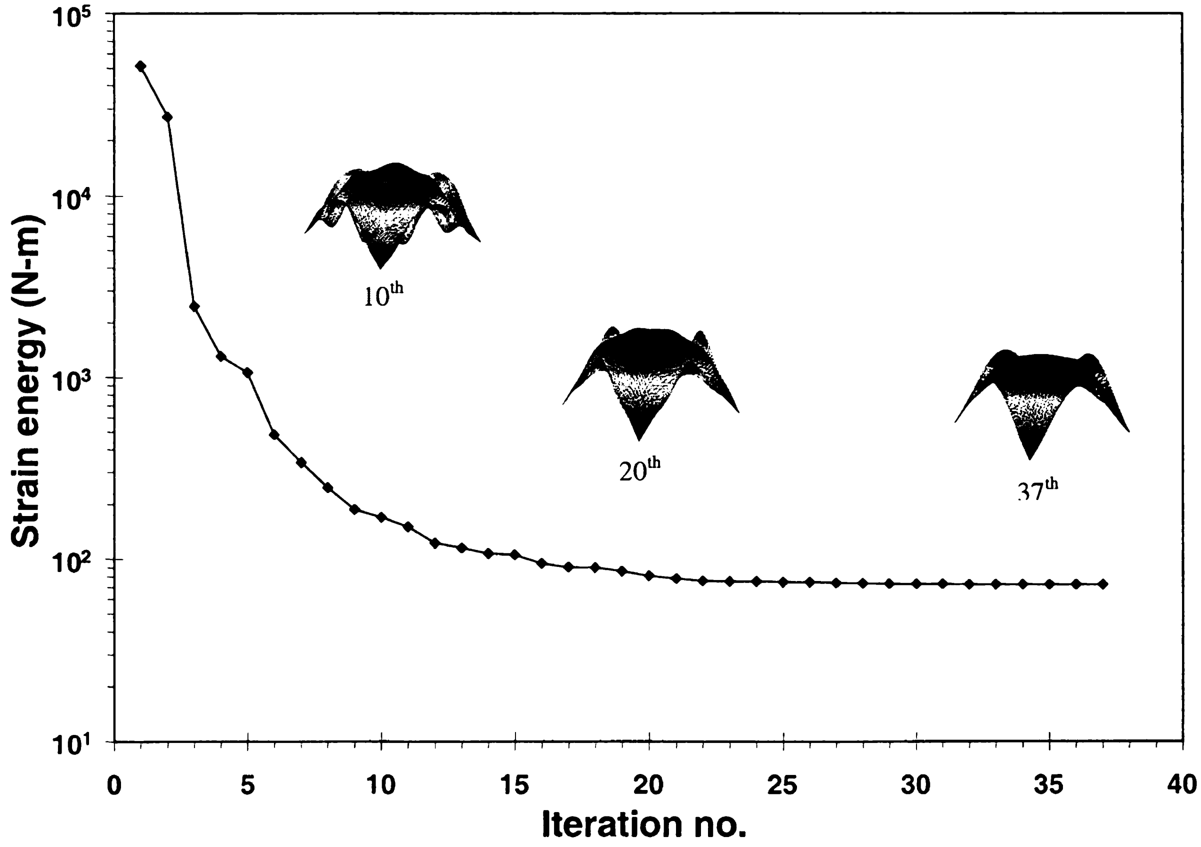

Figure 6–6 History of objective function – FRP Shell 2: $[45°/-45°/-45°/45°]_{6S}$

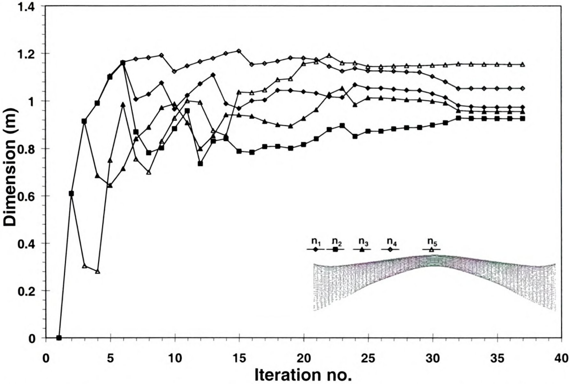

Figure 6–7 Histories of geometric design variables – FRP Shell 2: [45°/-45°/-45°/45°]$_{6S}$

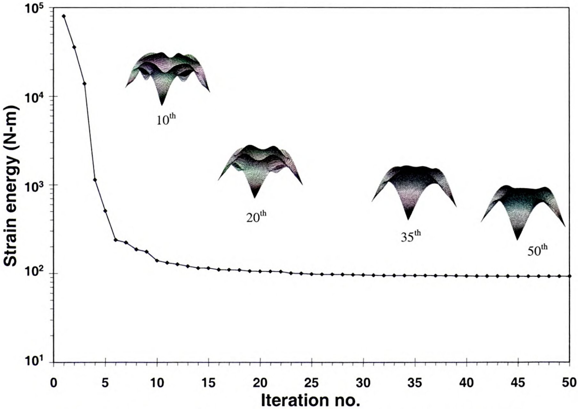

Figure 6–8 History of objective function – FRP Shell 3: [0°/90°/90°/0°]

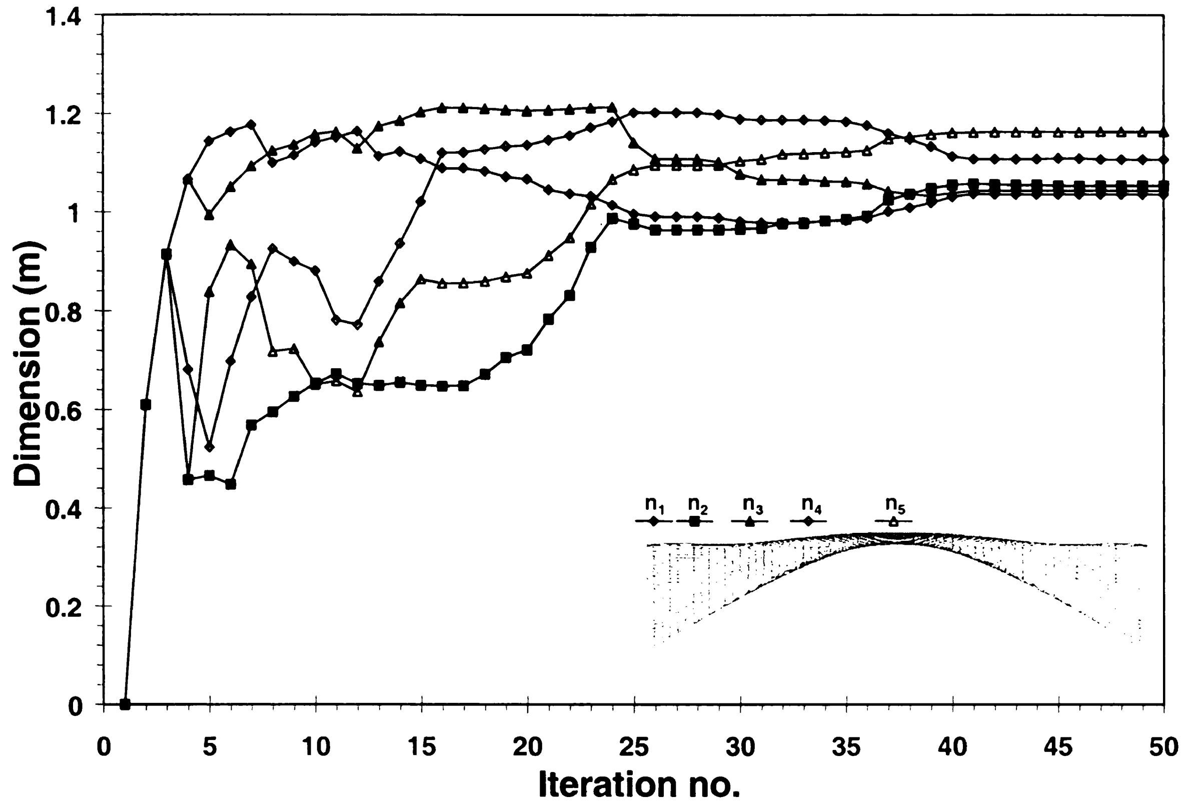

Figure 6–9 Histories of geometric design variables – FRP Shell 3: [0°/90°/90°/0°]

6.3 Comparison of three optimal shells

The structural response of all three optimal shells regarding strain energies, displacements and section resultants is summarized in Table 6–2 and Table 6–3, respectively.

Table 6–2 Summary of strain energies and displacements of optimal shells

	Optimal Shape	Strain Energy (N·m)	Max Deflection (mm)
Shell 1	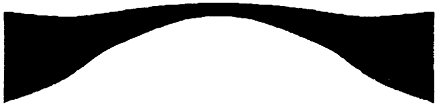	49.60	0.78
Shell 2	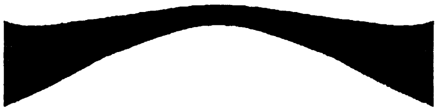	72.76	1.23
Shell 3	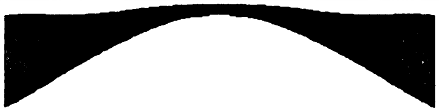	92.98	1.59

According to Table 6–2, the optimal shell obtained through the shape and laminate optimization (Shell 1) has the maximum structural stiffness, that is, the smallest vertical displacement and the smallest strain energy among all three shells. Shell 2, constructed by the laminate of $[45°/-45°/-45°/45°]_{6S}$, was found to be better than Shell 3, constructed by the laminate of [0°/90°/90°/0°] with respect to the structural stiffness.

The inherent nature of shape optimization for membrane structures and thin shells is to minimize bending stresses thus ensuring in-plane only response. Achievement of this objective was evaluated by comparing the section resultants between initial and optimal structures for all three shells. As shown in Table 6–3, the bending moments are reduced significantly after the optimization process. Meanwhile, membrane compressions are developed in all three optimal shells compared to the zero in-plane response of the initial structures. Contours of the force (SF1) and moment (SM1) section resultants (see Figure 6–10 for element axis orientation) are also compared for the initial and optimal structures in Figure 6–11. Figure 6–11 makes evident that bending behavior is minimized while the in-plane behavior becomes dominant. Additionally the results in Figure 6–11 show that the section resultants seek to be uniformly distributed throughout the entire structure.

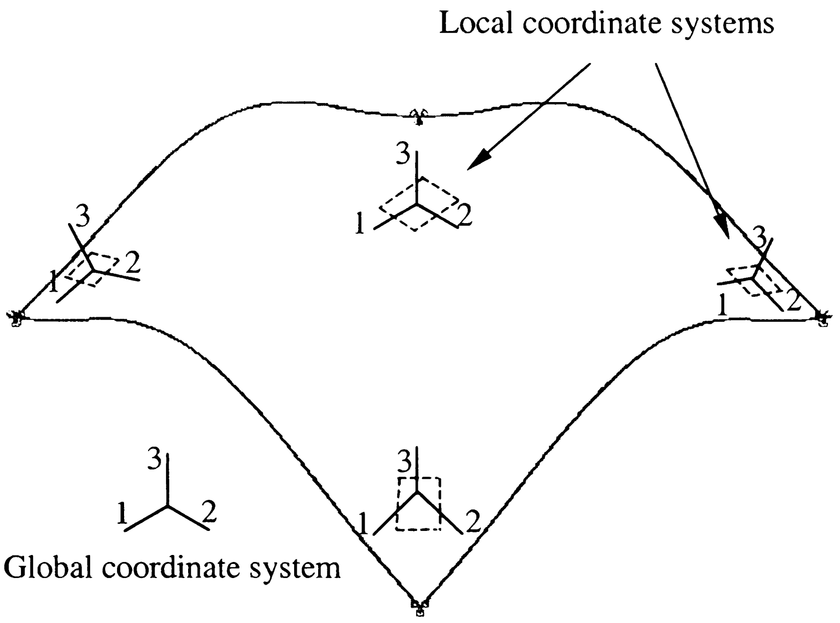
Local coordinate systems
3
1
2
3
1
2
3
1
2
3
1
2
3
1
2
Global coordinate system

Figure 6–10 Global and local coordinate systems

Table 6–3 Summary of structural responses of initial and optimal shells

		Shell 1		Shell 2		Shell 3	
		Initial	Optimum	Initial	Optimum	Initial	Optimum
SF1	Max	≈0	235.195	≈0	192.815	≈0	412.599
(kN/m)	Min	≈0	-744.289	≈0	-755.147	≈0	-820.294
SF2	Max	≈0	241.325	≈0	192.990	≈0	415.226
(kN/m)	Min	≈0	-945.860	≈0	-953.566	≈0	-1012.41
SM1	Max	-0.287	0.329	108.288	0.395	123.407	0.355
(kN·m/m)	Min	-24.957	-0.368	-24.932	-0.283	-64.117	-0.171
SM2	Max	-0.158	0.298	108.288	0.387	114.982	0.195
(kN·m/m)	Min	-54.077	-0.478	-24.932	-0.358	-41.885	-0.067

SF1, SF2: Direct membrane force per unit width in local 1-, 2-axis of elements

SM1, SM2: Bending moment force per unit width about local 2-, 1-axis of elements

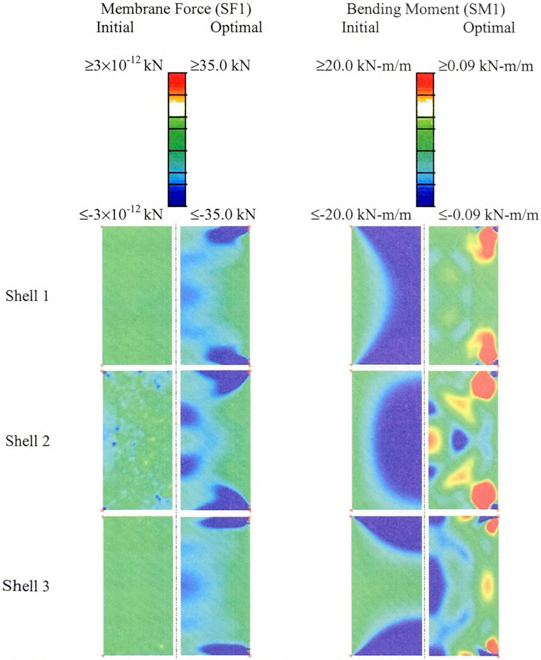

SF1: Direct membrane force per unit width in local 1-axis of elements
SM1: Bending moment force per unit width about local 2-axis of elements

Figure 6–11 Structural responses of initial and optimal shells

Images in this thesis/dissertation are presented in color.

It should be noted that stress leveling within the shell is not an optimization criterion to achieve maximum structural stiffness. For example, the shape-and-material optimal shell (Shell 1) attained the minimum strain energy and had the lowest membrane force and highest bending moment specific values (i.e., value at a given location) than the other two shape-only optimal shells. However, this does not conflict with the objective to minimize the strain energy of the entire structure by reducing bending moments. The in-plane structural performance can be best evaluated by comparing the stress-state in individual elements, which are summarized in Table 6–3. Thus, as shown in Figure 6–12, 90% of Shell 1 is subject to membrane forces ranging between -45 and 0 kN/m, compared to 79% and 84% for Shell 2 and Shell 3, respectively. The efficiency of Shell 1 is more obviously shown in Figure 6–13 regarding the bending moment SM1. Thus, although Shell 3 has the smallest range of bending moments among all three optimal shells, only 32% of Shell 3 is subject to bending moments of small magnitude, i.e., between –30 and 30 kN·m/m, compared to 74% and 47% for Shell 1 and Shell2, respectively.

According to the analyses described above, the stiffness of bending structures is in fact improved by achieving the objective of minimizing the structure's strain energy. In addition, the structural performance of laminated FRP shells can be further enhanced by the integration of shape and material optimization. Therefore, the shape and material objective function of minimizing strain energy leads to structural geometries and material properties that are dominated by in-plane response with minimum bending demands.

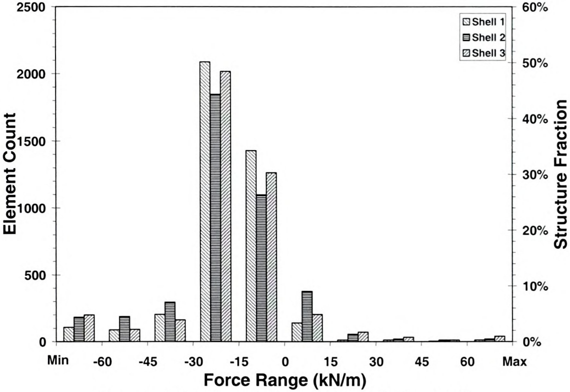

Figure 6–12 Membrane force distribution of optimal shells

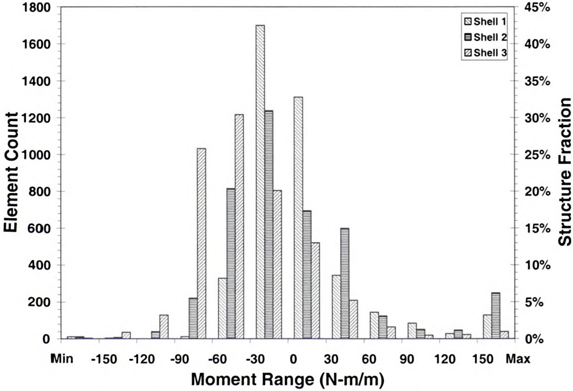

Figure 6–13 Bending moment distribution of optimal shells

6.4 Buckling analyses of optimized laminated FRP shells

As it is well known, shape-resistant structures carry their design loads primarily by axial or membrane action, rather than by bending action. When subjected to compression forces as in the case of shells, these stiff thin structures are sensitive to buckling. Considering that a structural stability criterion was not implemented in the presented integrated optimization approach, the structural buckling performance was evaluated and compared among the optimized shells.

Eigenvalue buckling analyses are generally used to provide useful estimates of the critical buckling loads and collapse mode shapes of stiff structures. To evaluate the buckling response of the optimized shells, the unloaded optimal shells are chosen as the base state and buckling loads are calculated relative to the base state of the structure. The optimization load-generating load case of 6.9 kN/m^2 applied in the gravity direction is used gain to introduce the linear perturbation. The subspace iteration extraction method is used to explore the eigenvalues and eigenvectors of the first five buckling modes. The results for Shell 1, Shell 2, and Shell 3 are summarized in Table 6–4, Table 6–5, and Table 6–6, respectively.

As judged by the values for the first buckling eigenvalue given in Table 6–4 through Table 6–6, structural buckling capability is improved by the shape and FRP laminate optimization along with maximizing structural stiffness. The general-optimized shell (Shell 1) has the highest buckling capacity ($\lambda_1^1 = 8.05$), compared to Shell 2 ($\lambda_1^2 = 4.29$) and Shell 3 ($\lambda_1^3 = 3.49$). On the other hand, although the buckling mode shapes vary significantly in character, it can be seen that the first three eigenvalues are closely spaced. The series of closely spaced eigenvalues indicates that the optimized shells are imperfection sensitive. In addition, the smaller spacing of eigenvalues for Shell 1 further implies Shell 1 is more buckling-sensitive compared to Shell 2 and Shell3. Therefore, it can be concluded that a stiffer structure will increase buckling resistance but suffer from higher buckling sensitiveness.

Table 6–4 Buckling analyses of Shell 1

Mode	Eigenvalue	Buckling shapes Side view Axis 1-3	 Side view Axis 2-3
Base State	-	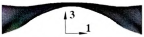	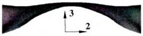
1	8.05	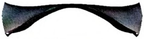	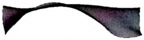
2	8.06	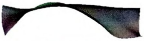	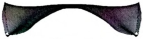
3	8.88	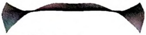	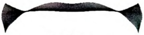
4	13.38	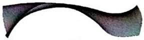	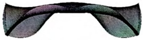
5	13.49	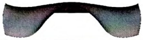	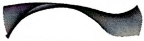

Table 6–5 Buckling analyses of Shell 2

Mode	Eigenvalue	Buckling shapes Side view Axis 1-3	 Side view Axis 2-3
Base State	-	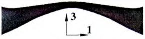	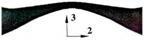
1	4.29	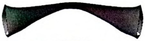	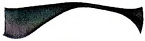
2	4.37	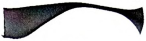	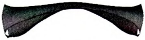
3	4.82	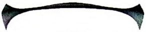	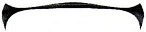
4	6.70	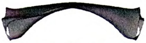	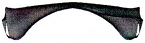
5	9.46	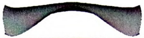	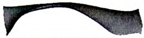

Table 6–6 Buckling analyses of Shell 3

Mode	Eigenvalue	Buckling shapes (eigenvectors) Side view Axis 1-3	 Side view Axis 2-3
Base State	-	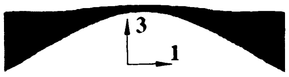	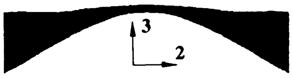
1	3.49	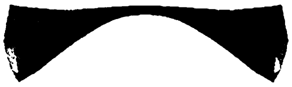	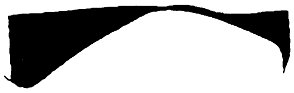
2	3.53	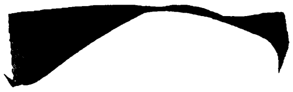	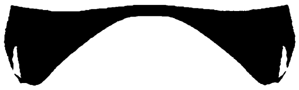
3	3.64	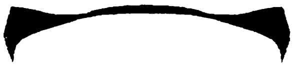	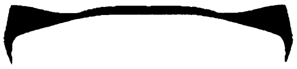
4	4.63	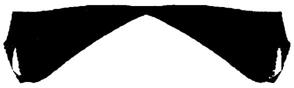	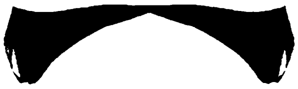
5	11.55	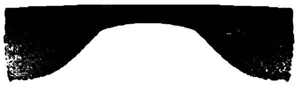	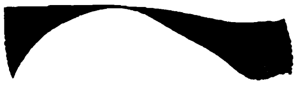

6.5 Summary

In this chapter, the optimization procedure of the integrated approach was evaluated and validated by optimizing FRP shells. It was illustrated in the comparison of a general-optimized shell and shape-only optimized FRP shells that the structural performance of a shape resistant structure can be improved by using FRP laminates with optimized material design. Stability evaluation of the optimized shells showed that buckling capacity should be an essential constraint of the integrated approach for shape resistant structures subject to compression.

References

Hibbitt, Karlsson & Sorensen, Inc. (2001). ABAQUS standard user's manual Version 6.2.

Isler, H. (1991). Generating shell shapes by physical experiments, IASS Bulletin: 34, 53-63.

Isler, H. (1994). Concrete shells derived from experimental shapes. Structural Engineering international: 3, 142-147.

Ramm, E., (1992). Shape finding methods of shells. IASS Bulletin: 33, 89-99.

Ramm, E., Kemmler, R. and Schwarz, S., (2000). Form finding and optimization of shell structures, In: Proc IASS-ICAM 2000. Fourth International Colloquium on Computation of Shell and Spatial Structures: Chania-Crete, Greece.

Ramm, E. and Mehlhorn G., (1991). On shape finding methods and ultimate load analysis of reinforced concrete shells. Engineering Structures:13, 178-198.

7 FRP Composite Membrane-Based Bridge Systems

Laminated FRP composites have been widely applied in strengthening and rehabilitating aging bridge systems and proved to be efficient. However, the application of laminated FRP composites for an entire structure is still limited. Although technical advances in manufacturing FRP composites have significantly reduced the manufacturing cost, their high material cost and the lack of proven design philosophies compared to conventional materials still confines the use of laminated FRP composites in primary structural components of bridge systems. However, the use of FRP composites in conjunction with conventional structural materials has shown that technical efficiency can be achieved within competitive economical constraints [Burgueño, 1999; Seible et al., 1999]. Furthermore, it was proved that the use of the high in-plane strength and stiffness of FRP composites can be maximized by material-adapted concepts of employing shape resistant structures of membrane/shells. Therefore, FRP composites membrane-based bridge systems are proposed as analytical studies for the application of laminated FRP composites in bridge systems.

The use of optimized laminated FRP composites in bridge systems is conceptualized in two bridge designs that can effectively employ the in-plane stiffness of FRP laminates. Both bridge types consist of a laminated FRP membrane together with a conventional reinforced concrete deck, in which the laminated FRP membrane provides the in-plane strength and the concrete deck provides the live load transfer and resists the majority of the compression forces. The developed optimization approach will be implemented and evaluated through analytical studies on these two types of FRP membrane-based bridges.

7.1 FRP composite membrane beam (CMB) bridges

Based on the concept of girder-slab bridges, an FRP Composite Membrane Beam (CMB) bridge (Figure 7–1) is considered as a case study for the proposed optimization approach. Because of the high stiffness provided by double-curvature surfaces, the system uses a hyperbolic paraboloid laminated membrane working compositely with a conventional reinforced concrete deck as schematically shown in Figure 7–1. The proposed system behavior is such that the FRP laminate is to carry the in-plane tensile and shear forces while the concrete deck carries the compressive force. The developed shape and FRP laminate optimization approach was thus used to obtain the optimal shape and laminate design of the membrane element for the CMB bridge system.

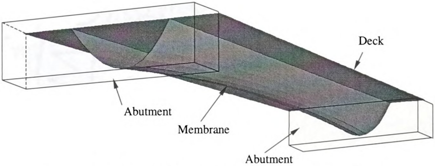

Figure 7–1 Composite membrane beam (CMB) bridge

7.1.1 Bridge system description

The proposed CMB Bridge for optimization studies is a 10.06 m long simple-span bridge girder with a 2.44 m wide compression flange (Figure 7–2). The flange is a 203.2 mm thick concrete deck with a density of 2402.8 kg/m^3. In order to reduce difficulties of finite element modeling, the abutments were not modeled in the finite element analyses. Rather, the abutment stiffness was taken into account in the computational model by constraining the plane section motion that it imposes on the rotations and displacements at both ends of the bridge (Figure 7–2). The laminates used in the CMB bridge systems are assumed to be from medium-performance carbon/epoxy FRP lamina, of which the lamina orthotropic properties are taken as: E_{11} = 88.253 GPa, E_{22} = 48.884 GPa, G_{12} = 4.557 GPa, G_{13} = 4.557 GPa, G_{23} = 0.456 GPa, and ν_{12} = 0.513.

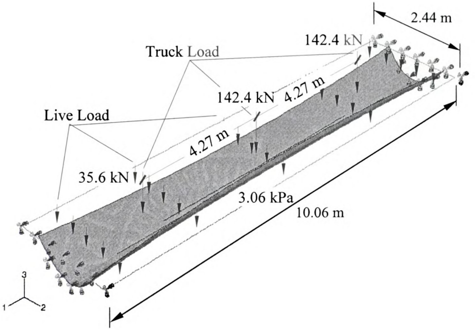

Figure 7–2 Computational model of the CMB bridge

Table 7–1 Load case specification for CMB bridge optimization

Limit State	Load Case Specification	Design Criteria	
		Stress	Deflection
Optimization	1.0×DL + 1.0×LL	$0.05\sigma_u$	-
Service	1.0×DL + 1.0×(LL + 1.33×TL)	$0.25\sigma_u$	L/800
Strength	1.25×DL + 1.75×(LL + 1.33×TL)	$0.50\sigma_u$	-

According to the AASHTO Bridge Design Specification [AASHTO, 1998], the simple-span CMB bridge is to be designed to load combinations that include dead load (DL), live lane load (LL) and concentrated loads from a three-axle truck (TL). The design

lane load consists of a uniformly distributed pressure of 3.06 kPa over each lane while the design truck load consists of three concentrated loads spaced at 4.27 m (Figure 7–2). The load case used in the integrated optimization procedure takes into account the dead and uniform live load with unit, or service load factors (Table 7–1). In addition to the optimization load case, the service and strength load cases (Table 7–1), in which the loads are combined with different load factors also need to be considered [AASHTO, 1998]. The influence of these two load cases on the optimal CMB bridge design was studied through post optimality analyses.

Two design criteria, namely stress and deflection are used for the CMB bridge designs. The stress criterion chooses a percentage, or stress index, of ultimate material failure for each limit state. The prediction of the ultimate material failure varies with different failure stress criteria, which define different failure surfaces surrounding the origin in three-dimensional space $\{\sigma_{11}, \sigma_{22}, \sigma_{12}\}$. The stress index is used to measure the proximity to the failure surface. The material failure determinations by different stress criteria are all depended on the stress limits of the individual lamina measured along the material directions. Following knowledge gained through experiments on carbon/epoxy FRP laminates, 1% and 0.5% of the Young's modulus of the corresponding direction respectively are commonly used as the tensile and compressive stress limits, while 0.5% of the shear modulus was chosen as the shear limit. Therefore, the tension and compression stress limits along the 1-axis (fiber-longitudinal direction) and 2-axis (fiber-transverse direction) were chosen to be: $X_T = 0.883$ GPa, $X_C = -0.442$ GPa and $Y_T = 0.489$ GPa, $Y_C = -0.244$ GPa, respectively, and the shear stress limit in the 1-2 plane was taken as $S = 22.9$ MPa.

In addition, the maximum structural deflection of L/800 [AASHTO, 1998] was chosen as another design criterion for the service limit state. Although the AASHTO [1998] bridge design specifications recommend the deflection limit of L/800 to apply for live load only, this limit is used conservatively in this work together with the system dead load.

7.1.2 Integrated optimization of CMB bridges

Based on the above-mentioned geometry, properties, and loading of the CMB bridge system, the integrated optimization approach was applied to design CMB bridges by sequentially employing the shape and laminate-property optimization and the laminate design optimization procedures.

7.1.2.1 Shape and material-property optimization

The shape design variables for the CMB bridge are the width and depth of the FRP membrane at the middle (w_2, h_2) and ends (w_1, h_1) of bridge component (Figure 7–3). These variables are used to define the hyperbolic paraboloid shape of the membrane through a CAGD algorithm. The laminate design variables are the lamination parameters $\{V_{1A}, V_{3A}, V_{1D}, V_{3D}\}$ controlling the in-plane tension stiffness and out-plane bending stiffness.

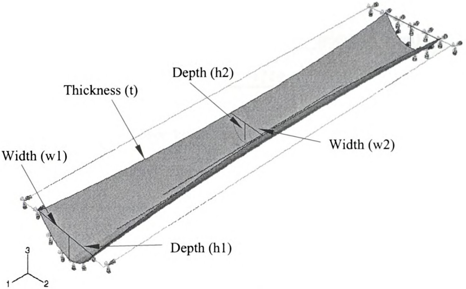

Figure 7–3 Geometric key points for CMB bridge shape optimization

It is well known that structural stiffness is improved when the amount of material increases. Therefore, the mass of materials needs to be constrained during shape optimization when the objective is maximizing structural stiffness. An inequality constraint, instead of using an equality constraint, is used to limit the mass of materials used in the structure. Considering that the geometry of the concrete deck remains constant during the optimization process, the material constraint is thus implemented by setting a lower and upper bound for the geometric design variables that are controlling the geometric dimensions and the thickness of laminated FRP composite (Table 7–2). Maximum stresses evaluated at the top and bottom surface of the laminate and the maximum deflection of the entire structure are two additional constraints taken into account in the structural design criteria for the integrated optimization procedure.

Table 7–2 Dimensional constraints for geometric design variables

Bound	w_1 (mm)	w_2 (mm)	h_1 (mm)	h_2 (mm)	t (mm)
Lower	609	609	609	305	6.35
Upper	2438	2438	1219	1219	19.05

The structural design achieved by an optimization process is normally obtained for a single load case. Due to the random nature of the truck loading position the optimization load case for the CMB bridge was taken as the combination of the dead load and live lane load with unit (service) factors (Table 7–1). This assumption was found to be conservative in the post optimality analyses (Section 7.2.4) as truck loading governs the demands in short-span bridges.

In the finite element analyses, the strains on the FRP laminates and concrete are expected to remain in the linear elastic range. Furthermore, the approximation of formulating the structure stiffness matrix in the reference (original) configuration is expected to have an error of 10^{-3} order compared to unity because of the small rotations and displacements under the loads. Thus, material linear elasticity and geometric linearity were used in the structural finite element analyses.

The stability of the proposed optimization approach was studied by searching for the optimal CMB bridge design from three different starting or initial designs. The initial designs considered are listed in Table 7–3. The optimization histories of the first-level shape and laminate-property optimization for the CMB bridges are shown in Figure 7–4 through Figure 7–12.

Table 7–3 Initial designs of CMB Bridges

Initial design	Model A	Model B	Model C
$\{w_1, w_2, h_1, w_2, t\}_{(\mathrm{mm})}$	{1625.6, 1016, 609.6, 609.6, 19.05}	{1625.6, 1016, 609.6, 609.6, 19.05}	{1219.2, 1219.2, 812.8, 508, 6.35}
$\{V_{1A}, V_{3A}, V_{1D}, V_{3D}\}$	{0,1,0.75,1}	{0,-1,0,-1}	{0,1,0.75,1}
Laminate Design	$[0°/90°]_S$	$[\pm 45°]_S$	$[0°/90°]_S$

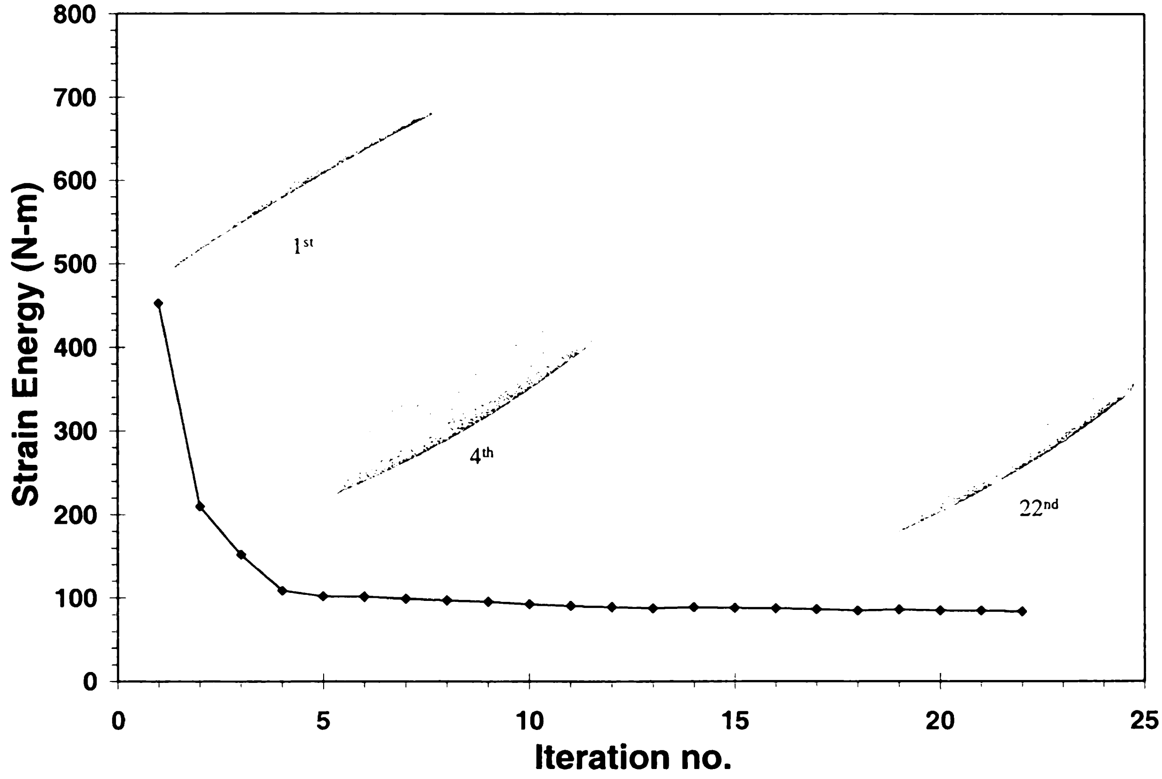

Figure 7–4 History of objective function – CMB Model A

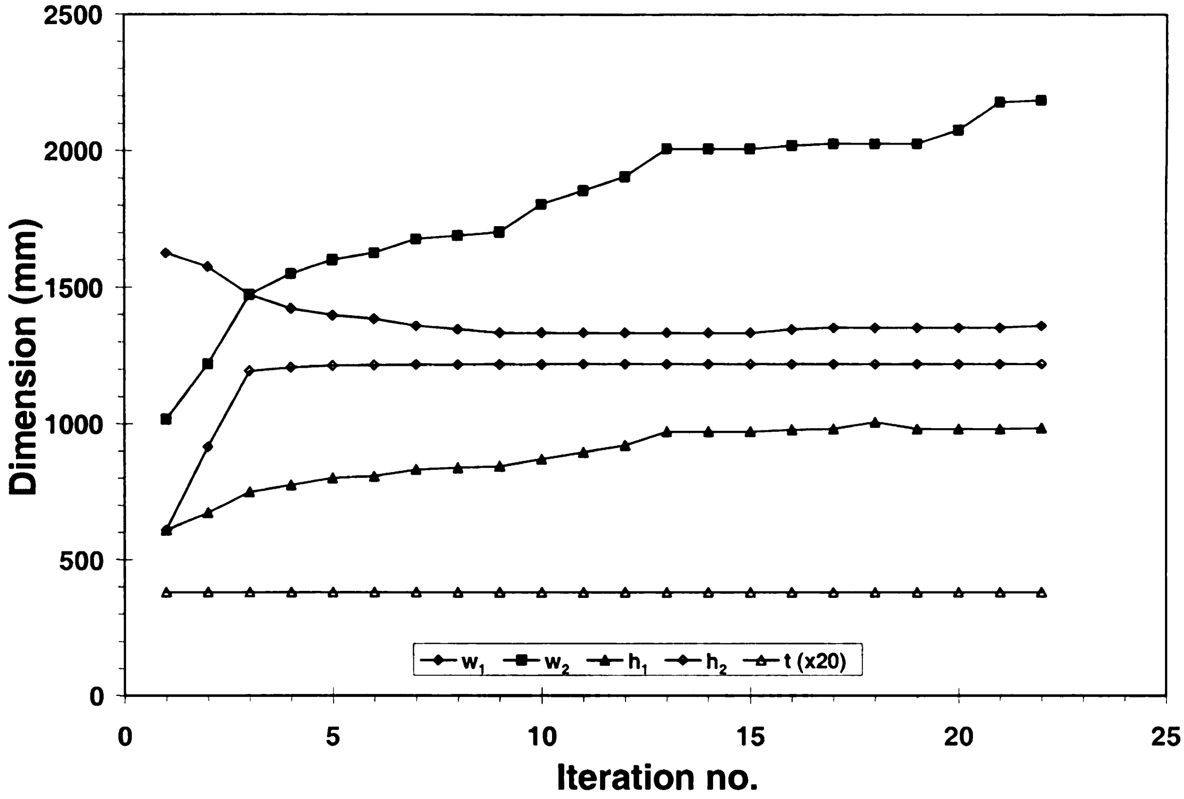

Figure 7–5 History of geometric design variables – CMB Model A

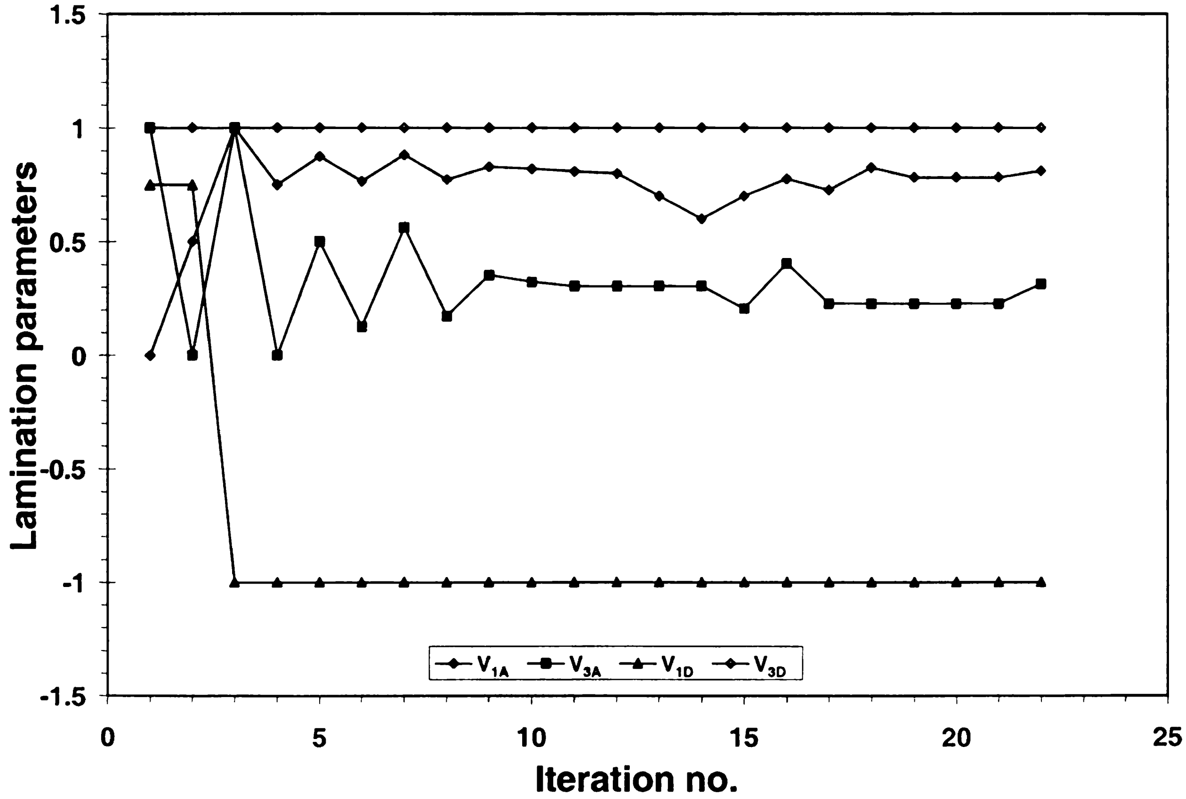

Figure 7–6 History of laminate-property design variables – CMB Model A

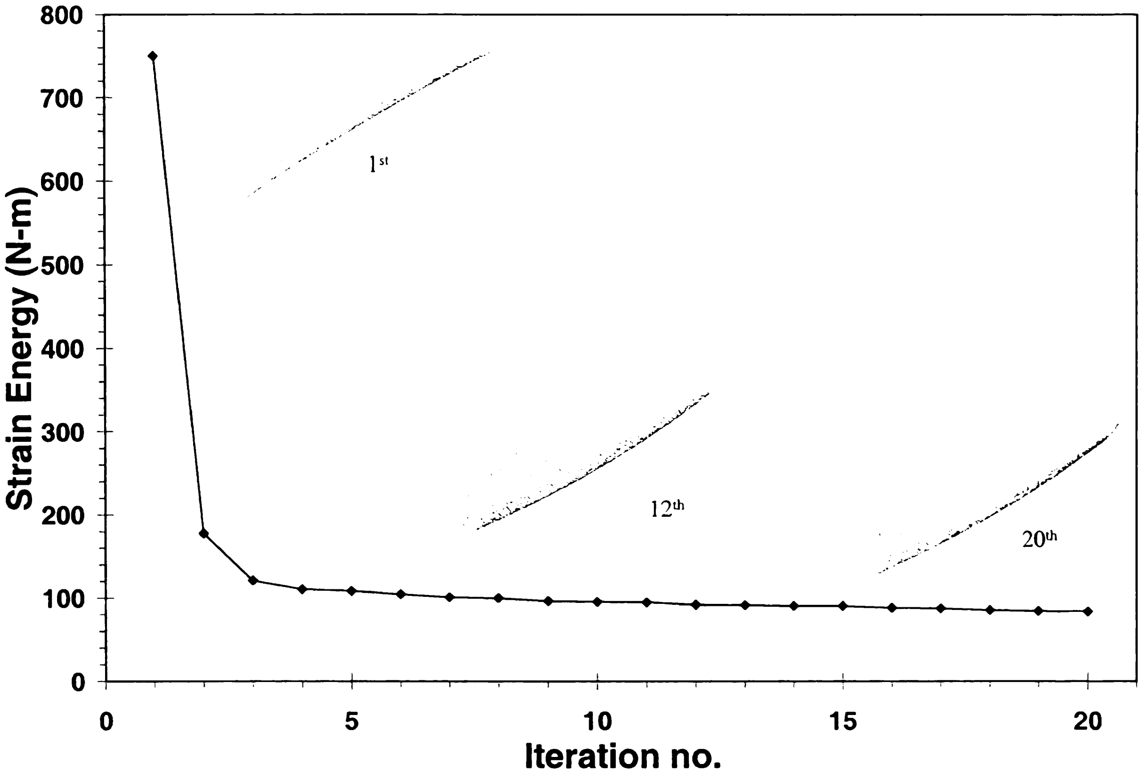

Figure 7–7 History of objective function – CMB Model B

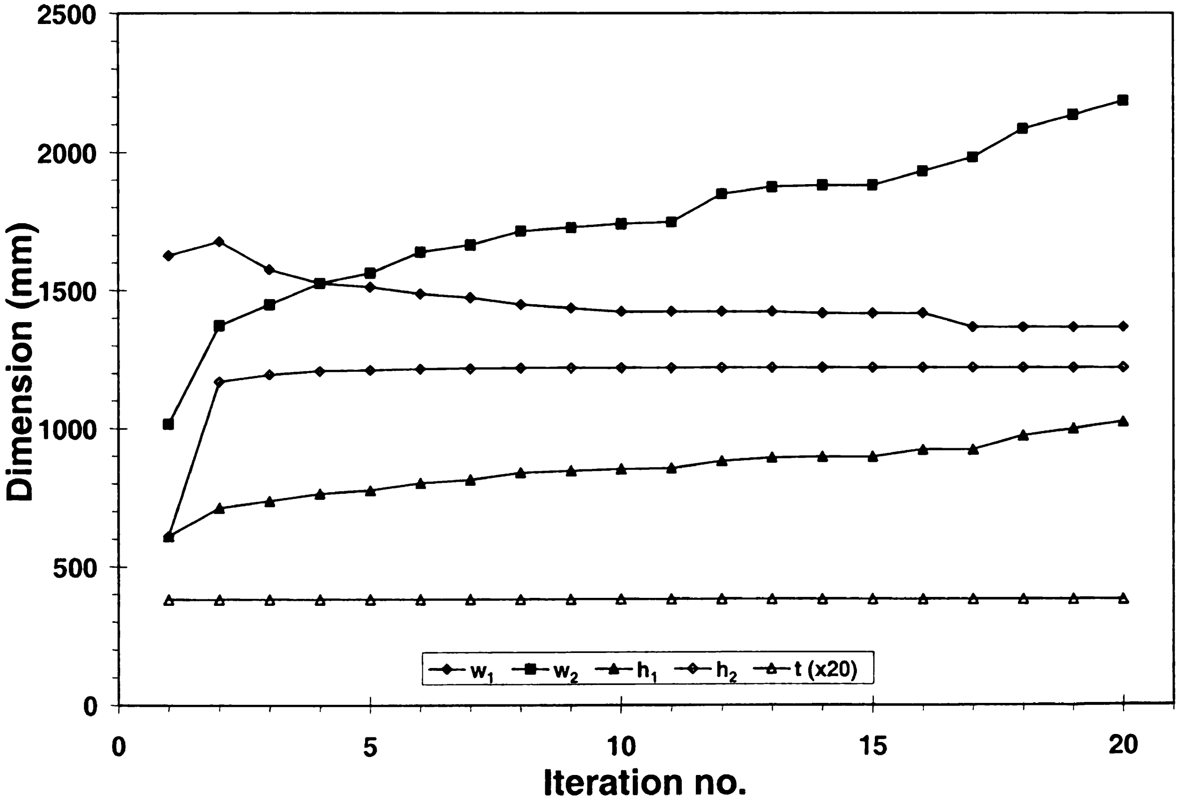

Figure 7–8 History of geometric design variables – CMB Model B

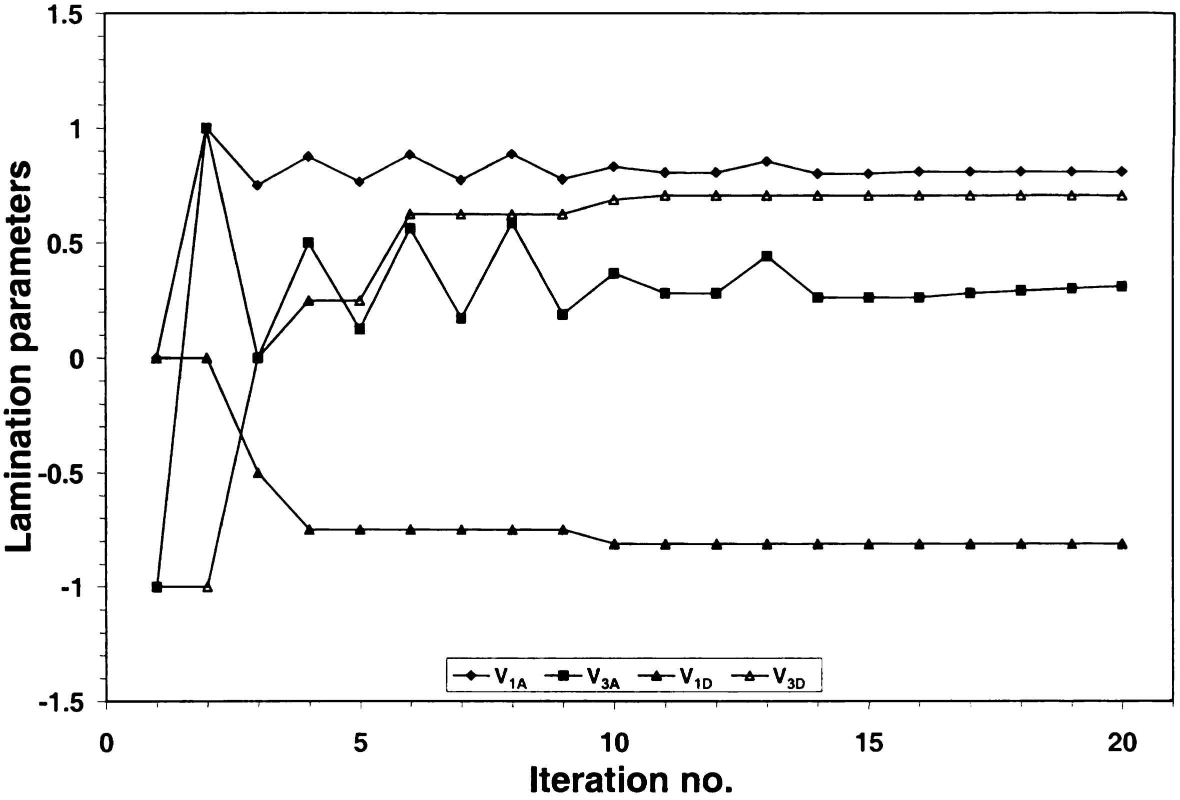

Figure 7–9 History of laminate-property design variables – CMB Model B

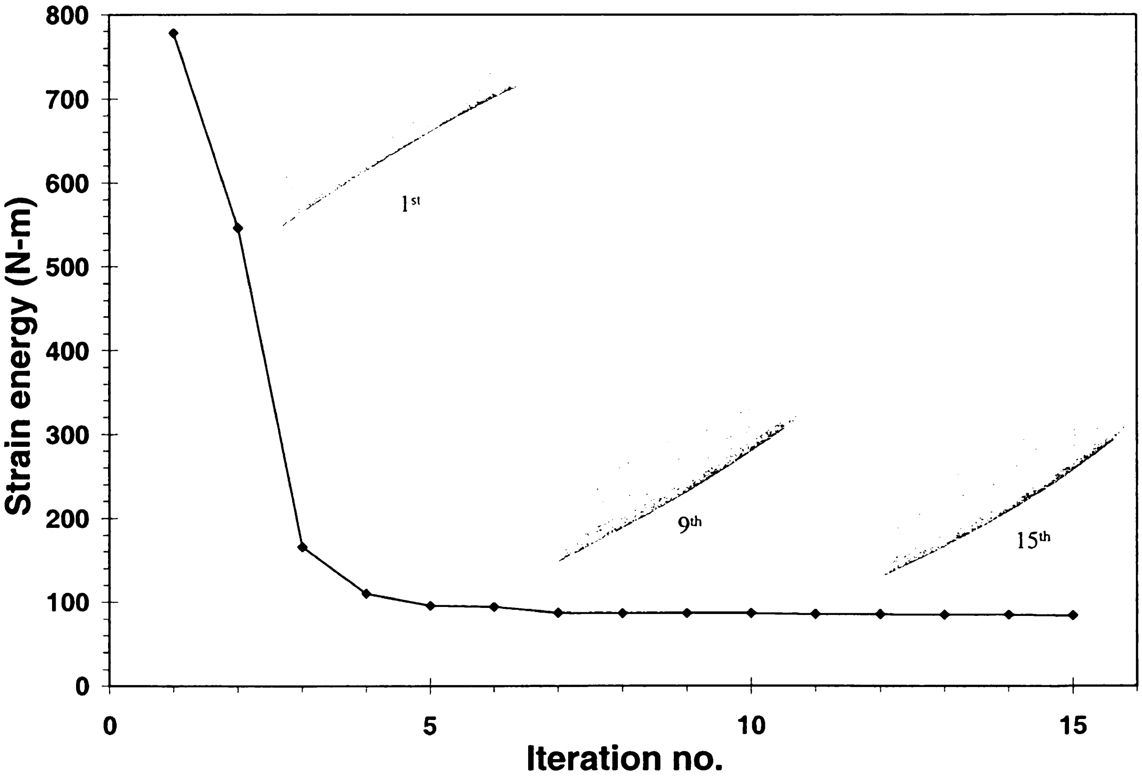

Figure 7–10 History of objective function – CMB Model C

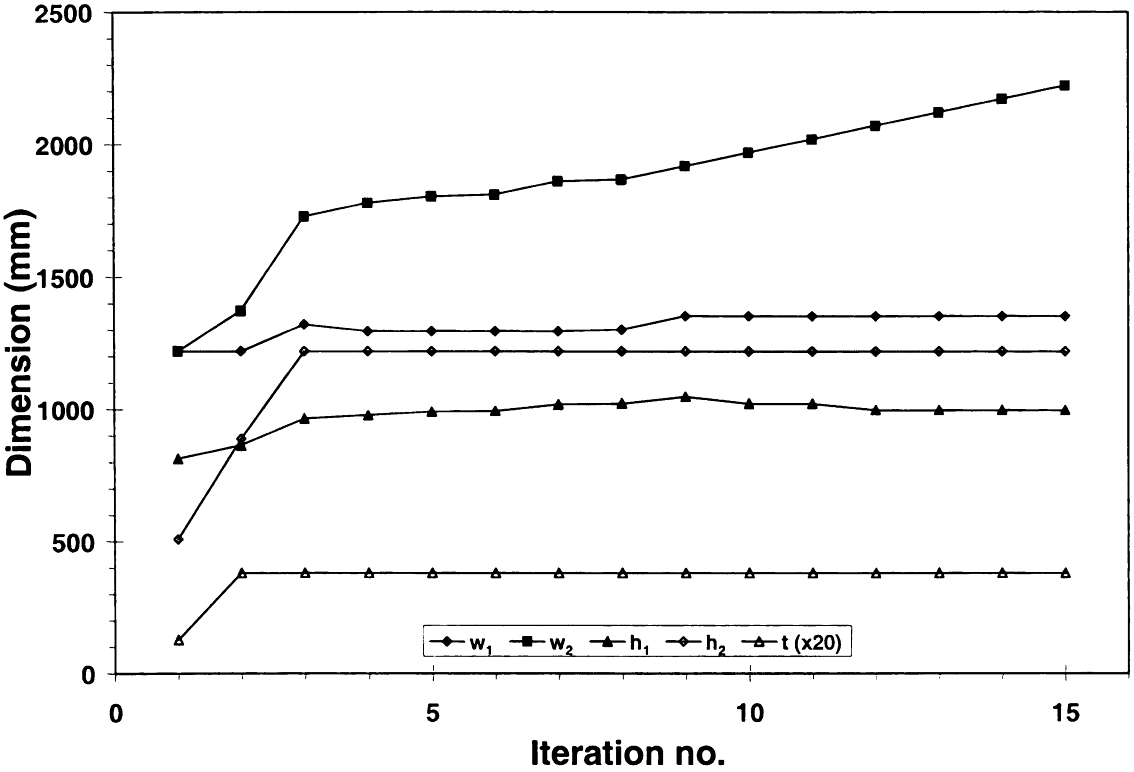

Figure 7–11 History of geometric design variables – CMB Model C

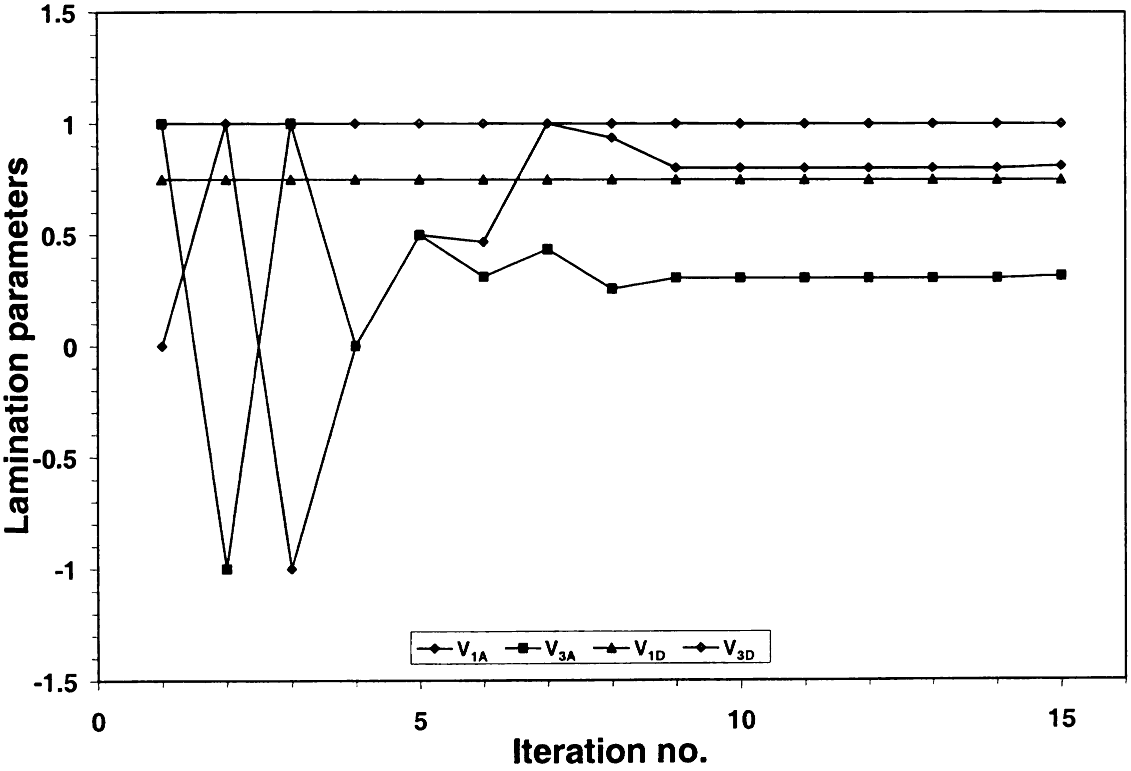

Figure 7–12 History of laminate-property design variables – CMB Model C

As summarized in Table 7–4, the shapes for all three CMB bridges (see Table 7–3) converged to a similar geometry with negligible differences. The optimization processes starting from three different initial attempts also resulted in the same in-plane lamination parameters (see Table 7–4). However, the out-plane lamination parameters were different.

Table 7–4 Optimum results of shape and material-property optimization

Optimal design	Model A	Model B	Model C
Strain Energy (N-m)	83.85	83.85	83.85
$\{w_1,w_2,h_1,w_2,t\}$ (mm)	{1359.0, 2184.4, 984.3, 1219.2, 19.05}	{1365.2, 2184.4, 1022.4, 1219.2, 19.05}	{1352.6, 2222.4, 997.0, 1219.2, 19.05}
$\{V_{1A},V_{3A},V_{1D},V_{3D}\}$	{0.81,0.31,-1,1}	{0.81,0.31,-0.8,0.7}	{0.81,0.31,0.75,1}

In fact, it was noted that the lamination parameters governing out-plane bending stiffness of membranes remain unchanged beyond certain iteration steps. This behavior does not significantly disturb the solution since the strain energy minimization process leads to a system dominated by in-plane stress resultants, i.e., bending resultants become negligible. Therefore, the out-plane lamination parameters, which determine the flexural stiffness, have a smaller influence on the optimization process when the structure becomes dominated by in-plane behavior.

7.1.2.2 Laminate design optimization

Assuming that only the in-plane lamination parameters govern the sectional stiffness of the FRP laminate, the optimal lay-up of the laminate can be solved by an alternate method presented by Gürdal et al. [1999]. This method allows finding the optimal lay-up for a 4-layer laminate with only two distinct orientation angles for a given volume fraction. By this method, the lay-up corresponding to the optimal section stiffness, which is defined by the optimal lamination parameters of $\{V_{1A}, V_{3A}\}=\{0.81, 0.31\}$ is found to be $[17°/19°]_S$. This result is later compared to the solution found by the developed laminate design optimization.

Symmetric and balanced laminates with certain number of distinct fiber orientations, which are defined by the design variables, were determined by the laminate design optimization process. In order to be able to compare the results with the previous optimal laminate design, optimal 8-layer symmetric and balanced laminates that have two distinct orientation angles were searched by the laminate design optimization algorithm. Furthermore, as it was discussed in Section 2.3, the bend-twist (D_{16} and D_{26} terms) coupling effect is minimized by increasing the number of plies in a symmetric and balanced laminate. Therefore, optimal 48-layer symmetric and balanced laminates (an arbitrarily selected large number of plies), which have twelve distinct fiber orientations, were also investigated.

In the second-level optimization, an optimal laminate is achieved by minimizing the difference of the lamination parameters of the searched laminates from the optimal lamination parameters derived from the first-level optimization. Therefore, the optimum criterion of the laminate design optimization is an allowable value of discrepancy. For the current research, a maximum error of 1% was considered acceptable for the optimum laminate design.

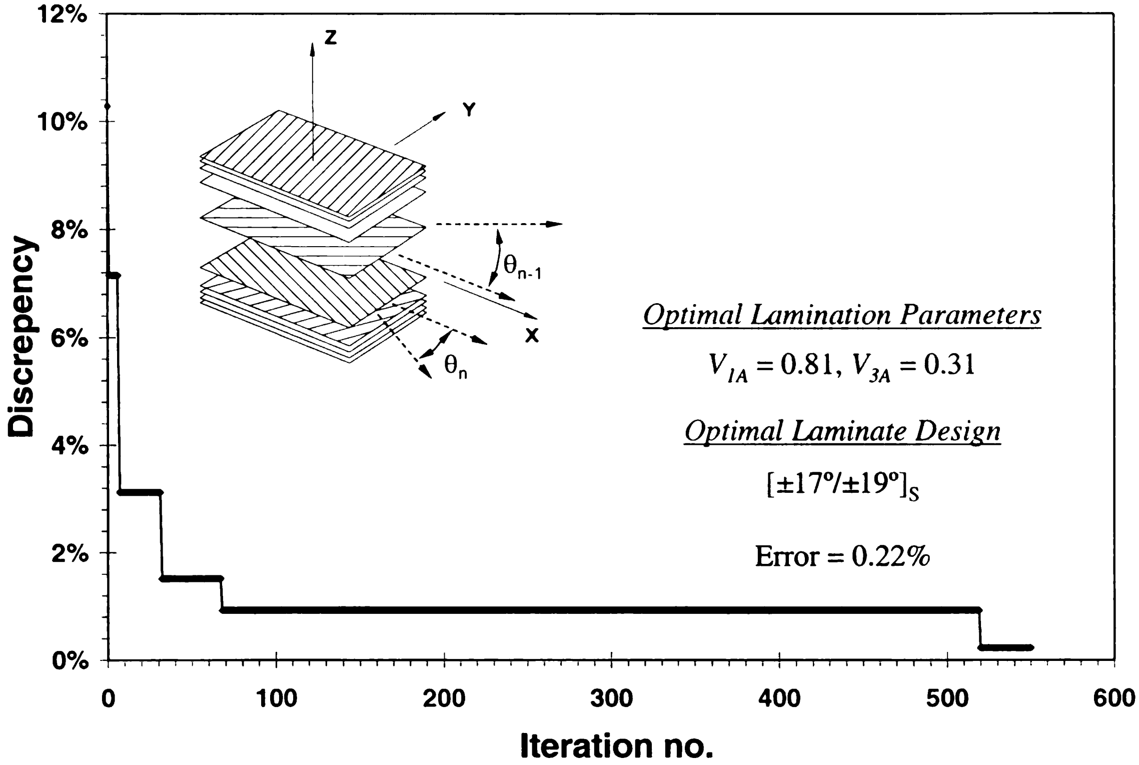

Figure 7–13 Laminate design optimization for 8-layer laminates

The optimal 8-layer laminate was found to be composed of $[\pm 17^\circ/\pm 19^\circ]_S$ with an error of 0.22% with respect to the optimal in-plane section properties from the first-level optimization. The resulting laminate design is thus the same as that previously obtained neglecting out-of-plane behavior through Gürdal et al.'s [1999] method. The optimization history of the objective function (lamination parameter error minimization) is shown in Figure 7–13. The optimal 48-layer symmetric and balanced laminate was found to be $[\pm 17^\circ/\pm 21^\circ/\pm 19^\circ/\pm 25^\circ/\pm 21^\circ/\pm 5^\circ/\pm 22^\circ/\pm 12^\circ/\pm 25^\circ/\pm 14^\circ/ \pm 17^\circ/\pm 12^\circ]_S$ with an error of 0.73%. Its optimization history is shown in Figure 7–14.

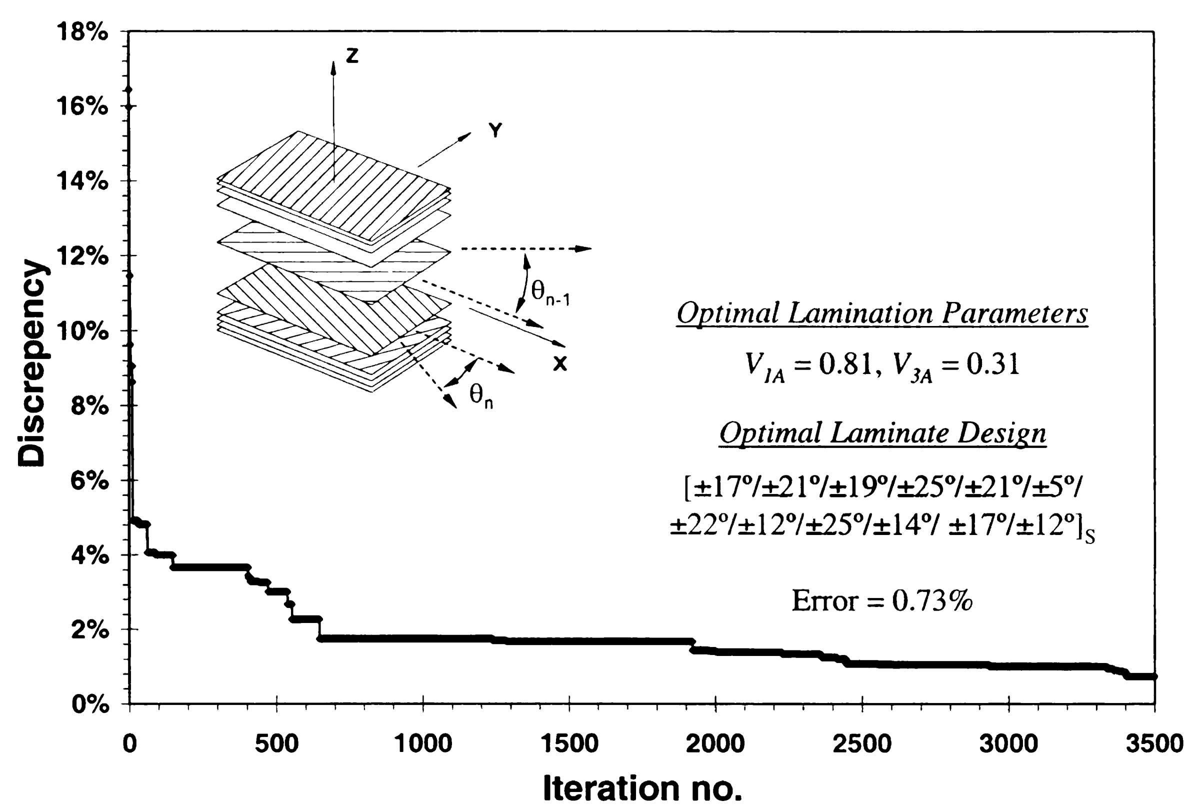

Figure 7–14 Laminate design optimization for 48-layer laminates

The lamination parameters and the section stiffness of the three optimal laminate are compared and summarized in Table 7–5. As shown in the table, all three optimal laminates have the same in-plane section properties and in-plane lamination parameters while the major terms of the out-of-plane section stiffness $\{D_{11}, D_{12}, D_{22}, D_{66}\}$ and the out-plane lamination parameters $\{V_{1D}, V_{3D}\}$ are only slightly different. However, the bend-twist coupling terms (D_{16} and D_{26}) of the out-plane stiffness are different for all three laminates. Thus, as expected, balanced and symmetric laminates have less bend-twist coupling effects than symmetric-only laminates. It also can be noted that the bend-twist coupling terms can be further reduced by increasing the distinct groups of balanced fiber orientations.

Table 7–5 Optimal laminates from laminate design optimization process

Optimal laminate		Lamination parameters $\{V_{1A}, V_{3A}, V_{1D}, V_{2D}, V_{3D}, V_{4D}\}$	A matrix (10^3 kN)	D matrix (kN-m)
4-layer	[17°/19°]s	{0.809, 0.308, 0.824, 0.566, 0.358, 0.933}	$\begin{bmatrix} 36.2 & 6.01 & 0 \\ & 20.7 & 0 \\ & & 6.98 \end{bmatrix}$	$\begin{bmatrix} 43.6 & 6.67 & 10.8 \\ & 25.0 & -4.41 \\ & & 7.91 \end{bmatrix}$
8-layer	[±17°/±19°]s	{0.809, 0.308, 0.824, 0.215, 0.358, 0.352}	$\begin{bmatrix} 36.2 & 5.96 & 0 \\ & 20.7 & 0 \\ & & 6.98 \end{bmatrix}$	$\begin{bmatrix} 43.6 & 6.67 & 4.07 \\ & 25.0 & -1.58 \\ & & 7.91 \end{bmatrix}$
48-layer	[±17°/±21°/±19°/±25°/ ±21°/±5°/±22°/±12°/ ±25°/±14°/±17°/±12°]s	{0.803, 0.310, 0.800, -0.037, 0.231, -0.056}	$\begin{bmatrix} 36.1 & 5.96 & 0 \\ & 20.8 & 0 \\ & & 6.98 \end{bmatrix}$	$\begin{bmatrix} 42.1 & 7.80 & -0.68 \\ & 24.4 & 0.23 \\ & & 8.93 \end{bmatrix}$

7.1.3 System characteristics of optimal CMB bridges

The system characteristics of the optimized CMB bridge systems were investigated by studying their structural behavior for the optimal load case and their buckling sensitivity. Due to the slight geometric variations existing in the optimum designs, the CMB bridge chosen for the system evaluation studies has a shape with average dimensions of the obtained optimal bridges (see Table 7–4). The optimal 8-layer laminate design is used for FRP membrane in system characteristic studies. The variations to the optimum design by using an average geometry and the 8-layer laminate with non-zero bend-twist coupling will be studied in post optimality analyses.

7.1.3.1 Structural behavior of optimal CMB bridges

As shown in Figure 7–4, Figure 7–7 and Figure 7–10, the optimal geometry of the FRP membrane is that of a hyperbolic paraboloid. A hyperbolic paraboloid is obtained by translating a parabola along the longitudinal direction of another parabola. This shape obviously follows as a direct consequence of the moment diagram of the loaded CMB bridge to assure in-plane behavior of the FRP membrane.

The results illustrated in Table 7–6 and Table 7–7 clearly show that the FRP membrane of the optimized CMB bridge is dominated by an in-plane stress-state by comparing the in-plane and out-of-plane section resultants. In addition, the FRP membrane also provides a shear force resistance, which reaches maximum values at both ends of the bridge structure. However, the bar chart in Figure 7–15 shows that 91% of the FRP membrane is subjected to longitudinal tension ranging from 0 kN/m to 133.9 kN/m, while only 9% of the membrane is subjected to longitudinal compressions with values les than 25 kN/m. Figure 7–16 reveals that the transverse section stress resultants of the FRP membrane due to the Poisson effect are mainly compression forces with values close to zero. The shear membrane force distribution shown in Figure 7–17 further indicates that the high level of shear forces is a local behavior and most of the FRP membrane is subjected to a low level shear forces, i.e., values close to zero. Therefore, the FRP membrane is primarily subjected to longitudinal tensile stresses rather than transverse stresses.

According to Table 7–6 and Table 7–7, although the concrete deck is subjected to higher out-of-plane section resultants than the FRP membrane, the concrete deck is still dominated by in-plane membrane forces. Furthermore, the deck is mainly subjected to longitudinal compression (Figure 7–15), which introduces a small level of transverse tension due to the Poisson effects (Figure 7–16). Therefore, the optimized FRP CMB bridge behavior is such that the FRP membrane carries the in-plane longitudinal tensile and shear forces while the concrete deck carries the compressive forces.

Table 7–6 Section forces for the optimal CMB bridge

Section Forces		SF1 (kN/m)	Min Max	SF2 (kN/m)	Min Max	SF3 (kN/m)	Min Max
Deck	Max	32.28	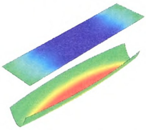	12.63	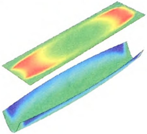	35.03	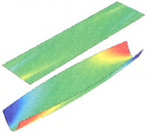
	Min	-105.16		-10.23		-35.06	
Membrane	Max	133.87		1.20		52.33	
	Min	-10.51		-13.79		-52.31	

SF1, SF2: Direct membrane force per unit width in local 1-, 2-axis of elements.
SF3: Shear membrane force per unit width in local 1-2 plane.

Table 7–7 Section moments for the optimal CMB bridge

Section Forces		SM1 (kN-m/m)	Min Max	SM2 (kN-m/m)	Min Max	SM3 (kN-m/m)	Min Max
Deck	Max	3.76	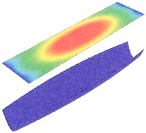	4.18	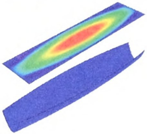	0.57	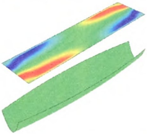
	Min	0.11		-0.43		-0.57	
Membrane	Max	0.15		0.06		0.02	
	Min	-0.13		-0.08		-0.02	

SM1, SM2: Bending moment force per unit width about local 2-, 1-axis of elements.
SM3: Twisting moment force per unit width in local 1-2 plane.

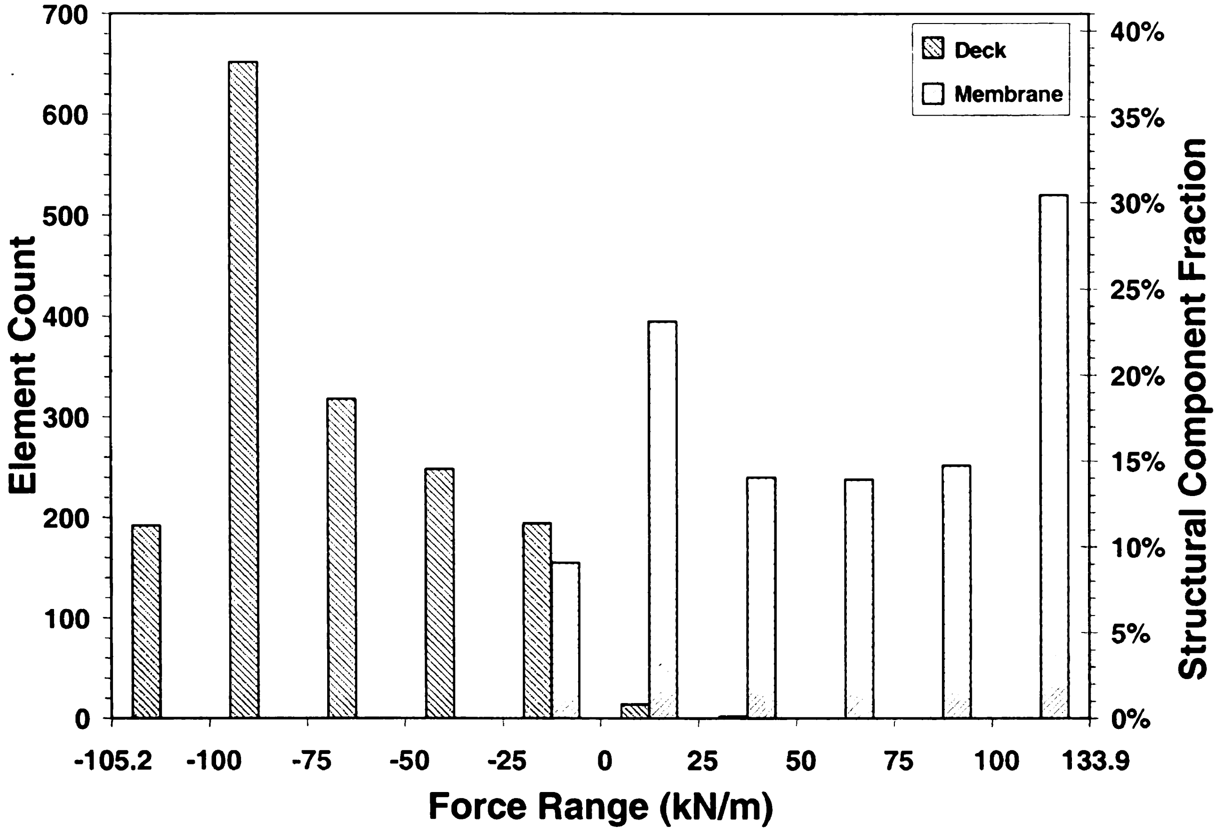

Figure 7–15 Section force (SF1) distribution

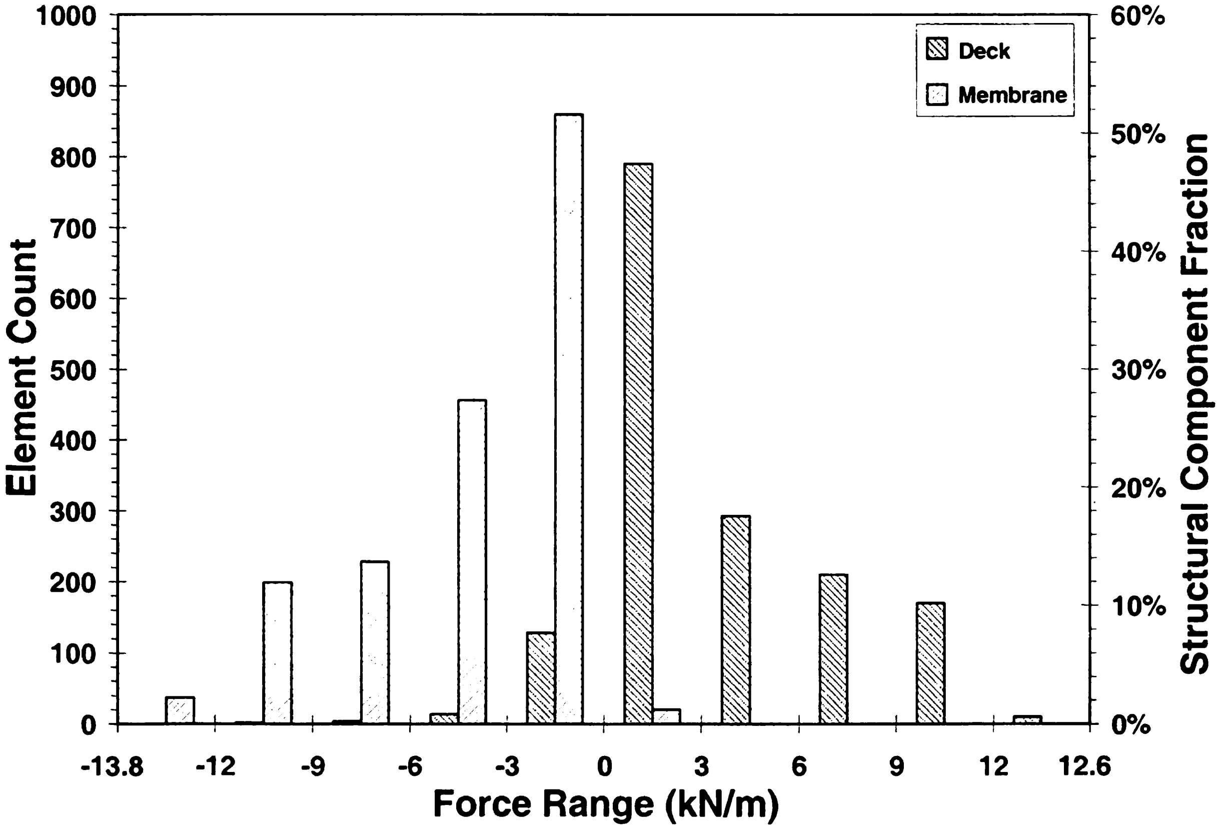

Figure 7–16 Section force (SF2) distribution

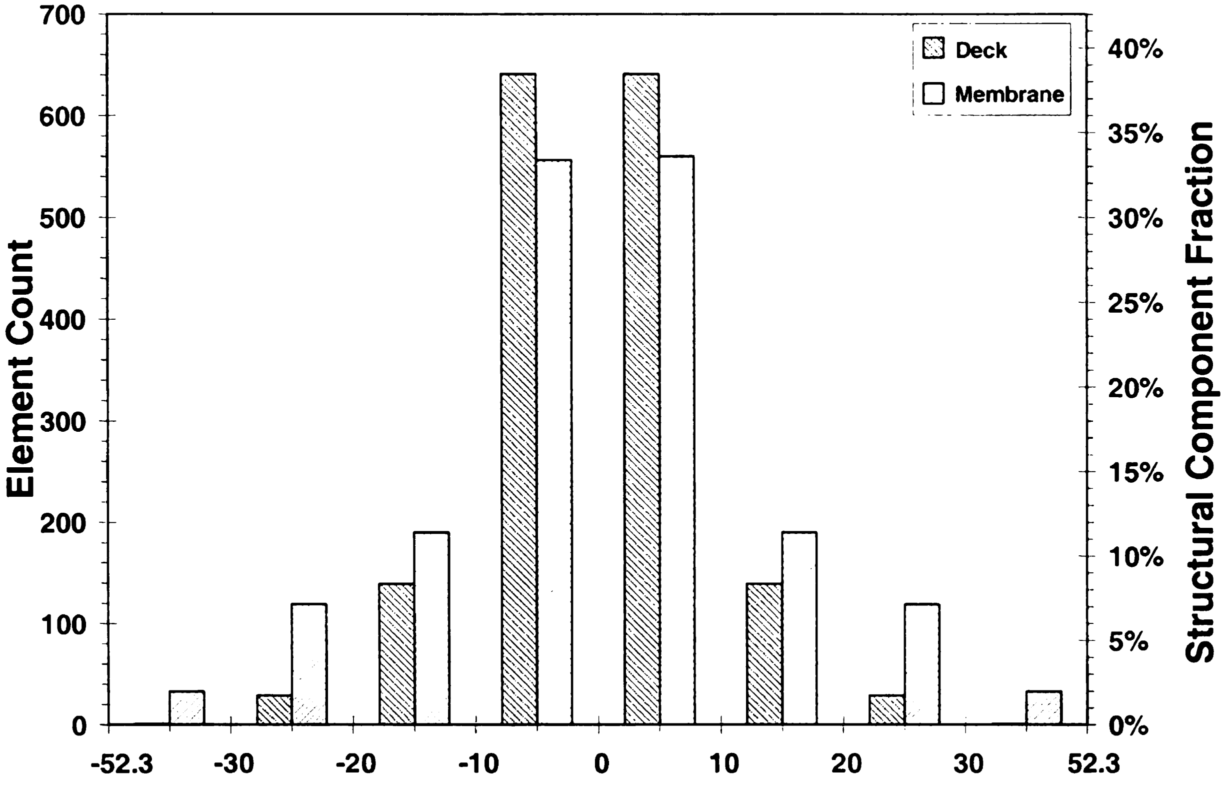

Figure 7–17 Shear section force (SF3) distribution

7.1.3.2 Stability evaluation

As previously discussed, shape optimization of a shape resistant structure will improve their structural stiffness. Such optimized structures become stiffer and carry their design loads primarily by axial or membrane action rather than bending. This leads to a response that usually involves very small deformations prior to buckling. Therefore, shape optimized structures are stability sensitive. The stability of the optimized CMB bridge was investigated by eigenvalue buckling analyses, which are generally used to estimate the critical buckling loads and potential collapse shapes of stiff structures.

Considering that the material properties of the optimal 8-layer laminate were only slightly different to the optimal 48-layer laminate, the laminate design of $[\pm 17^\circ/\pm 19^\circ]_S$ was employed to reduce the computational cost of the buckling analyses. The buckling analysis of the optimal CMB bridge considered a perturbation uniform load of 6.9 kN/m^2 on the concrete deck acting in the gravity direction. The method of subspace iteration eigenvalue extraction [HKS, 2000] was used to predict the first five eigenvalues and the corresponding eigenmodels for the optimal CMB bridge as summarized in Table 7–8.

Table 7–8 Buckling eigenvalues and eigenvectors of the optimal CMB bridge

Mode	Eigenvalue	Eigenmodel
1	-76.909	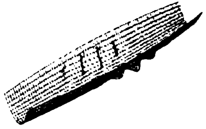
2	-76.909	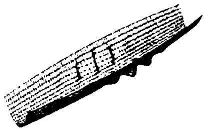
3	-77.137	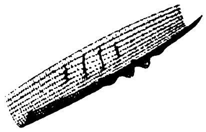
4	-77.137	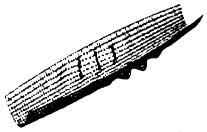
5	-79.923	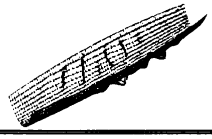

As shown in Table 7–8, negative eigenvalues were obtained from the buckling analyses. Such negative eigenvalues indicate that the optimized CMB bridge would buckle if the perturbation load were applied opposite to the gravity direction. However, the first five buckling modes show that the structure has closely spaced eigenvalues, which indicates that the structure is imperfection sensitive. Therefore, further consideration to buckling stability is required for CMB bridges if the applied loading can act in a direction opposite to that of gravity.

7.1.4 Post optimality analyses

Structural designs by optimization methods are obtained with optimal parameters achieved regarding certain optimization conditions. For example, the optimum design defined by the optimal geometric and material parameters for the CMB bridge is achieved with respect to an optimization load case. However, the CMB bridge might not be constructed exactly to the optimal geometry and the optimal laminate specified by the optimal design variables may not be easily achieved in practice. Furthermore, multiple load cases that must be resisted with corresponding performance limit states are typically considered for the design of bridge structures. The performance of an optimized structure could thus be compromised due to changes in structural geometry, loading and material properties. Therefore, the response of the optimum solution to the CMB bridge system due to geometric imperfections, loading alterations and material property changes (bend-twist coupling effects) was investigated. The CMB bridge model used in the post optimality analyses was constructed by averaging dimensions of the three optimized CMB bridges previously obtained (see Table 7–4).

7.1.4.1 Influence of bending twisting coupling effect of laminate properties

The influence of material coupling effects to the optimal CMB model was investigated by analyzing CMB bridge systems with different optimal laminates for the FRP membrane that varied only in their coupling stiffness terms (i.e., D_{16} and D_{26}). The previously obtained optimal 8-layer and 48-layer laminates, which varied in the out-plane material properties (see Table 7–5), are thus used in this analysis. The structural responses of the two CMB models constructed by these two balanced-and-symmetric laminates are compared in Table 7–9.

Table 7–9 Structural response of optimal CMB bridge with different optimal laminates

CMB membrane model		In-plane section resultants (kN/m)			Out-of-plane section resultants (kN-m/m)			Max Deflection (mm)	Strain Energy (N-m)
		SF1	SF2	SF3	SM1	SM2	SM3		
8-layer	Max	133.87	1.20	52.33	0.15	0.06	0.02	1.692	84.51
	Min	-10.51	-13.79	-52.31	-0.13	-0.08	-0.02		
48-layer	Max	133.88	1.29	52.31	0.15	0.06	0.02	1.692	84.51
	Min	-10.47	-13.76	-52.31	-0.13	-0.07	-0.02		

SF1, SF2: Direct membrane force per unit width in local 1-, 2-axis of elements.
SF3: Shear membrane force per unit width in local 1-2 plane.
SM1, SM2: Bending moment force per unit width about local 2-, 1-axis of elements.
SM3: Twisting moment force per unit width in local 1-2 plane.

According to Table 7–9, both of the material-modified CMB bridges have the same strain energy while maximum deflection and the in-plane section resultants in the membrane vary slightly. This can be explained by the in-plane dominated behavior of the optimized CMB bridge. The optimized CMB bridge is primarily subjected to in-plane longitudinal tension rather than out-of-plane section resultants. Furthermore, the small magnitudes of the bend-twist coupling terms (D_{16} and D_{26}) compared to the other major bending stiffness terms (D_{11} and D_{22}) also partially reduce the bending-twisting coupling effect. Therefore, material property changes in bend-twist coupling can be neglected for the structural behavior of the optimal CMB bridge.

7.1.4.2 Influence of geometric variations

Table 7–10 summarizes the geometric variations of the CMB bridge using average shape dimensions with respect to the three optimal CMB bridges in terms of geometric design variables. It can be noted that the maximum variation of 1.94% occurs for h_1 (the height at the end of the bridge) by using average dimensions. Consequently, the strain energy of the CMB bridge with average dimensions has an 0.7% increase (Table 7–4 and

Table 7–9). Although the CMB bridge combining several slightly-different optimal designs by averaging shape geometries can be still considered an optimum design in the current application, it can be anticipated that adequate performance of optimum designs can be compromised by geometric imperfections.

Table 7–10 Geometric variations of optimal CMB bridges

	w_1 (mm)	w_2 (mm)	h_1 (mm)	h_2 (mm)	t (mm)
Model A	1359.0	2184.4	984.3	1219.2	19.05
Model B	1365.2	2184.4	1022.4	1219.2	19.05
Model C	1352.6	2222.4	997.0	1219.2	19.05
Average	1358.9	2197.1	1001.2	1219.2	19.1
Variation	0.46%	1.00%	1.94%	0.00%	0.00%

Variation = (Standard deviation of a dimension) / (Average dimension)

7.1.4.3 Influence of loading alterations

Structural designs require a structure that meets design criteria (i.e. limit states) with respect to different load cases. However the CMB bridge was optimized with respect to a single load case. Other load cases, i.e., the service load case and the strength load case, are required to comply with structural design requirements for different limit states [ASSHTO, 1998]. Therefore, the performance of the optimized CMB bridge due to these two load cases was studied with respect to the corresponding design criteria.

Considering that most unidirectional laminated composites behave in a brittle manner, local failures generally can lead to complete fracture and total loss of load-carrying capacity. Therefore, the first-ply failure theory, which assumes failure of a composite laminate to take place when failure initiates in the most critical layer of the laminate, is used to evaluate the material strength of laminates. Several stress criteria have been developed to predict the material failure of FRP lamina under different limit states [Jones, 1999]. In addition to the maximum stress criterion implemented in the integrated optimization procedure, other three commonly used stress criteria were employed to calculate the ultimate strength of laminates in the study of load alternations. The criteria used were the Tsai-Hill [Tsai, 1968], Tsai-Wu [Wu, 1974] and Azzi-Tsai-Hill [Azzi and Tsai, 1965] models. These models are more accurate in comparison to the maximum stress criteria since they consider polynomialcombination of the stress state rather independent relations [Jones, 1999].

The structural responses and the stress indices of the optimized CMB bridge with respect to the different limit states are summarized in Table 7–11 and Table 7–12 respectively. As expected, the strength limit state has the maximum influence on the optimized CMB bridge as it results in maximum in-plane stress demands and a maximum deflection. With regards the deflection criterion, the maximum deflection obtained in the service limit state reached 5.237mm, which is 41.65% deflection limit (L/800) of 12.573 mm. It should be pointed out that the maximum stress index reached 5.39% of the material failure, that is 21.54% of the allowed service stress limit (Table 7–1). Therefore, the deflection criterion governed the design of the optimum CMB bridge under service loading. Furthermore, it can be noted that the stress indices are below the design limits proposed for each limit state (Table 7–1).

Although the optimized CMB bridge satisfied the design criteria specified in Table 7–1 for all limit states, the maximum stress criterion has the lowest stress index, which underestimates the stress level of laminates compared to the other failure stress criteria. Therefore, a more accurate material strength criteria should be applied in the stress constraint in future optimization studies.

Table 7–11 Laminate stresses of the optimized CMB bridge under different limit states

Load Case		S_{11} (N/mm^2)	S_{22} (N/mm^2)	S_{12} (N/m^2)	Max deflection (mm)
Optimization	Max	7.83	2.72	0.75	-1.692
	Min	-6.47	-4.04	-0.79	
Service	Max	20.76	7.81	1.86	-5.237
	Min	-16.39	-10.14	-1.96	
Strength	Max	33.96	12.94	3.03	-8.649
	Min	-26.71	-16.52	-3.19	

S_{11}, S_{22}: Direct stress in local 1-, 2-axis of elements.
S_{12}: Shear stress in local 1-2 plane.

Table 7–12 Stress indices of the optimized CMB bridge under different limit states

Load Case	MStrs (%)	TsaiH (%)	TsaiW (%)	AzziT (%)
Optimization	1.73	2.17	2.03	2.05
Service	4.31	5.39	5.02	5.07
Strength	7.01	8.76	8.17	8.24

In addition to the loading alteration by load cases corresponding different limit states, the structural response of the optimized CMB bridge due to the extreme loading effects introduced by the loading pattern of moving trucks in the strength limit state was also explored. Two extreme truck loading positions were considered. One loading pattern was introduced to create maximum torsion by placing the truck loads at the edge of the optimized CMB bridge (Figure 7–18). A second loading position sought to develop the maximum mid-span moment by placing the two axel loads (142.4 kN) in the middle of the bridge (Figure 7–19). The structural responses and stress indices for the optimized CMB bridge due to these two critical loading patterns are summarized in Table 7–13 and Table 7–14.

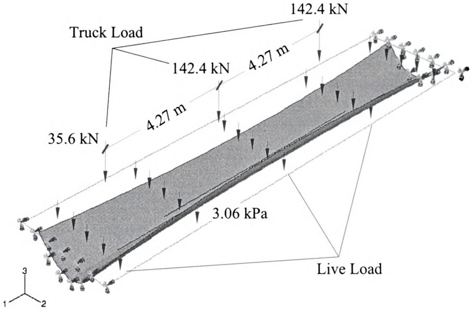
142.4 kN
Truck Load
142.4 kN
4.27 m
4.27 m
35.6 kN
3.06 kPa
Live Load
3
1
2

Figure 7–18 Load case for maximum torsion in the strength limit state

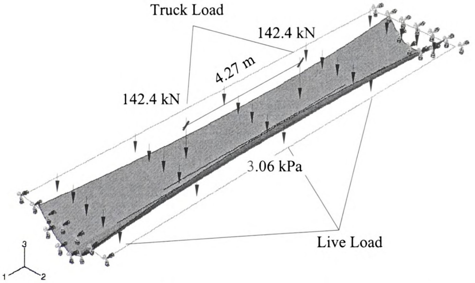
Truck Load
142.4 kN
4.27 m
142.4 kN
3.06 kPa
Live Load
3
1
2

Figure 7–19 Load case for maximum bending in the strength limit state

As shown in Table 7–13 and Table 7–14, the maximum structural response is developed due the load case of maximum torsion. The maximum deflection reached 11.82 mm and the maximum stress demand achieved about 21% of the material failure stress state (Table 7–14), which is 2 times greater than the maximum stress level of the

optimized CMB bridge under strength loads. Also, the transverse stresses (S_{22}) are obviously increased due to the twisting behavior introduced by the truck loads (Table 7–13). Although the optimized CMB bridge is still within the stress limit for the strength limit state (see Table 7–1), the structural responses under the critical load patterns are clearly different than those obtained for the optimum load case. Therefore, structural optimum designs with respect to a typical load pattern should be designed with strength reserves to allow possible increases of structural response due to non-optimal loading alterations while in service.

Table 7–13 Laminate stresses of the optimized CMB due to different extreme effects

Load Case		S_{11} (N/mm^2)	S_{22} (N/mm^2)	S_{12} (N/mm^2)	Max deflection (mm)
Strength	Max	33.96	12.94	3.03	-8.65
	Min	-26.71	-16.52	-3.19	
Maximum Torsion	Max	48.74	23.54	4.07	-11.82
	Min	-38.36	-50.43	-4.94	
Maximum Bending	Max	44.83	18.07	4.13	-9.50
	Min	-37.27	-22.73	-4.22	

S_{11}, S_{22}: Direct stress in local 1-, 2-axis of elements..
S_{12}: Shear stress in local 1-2 plane.

Table 7–14 Stress indices of the optimized CMB due to different extreme effects

Load Case	MStrs (%)	TsaiH (%)	TsaiW (%)	Azzit (%)
Strength	7.01	8.76	8.17	8.24
Maximum Torsion	20.63	21.14	21.44	21.14
Maximum Bending	9.30	11.94	10.76	10.83

7.2 FRP composite membrane suspension (CMS) bridges

Inspired by conventional cable suspension bridges, an FRP composite membrane bi-suspended (CMS) bridge (see Figure 7–20) was conceptualized as a second case study for the developed optimization approach. In CMS bridge systems, a deck system (either a conventional concrete slab or an FRP panel) is assumed to be placed on top of the FRP membrane such that it transfers the applied live loads through internal diaphragms or "bulkheads." Thus, the in-plane stiffness of the FRP membrane is employed in two-way tension under uniform loading from the deck system. A conceptual depiction of a three-span CMS bridge is shown in Figure 7–20.

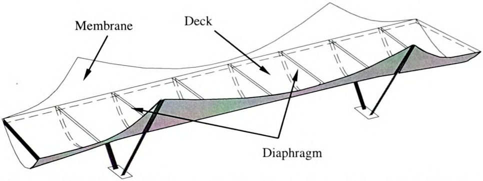

Figure 7–20 Concept for Composite Membrane Suspension (CMS) Bridges

7.2.1 Bridge system description

The CMS bridge proposed for optimization studies is a 60.96 m long three-span bridge with a 10.36 m wide concrete deck to accommodate two 3.66 m traffic lanes and essential shoulders (Figure 7–21). The concrete deck is 304.8 mm thick with a density of 2400 kg/m^3 for normal concrete. The loads acting on the bridge include the self-weight of the concrete deck, and the live lane and truck vehicular loads. The live lane load, which acts over the 3.05 m wide lane, is assumed to be distributed over the entire surface of the deck, resulting in a pressure of 3.06 kN/m^2. The total truck loads introduced by two trucks for two lanes are also considered to be ideally distributed over the FRP membrane through diaphragms as a pressure of 1.014 kN/m^2. The laminates used for this bridge system are based on typical medium-performance carbon/epoxy material system for use

in civil structures. Thus the lamina orthotropic properties are taken as: E_{11} = 155.025 GPa, E_{22} = 10.335 GPa, G_{12} = 6.89 GPa, G_{13} = 6.89 GPa, G_{23} = 0.689 GPa, and ν_{12} = 0.3.

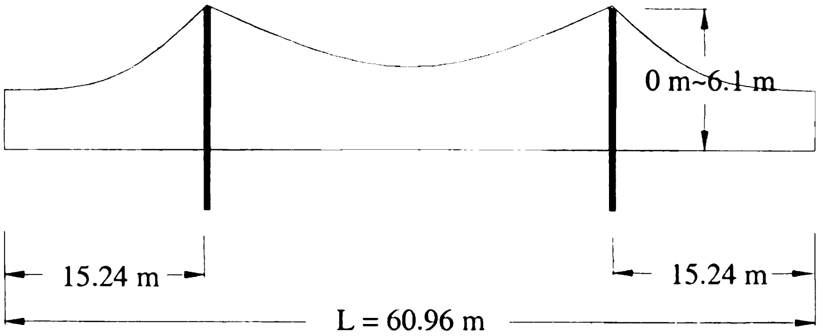
0 m~6.1 m
15.24 m
15.24 m
L = 60.96 m

(a) Side view

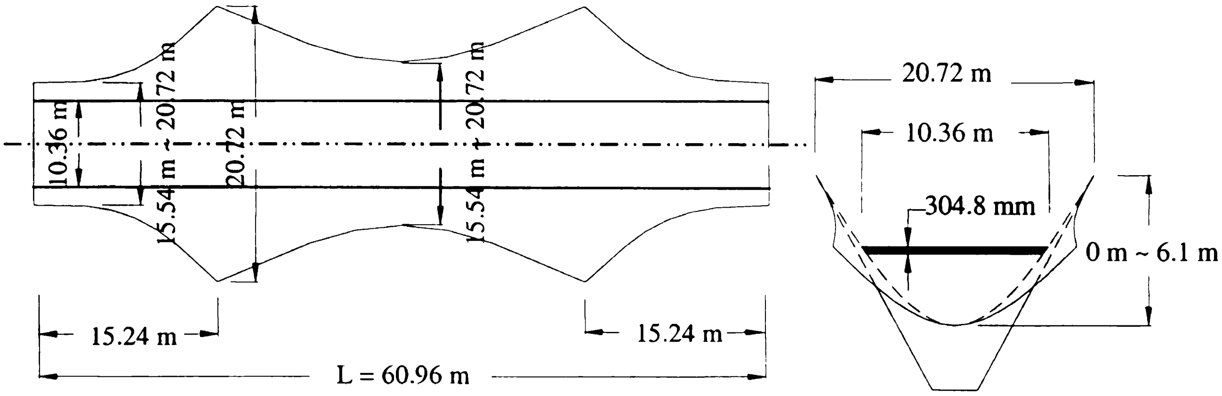
10.36 m
15.54 m ~ 20.72 m
20.72 m
15.54 m ~ 20.72 m
15.24 m
15.24 m
L = 60.96 m
20.72 m
10.36 m
304.8 mm
0 m ~ 6.1 m

(b) Plan view

(c) Cross view

Figure 7–21 Geometry of the CMS bridge

The CMS bridge is subjected to dead loads (DL), two lanes of uniformly distributed lane loads (LL) and two three-axel truck loads (TL) [AASHTO, 1998]. Two load cases using different combinations of the applied loads, which are specified in Table 7–15, were selected to analyze the CMS bridges for service and strength limit states.

As previously used for CMB bridges, the tension and compression stress limits based on the material properties for 1-axis (fiber-longitudinal direction) and 2-axis (fiber-transverse direction) were chosen as X_T = 1.55 GPa, X_C = -0.775 GPa and Y_T = 0.103

GPa, Y_C = -0.052 GPa respectively, and the shear stress limit in 1-2 plane is taken as S =34.45 MPa. The ultimate material failure σ_u is then determined by combining the stress limits measured on the material directions according to a stress criterion.

Table 7–15 Load cases specification for CMS bridges

Load Cases	Specification	Design Criteria		Limit State
		Stress Strength	Deflection	
Service load case	1.0×DL + 1.0×(LL + 1.33×TL)	$0.25\sigma_u$	L/800	Service
Strength load case	1.25×DL + 1.75×(LL + 1.33×TL)	$0.50\sigma_u$	–	Strength

7.2.2 Integrated optimization of CMS bridges

Based on the above-mentioned geometric, material, and loading definition for the bridge systems, the integrated optimization approach was applied to design FRP CMS bridges starting with the shape and laminate-property optimization and then followed by the laminate design optimization.

7.2.2.1 Shape and FRP laminate-property optimization

Taking advantage of structural symmetry, the hyperbolic profile of the CMS membrane can be controlled by four key points as shown in Figure 7–22. The shape design variables were therefore the six degrees of freedom of the four geometric key points. The membrane system was completely defined by spline interpolation of the key points. The positions of the pier supports (Figure 7–21 (a)) are constant throughout the optimization process. The rational of this assumption will be discussed in Section 7.3.3. The laminate design variables are the lamination parameters $\{V_{1A}, V_{3A}, V_{1D}, V_{3D}\}$ controlling the in-plane tension stiffness and out-plane bending stiffness.

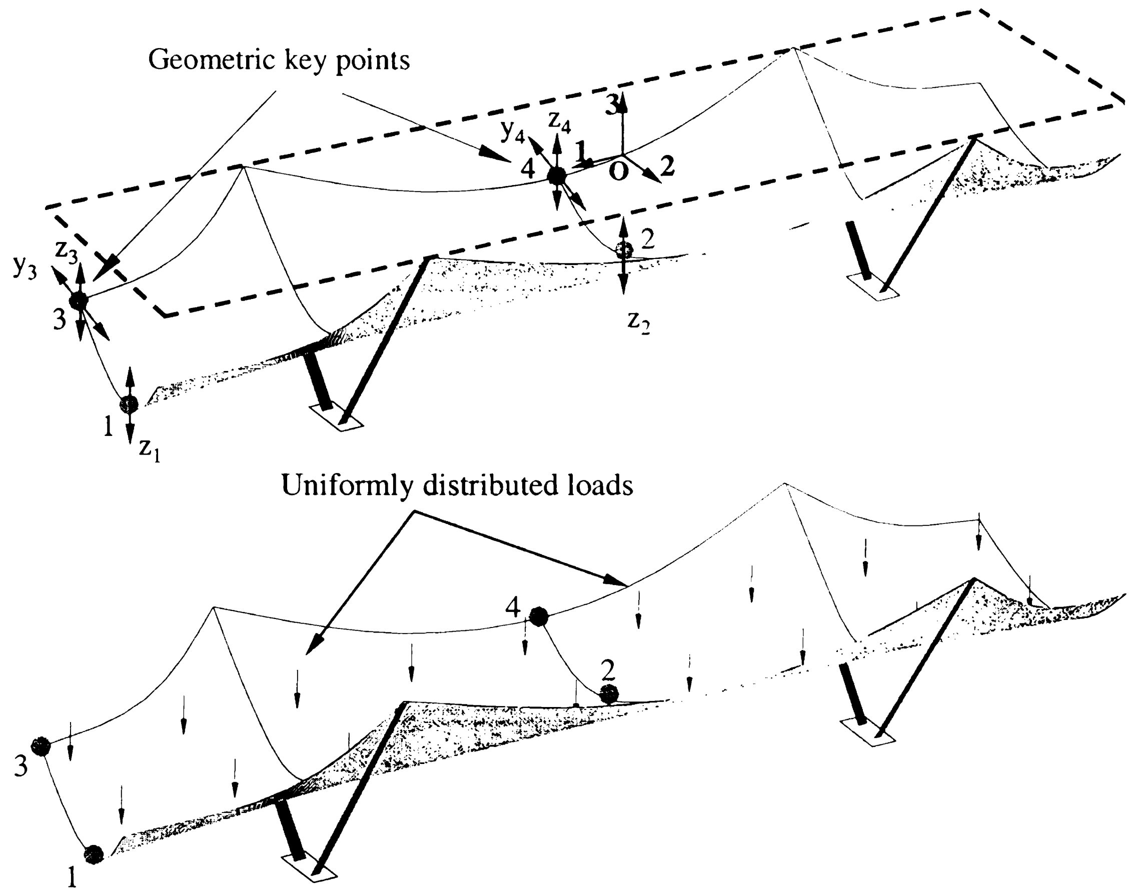

Figure 7–22 Loading and geometric key points for the CMS bridge

As applied in the integrated optimization of CMB bridges, an inequality constraint was employed to limit the used mass of the membrane FRP laminate. Therefore, a material constraint was implemented by setting a lower and upper bound for the coordinates of the shape key points (Table 7–16). Maximum stresses monitored at the top and bottom surface of the FRP laminate and maximum deflections of the complete system constituted two additional constraints required to enforce the structural design criteria in the integrated optimization procedure. Instead of only using dead load and live lane in the optimization load case, the load case for the service limit state (Table 7–15), which includes truck loads, was chosen as the optimization load case for the CMS bridges.

Table 7–16 Coordinates constraints for geometric design variables

Coordinate	P_1 (m)			P_2 (m)			P_3 (m)			P_4 (m)		
bound	x	y	z	x	y	z	x	y	z	x	y	z
Lower	30.48	0.0	-6.1	0.0	0.0	-6.1	30.48	-10.4	-6.1	0.0	-10.4	-6.1
Upper			0.0			0.0		-7.8	0.0		-7.8	0.0

Two typical boundary conditions for suspension bridges were considered in the CMS bridge analyses (Table 7–17) to evaluate the effect of boundary conditions on the optimized shape. Model A was provided with simple supports at the positions of the piers while Model B featured extra roller supports at both ends of the bridge.

Table 7–17 Initial designs of CMS Bridges

Initial design	Model A	Model B
Boundary conditions	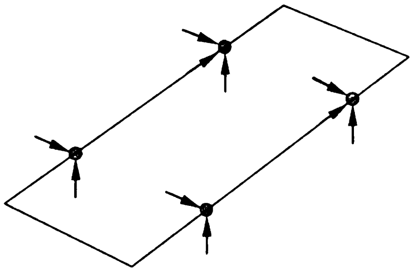	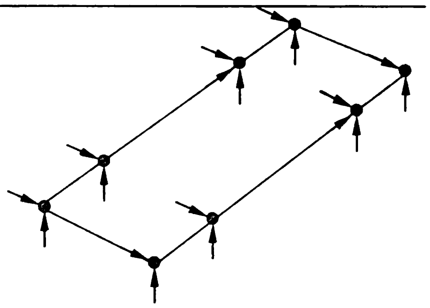
$\{z_1, z_2, z_3, z_4, y_3, y_4\}$ (m)	{0, 0, 0, 0, -10.4, -10.4}	
Laminate design	$[0°/90°]_S$	
$\{V_{1A}, V_{3A}, V_{1D}, V_{3D}\}$	{0,1,0.75,1}	

The integrated optimization approach was implemented as previously described and the performance and stability of the obtained results was assessed by studying a single initial design (geometry and laminate layup) for each CMS bridge model (Table 7–17). Both integrated optimizations were initiated with a plane FRP membrane constructed with a cross-ply laminate, i.e., a $[0°/90°]_S$. The first-level optimization history of the two CMS bridges is shown in Figure 7–25 and Figure 7–28, respectively.

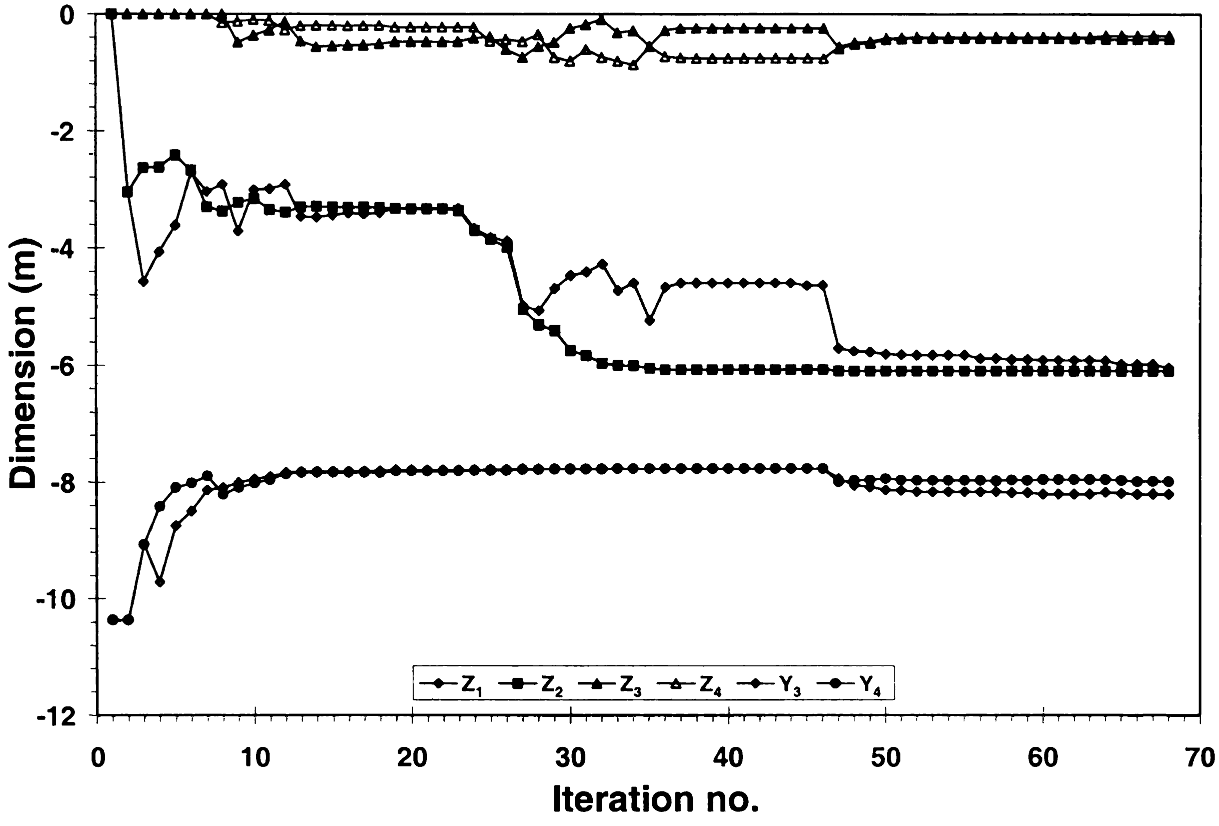

Figure 7–23 Histories of geometric design variables – CMS Model A

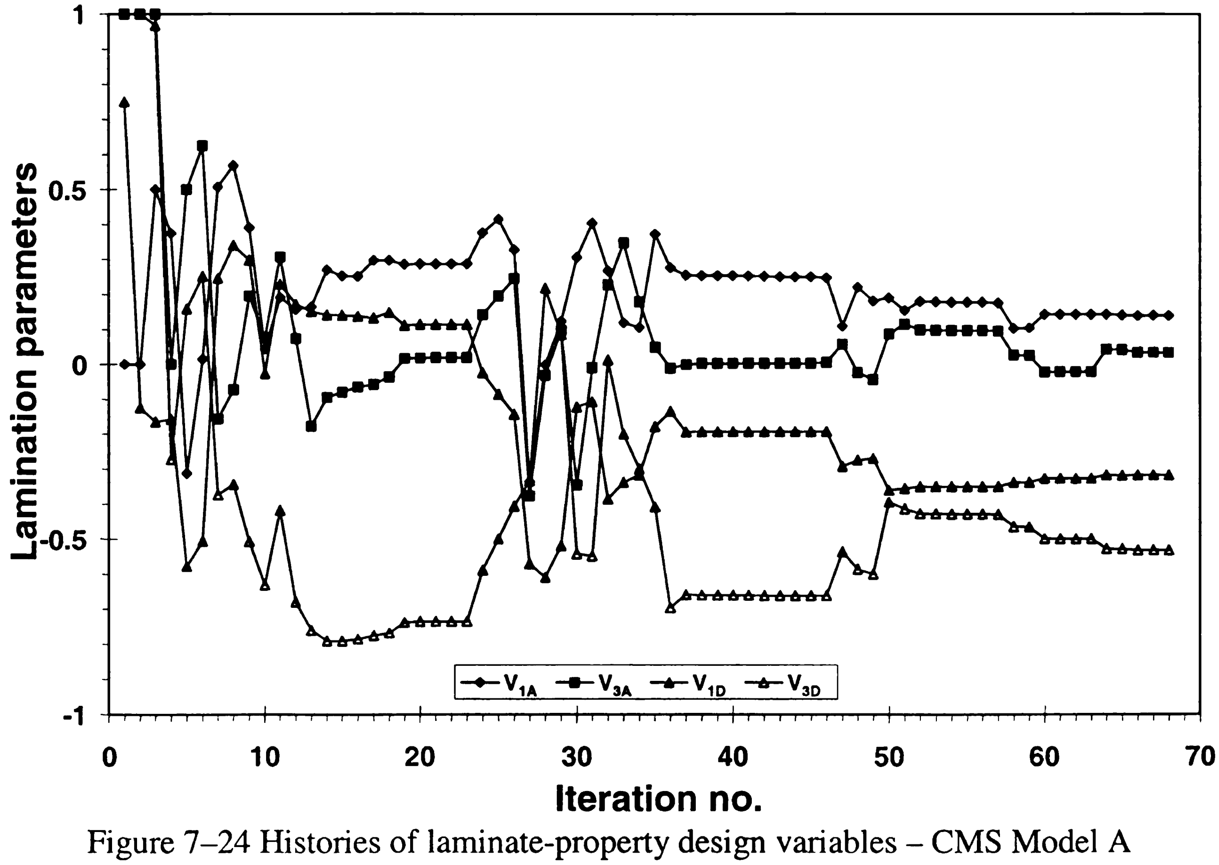

Figure 7–24 Histories of laminate-property design variables – CMS Model A

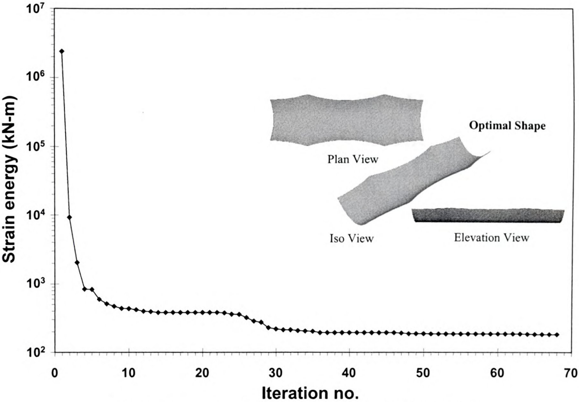

Figure 7–25 History of objective function – CMS Model A

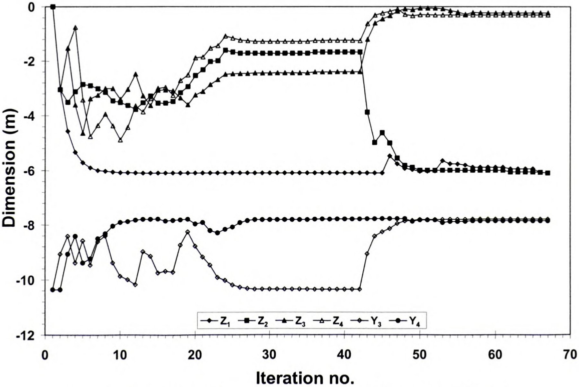

Figure 7–26 Histories of geometric design variables – CMS Model B

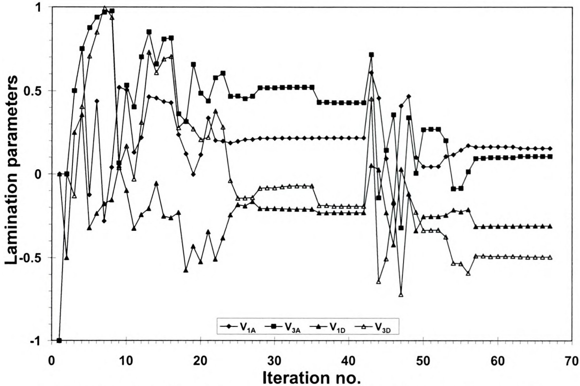

Figure 7–27 Histories of laminate-property design variables – CMS Model B

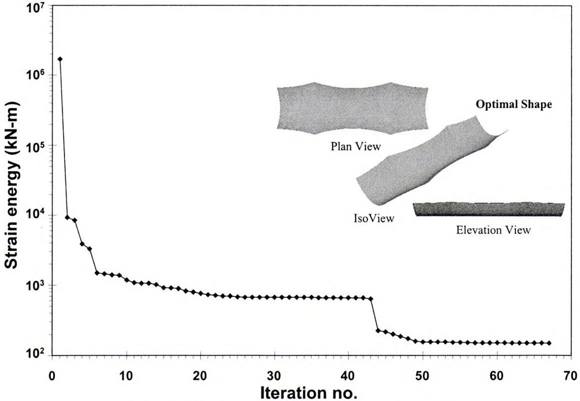

Figure 7–28 History of objective function – CMS Model B

The optimal results obtained from the first-level optimization are summarized in Table 7–18. It can be seen that although both models have a similar geometric shape, the optimized objective of Model B has a strain energy value 20% lower than that of Model A. The improvement in minimizing the strain energy came from changes in the laminate properties due to the different boundary conditions. In Chapter 6 it was demonstrated that structural optimization can be further improved by material optimization. Optimum laminates were thus also determined for the CMS bridges using the second-level optimization so as to achieve the obtained optimal lamination parameters.

Table 7–18 Optimal results of the first-level optimization for the CMS bridges

Optimum design	Model A	Model B
Strain energy (kN-m)	183.26	149.93
$\{z_1, z_2, z_3, z_4, y_3, y_4\}$ (m)	{-6.05, -6.10, -0.43, -0.37, -8.20, -7.99}	{-6.10, -6.10, -0.22, -0.30, -7.79, -7.85}
$\{V_{1A}, V_{3A}, V_{1D}, V_{3D}\}$	{0.138, 0.033, -0.317, -0.533}	{0.155, 0.106, -0.309, -0.494}

It should be noted in Figure 7–28 that the objective function experienced an abrupt decrease after a relative smooth development in the iteration history of CMS bridge optimization. The occurrence is thought to be inherent from the gradient properties of the objective function with respect to the design variables for this optimization case.

7.2.2.2 *Laminate design optimization*

In the second level optimization, the genetic optimization procedure was employed to design optimal laminates with a maximum error of 1% with respect to the optimal lamination parameters obtained from the first-level optimization.

The genetic iteration histories for the laminate designs of the two CMS bridge models are shown in Figure 7–29 and Figure 7–30, respectively. The optimal laminate for Model

A was found to be $[\pm51^\circ/\pm57^\circ/\pm60^\circ/\pm63^\circ/\pm50^\circ/\pm67^\circ/\pm62^\circ/\pm21^\circ/0^\circ_8]_S$ with a minimum error of 0.807% with respect to the optimal lamination parameters. The optimal laminate for Model B was $[\pm53^\circ/\pm51^\circ/\pm64^\circ_2/\pm53^\circ/\pm62^\circ/\pm64^\circ/\pm4^\circ/0^\circ_8]_S$ with a minimum error of 0.643%.

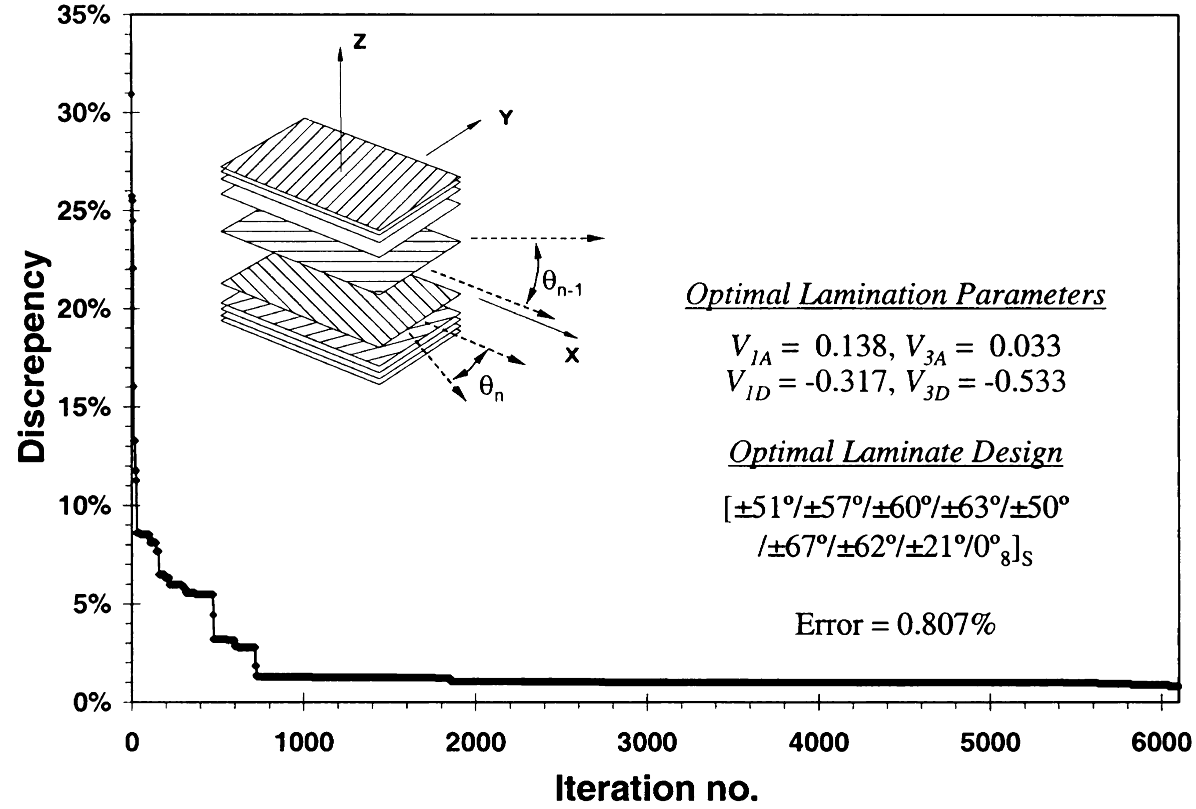

Figure 7–29 Second-level optimization process of Model A

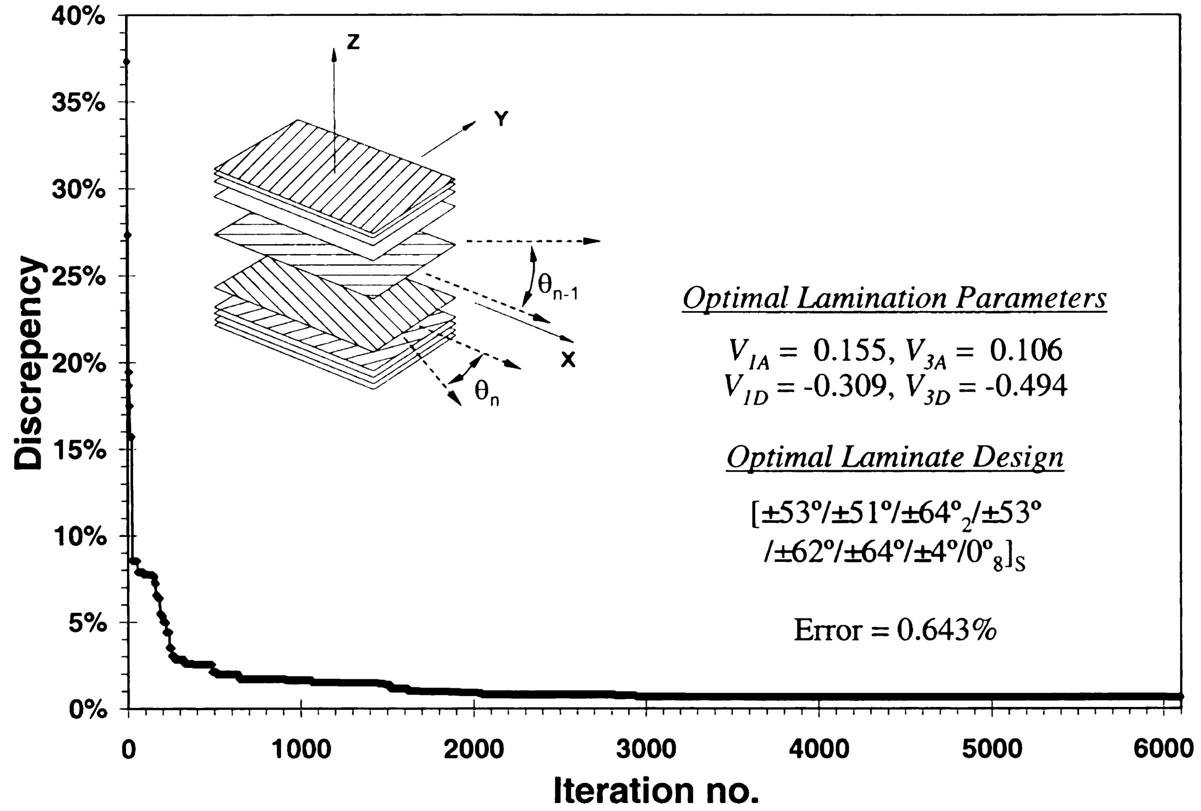

Figure 7–30 Second-level optimization process of Model B

7.2.3 System characteristics of optimal CMS bridges

The system characteristics of the optimized CMS bridges was investigated by studying the structural response of the bridge systems under the optimal load case and the stability of the optimized CMS FRP membrane. The influence of boundary conditions on the optimum designs was evaluated by comparing the results from both models.

7.2.3.1 Structural behavior of optimal CMS bridges

The section forces and moment resultants for the CMS bridges are given in Table 7–19 and Table 7–20, respectively. From these tables it is clearly seen that the FRP membrane of both CMS bridges is dominated by in-plane stress demands. In addition, a further review of the section forces along the local 1- and 2-direction (Figure 7–31)

shows that the FRP membrane is subjected to two-way tension, as the relative magnitude of both of these stress fields is similar. Therefore, the behavior of FRP CMS bridges is such that the FRP membrane acts as a membrane structure carrying distributed loads primarily through bi-directional tension.

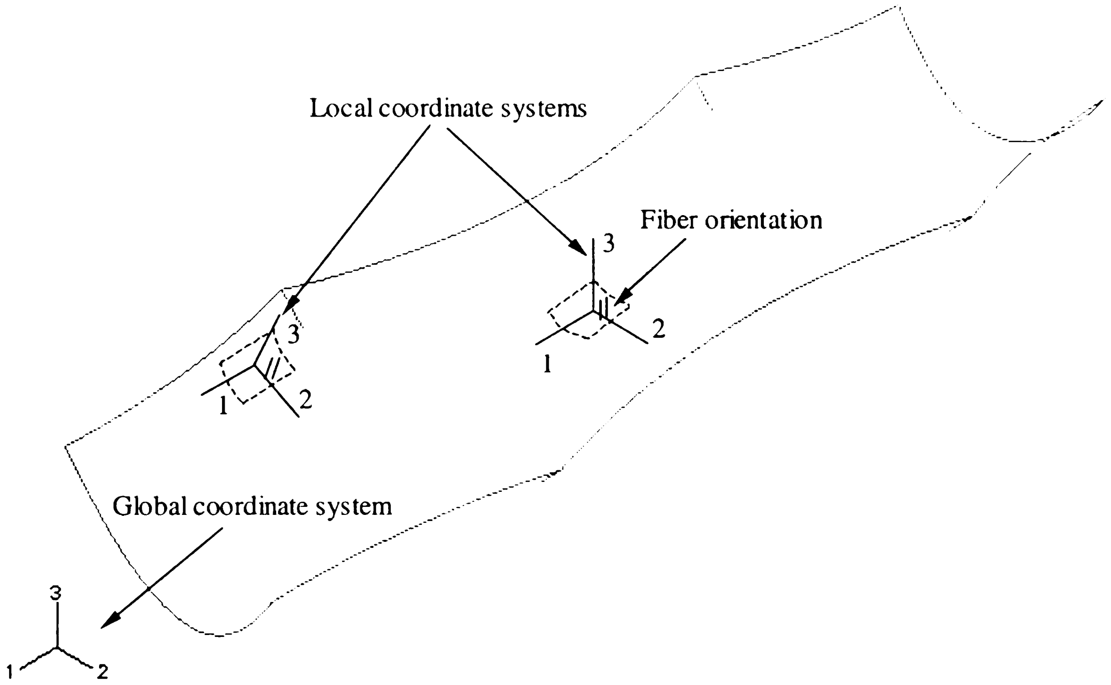
Local coordinate systems
Fiber orientation
3
3
1
2
1
2
Global coordinate system
3
1
2

Figure 7–31 Coordinate systems

Table 7–19 Section forces for optimal CMS bridges

Section Forces		SF1 (kN/m)	Min Max	SF2 (kN/m)	Min Max	SF3 (kN/m)	Min Max
Model A	Max	2818.32	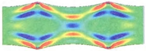	2472.79	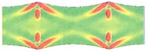	1910.28	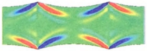
	Min	-1113.46		-611.19		-1910.46	
Model B	Max	2116.41	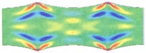	2403.27	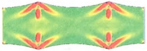	1619.22	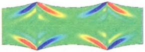
	Min	-820.47		-717.67		-1619.22	

SF1, SF2: Direct membrane force per unit width in local 1-, 2-axis of elements.
SF3: Shear membrane force per unit width in local 1-2 plane.

Table 7–20 Section moments for optimal CMS bridges

Section Forces		SM1 (kN-m/m)	Min Max	SM2 (kN-m/m)	Min Max	SM3 (kN-m/m)	Min Max
Model A	Max	2.64	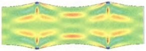	5.18	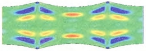	4.87	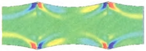
	Min	-8.29		-8.70		-4.87	
Model B	Max	2.82	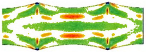	6.26	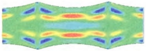	5.80	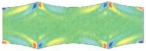
	Min	-6.45		-6.45		-5.80	

SM1, SM2: Bending moment force per unit width about local 2-, 1-axis of elements.
SM3: Twisting moment force per unit width in local 1-2 plane.

7.2.3.2 Stability

From above-discussed results, the optimized CMS bridges are shape resistance structures in which high structural stiffness is primarily gained by in-plane membrane actions rather than flexural actions. As previously addressed, such structures are buckling sensitive and usually require only small deformations prior to experiencing buckling. Therefore, the stability of the optimized CMS bridges was investigated through buckling sensitivity analyses.

Eigenvalue buckling analyses determined with ABAQUS [HKS, 2001] were used to predict critical buckling loads and potential collapse modes of CMS bridges. The loading of the service limit state was employed as the perturbation load required for the buckling analyses. The method of subspace iteration extraction was chosen to obtain the first four eigenvalues and corresponding eigenshapes, which are summarized in Table 7–21.

According to the results shown in Table 7–21, negative eigenvalues are reported for both CMS bridge models. Such eigenvalues imply that buckling of the optimal CMS bridges would happen only if the perturbation load were applied opposite to the gravity direction. Further comparison of the two models shows how the different boundary conditions will influence the buckling modes of the structures. Model A has obvious buckling deformations at the free ends of the bridge while buckling of Model B will primarily happen at the positions where the columns support the FRP membrane. Considering that Model B is stiffer due to its lower strain energy, it is understood that Model B is more sensitive to buckling and, therefore, has higher and more closely spaced eigenvalues than Model A.

Table 7–21 Buckling eigenvalues and eigenshapes of the optimal CMS bridges

Mode	Model A		Model B	
	Eigenvalue	Eigenshape	Eigenvalue	Eigenshape
Base State	-		-	
1	-0.037	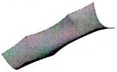	-0.2526	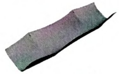
2	-0.114	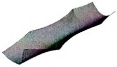	-0.3151	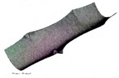
3	-0.120	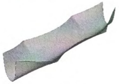	-0.3152	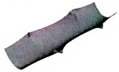
4	-0.125	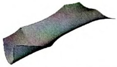	-0.3153	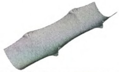

7.2.4 Post optimality analyses

Optimal structural designs are achieved by satisfying certain optimization paramters and constraints such as loading and boundary conditions. Change of such conditions can alter the optimum designs whose response may violate the constraints originally satisfied. Therefore, it is necessary to evaluate the influence of such changes on the behavior of optimum designs through post optimality analyses. The following analyses focus on the influence of loading and boundary-condition changes on the performance of the previously-obtained optimal CMS bridges.

7.2.4.1 Influences of loading alternations

Since the load case for the service limit state was used to achieve the optimal CMS bridges, the constraints of maximum deflection and maximum stresses were verified for the strength limit state load case on the optimal CMS bridges.

A first-ply failure analysis was applied to predict the material ultimate strength of the laminated FRP membrane. In addition to the independent maximum stress criterion implemented in the integrated optimization procedure, the coupled polynomial stress failure theories by Tsai-Hill [Tsai, 1968], Tsai-Wu [Wu, 1974] and Azzi-Tsai-Hill [Azzi and Tsai, 1965] were also used in a first-ply-failure criterion. These models are readily available in ABAQUS to estimate the stress failure of FRP laminates.

The structural responses and the stress indices of the optimized CMS bridges with respect to the different limit states, see Table 7–15, are summarized in Table 7–22 and Table 7–23, respectively. As shown in the tables, although the maximum stresses and maximum deflection are increased from the service limit state to the strength limit state, the stress indices for both models of the optimized CMS bridges indicate that the load case associated to the service limit state is still the critical load case for the bridge system. It should be noted that the stress index evaluated by the maximum stress criterion employed in the optimization process predicted that the stress level in the laminates was within the allowable limits and the material strength. However, as seen in Table 7–23, the bi-axial stress failure criteria indicate that the stresses on the FRP laminate exceed the service stress limits. Therefore, multiple stress failure criteria should be considered as stress constraints during optimization processes.

Table 7–22 Structural response of optimized CMS bridges for different limit states

Model	Load Case		S_{11} (N/mm^2)	S_{22} (N/mm^2)	S_{12} (N/mm^2)	Max deflection (mm)
A	Service	Max	525.08	39.22	20.96	400.30
		Min	-133.91	-15.08	-11.41	
	Strength	Max	715.88	53.48	28.57	545.59
		Min	-182.57	-20.55	-15.55	
B	Service	Max	613.59	46.30	19.57	139.95
		Min	-187.88	-19.06	-15.52	
	Strength	Max	836.54	63.12	26.68	191.01
		Min	-256.15	-25.99	-21.17	

S_{11}, S_{22}: Direct stress in local 1-, 2-axis of elements.
S_{12}: Shear stress in local 1-2 plane.
SP_1, SP_2: Minimum, maximum principal stresses

Table 7–23 Stress indices of optimized CMS bridges for different limit states

Model	Load Case	MStrs (%)	TsaiH (%)	TsaiW (%)	AzziT (%)
A	Service	23.47	32.38	29.23	30.73
	Strength	32.01	44.14	39.84	41.88
B	Service	20.78	27.20	25.30	25.83
	Strength	33.86	45.70	52.90	45.70

MStrs: Maximum stress theory failure measure
TsaiH: Tsai-Hill theory failure measure.
TsaiW: Tsai-Wu theory failure measure.
AzziT: Azzi-Tsai-Hill theory failure measure.

In the optimization procedure, the design loads applied on the FRP membrane were ideally considered to be uniformly distributed over the area that the concrete deck projects onto the FRP membrane. However, in practice, it is conceptualized that the concrete deck weight and live loads will be transferred to the FRP membrane through diaphragms or "bulkheads." Therefore, spaced line loads (Figure 7–32), which simulate the pattern of the loads transferred from the diaphragms, were applied on the FRP membrane as a non-optimal loading pattern. The structural response of the optimal CMS bridges subject to spaced line loads at the service limit state will be used to verify the design criteria and is compared to the structural behavior of the optimal CMS bridge subjected to the distributed loading.

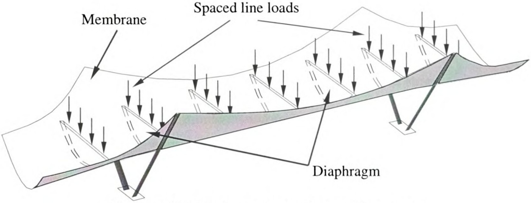

Figure 7–32 Loading pattern of spaced line loads

The structural response of the optimal CMS bridges subject to the spaced diaphragm line loading pattern is summarized in Table 7–24, Table 7–25, Table 7–26 and Table 7–27. By comparing the section forces and moments, it is shown that the response of both models still remains governed by in-plane stresses. However, it is easily seen in the figures of Table 7–26 and Table 7–27 that the distribution of the section forces and moments in the FRP membrane has obvious changes along the loading pattern, while the magnitude variation of the section forces and moments varied only modestly. A comparison of Table 7–22 and Table 7–24 shows that compressive forces noticeably increased in the FRP membrane of Model A after the loading pattern was altered. This lead to the stress index of the FRP membrane of Model A (see Table 7–23 and Table 7–25) to be almost twice than the stress demand limits chosen for the service limit state. However, the stress level and stress indices of Model B had smaller variations compared to Model A due to changes in the loading pattern.

It can be further noted for Model A that, although its section moments remained small compared to the in-plane forces, the magnitudes of the section moments increased considerably for the non-optimal loading pattern as compared to values obtained under the uniform load distribution (Table 7–26 and Table 7–27). Accordingly, the structural strain energy under the non-optimal load pattern is more than two times that of the optimal value previously obtained (Table 7–25). The increase in strain energy is caused by the increase in the section moments throughout the FRP membrane, which can be clearly seen in the figures and values given in Table 7–27. Consequently, optimal Model A, obtained by a uniform loading pattern, might not be considered as an optimal shape for the loading pattern of spaced line loads. On the other hand, the strain energy of Model B increased only moderately over the optimal strain energy value.

Table 7–24 Structural responses of the optimized CMS bridges subject to spaced line loads under the service limits state

Model		Stress				
		S_{11} (N/mm^2)	S_{22} (N/mm^2)	S_{12} (N/mm^2)	SP_1 (N/mm^2)	SP_2 (N/mm^2)
A	Max	439.21	25.99	27.65	17.43	439.29
	Min	-303.67	-20.02	-26.61	-304.75	-18.82
B	Max	506.56	36.96	19.74	36.71	506.74
	Min	-135.39	-13.40	-10.02	-135.75	-11.53

S_{11}, S_{22}: Direct stress in local 1-, 2-axis of elements.
S_{12}: Shear stress in local 1-2 plane.
SP_1, SP_2: Minimum, maximum principal stresses

Table 7–25 Stress indices of the optimized CMS bridges subject to spaced line loads under the service limits state

Model	Stress Index				Max deflection (mm)	Strain Energy (kN-m)
	MStrs (%)	TsaiH (%)	TsaiW (%)	AzziT (%)		
A	40.10	58.83	68.73	58.83	427.74	414.20
B	23.76	26.65	28.65	25.95	139.65	193.20

MStrs: Maximum stress theory failure measure
TsaiH: Tsai-Hill theory failure measure.
TsaiW: Tsai-Wu theory failure measure.
Azzit: Azzi-Tsai-Hill theory failure measure.

Table 7–26 Section forces of optimal CMS bridges subject to loading pattern changes

Section Forces		SF1 (kN/m)	Min Max	SF2 (kN/m)	Min Max	SF3 (kN/m)	Min Max
Model A	Max	2347.6	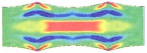	2332.0	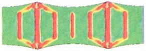	1795.2	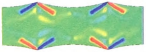
	Min	-1000.3		-470.0		-1801.2	
Model B	Max	2098.9	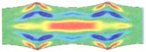	2492.1	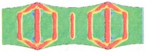	1647.1	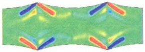
	Min	-834.3		-775.1		-1645.8	

SF1, SF2: Direct membrane force per unit width in local 1-, 2-axis of elements.
SF3: Shear membrane force per unit width in local 1-2 plane.

Table 7–27 Section moments of optimal CMS bridges subject to loading pattern changes

Section Forces		SM1 (kN-m/m)	Min Max	SM2 (kN-m/m)	Min Max	SM3 (kN-m/m)	Min Max
Model A	Max	9.49	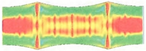	24.16	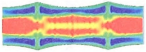	3.89	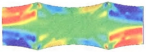
	Min	-4.92		-9.23		-3.69	
Model B	Max	3.78	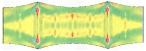	5.17	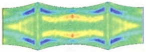	3.99	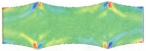
	Min	-5.95		-6.39		-3.96	

SM1, SM2: Bending moment force per unit width about local 2-, 1-axis of elements.
SM3: Twisting moment force per unit width in local 1-2 plane.

The summarized results point out that the performance of an optimum design can be significantly altered by changes in loading patterns. However, optimal CMS bridge Model B was found to be less sensitive to loading pattern changes than Model A (their difference arising from their boundary conditions). Thus, the optimal CMB bridge of Model B would behave better under changes in loading patterns during service.

7.2.4.2 Influence of boundary conditions

As previously discussed, the optimal CMS bridge designs show different performance detriments due to changes in loading patterns. The change in performance due to non-optimal loading patterns is largely originated from the difference in boundary conditions. Therefore, it is necessary to investigate the influence of boundary conditions on the optimum design of CMS bridges. This can be done by comparing the in-plane behavior of the two CMS bridge models under the service limit state.

The membrane forces of Model A and Model B are compared in Figure 7–33 and Figure 7–34. According to Figure 7–34, both models are primarily subjected to in-plane tensile forces and have an almost equal force distribution in the transverse direction of the bridge. However, although both models are subjected to tension and compression in longitudinal direction, their in-plane structural behavior, demonstrated by the distribution of transverse section forces, is different. Figure 7–33 shows that about 85% of Model B is subjected to membrane forces with 300 kN/m or less while 15% is subjected to membrane forces higher than 300 kN/m. In contrast, about 30% of Model A has membrane forces over 300 kN/m. This is the reason that Model A has a higher optimal strain energy than Model B. The variation in section force distribution is caused by the difference in boundary conditions between the two models. These results, combined the

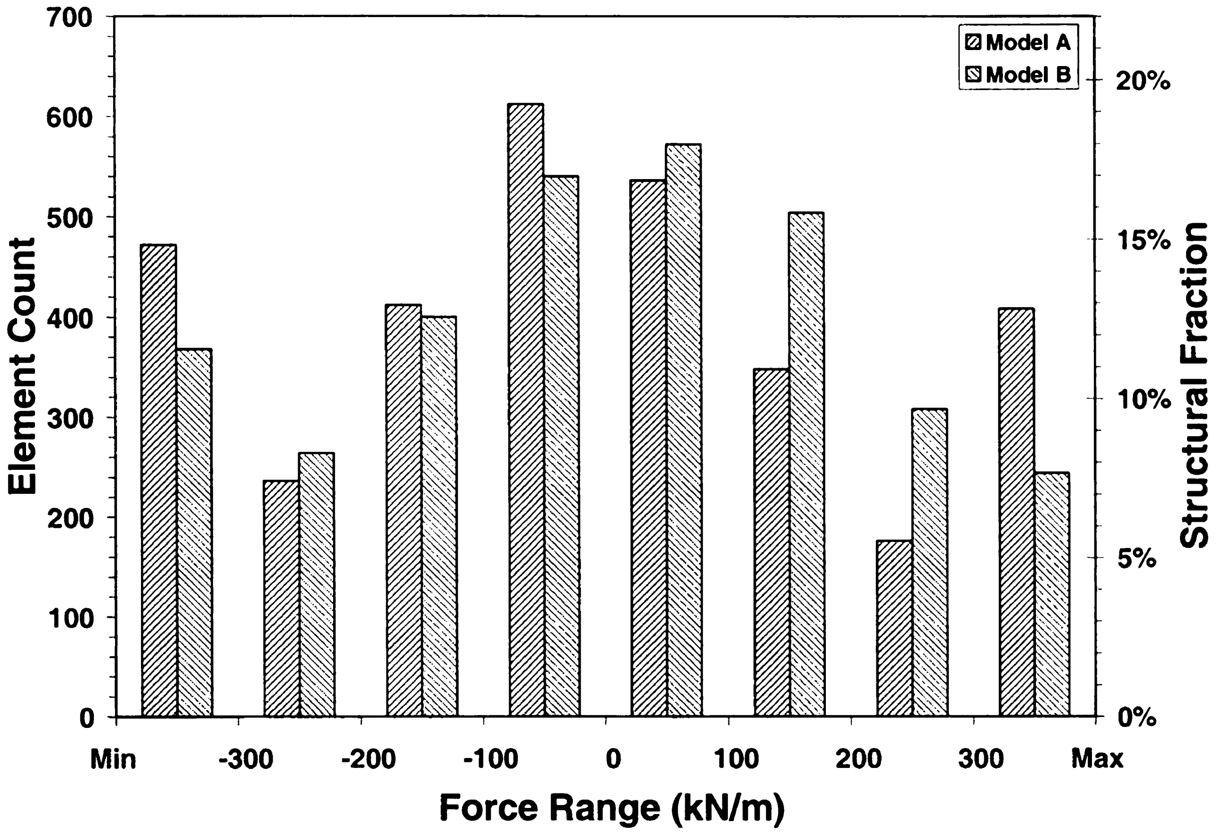

Figure 7–33 Section force (SF1) distribution in CMS optimal designs

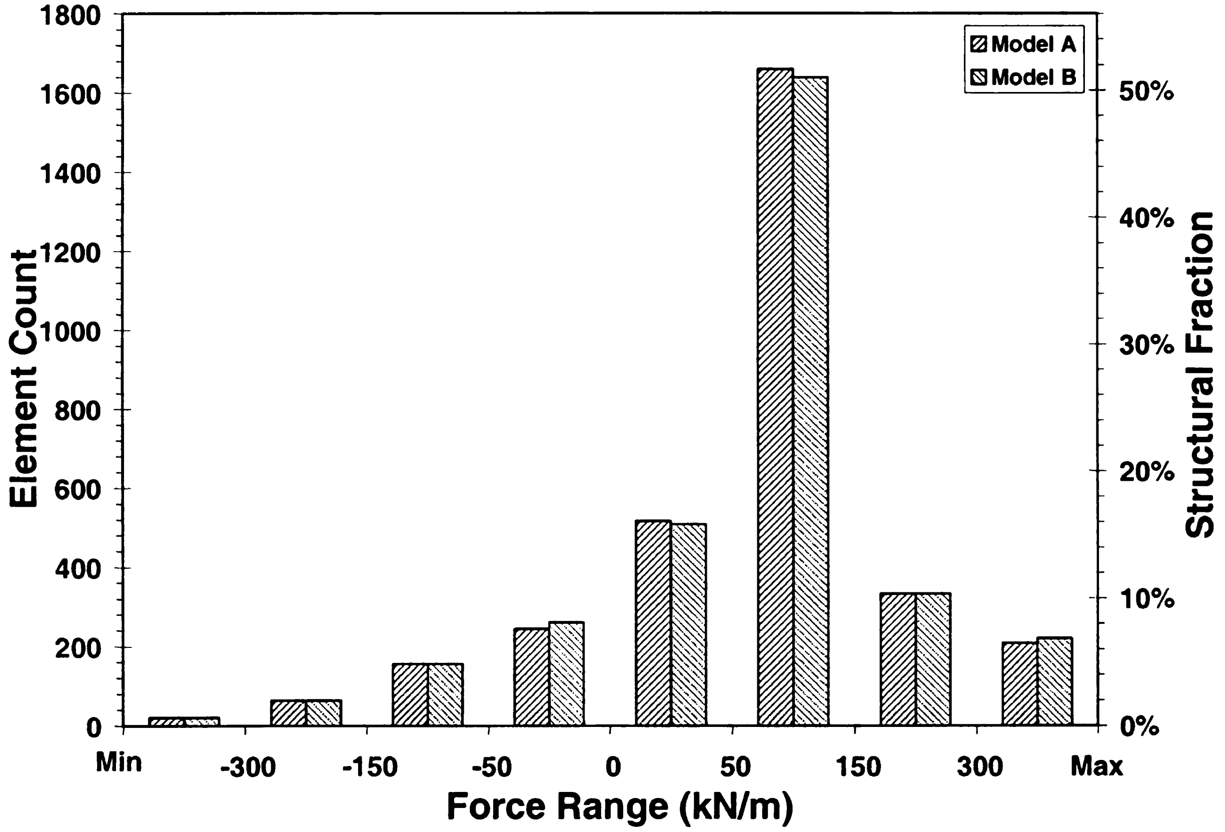

Figure 7–34 Section force (SF2) distribution in CMS optimal designs

issues discussed in the system characteristics and the load variation studies, lead to the conclusion that Model B has a more effective and stable in-plane behavior than Model A. This improved in-plane behavior is achieved by the addition of supporting boundaries at both ends of Model B (Table 7–17), which strengthens the dual hanging concept of the CMS bridge system.

7.3 Discussion of FRP membrane-based bridge systems

In this section, the conceptualized FRP composite membrane-based bridge systems (CMB, CMS-A, and CMS-B) are evaluated by comparing their structural behavior in terms of material use efficiency. In addition, the selection of an objective function that could further improve the integrated shape and laminate optimization approach is also discussed.

7.3.1 Comparison of FRP membrane-based bridge systems

As shown through the studies of system characteristics, the performance of both types of composite membrane-based bridges is improved by their in-plane behavior as tension structures after the integrated optimization. However, efficient performance under in-plane behavior is gained through different schemes for both composite membrane-based bridges.

The system characteristic studies of the optimal CMB bridges showed that the structural stiffness used by CMB bridges to carry external loadings is obtained by developing a force couple between the longitudinal tension forces in the FRP membrane and the longitudinal compression in the concrete deck. The in-plane section resultants of the FRP membrane and the concrete deck in the transverse direction are due primarily to the Poisson effect and are two orders of magnitude less than the longitudinal in-plane resultants. Therefore, CMB bridges achieve mainly unidirectional in-plane behavior. However, the system characteristic studies for the optimal CMS bridges indicated that the FRP membrane in optimal CMS bridges are subject to in-plane longitudinal and transverse tensions. The structural stiffness of CMS bridges is thus acquired by achieving the bi-directional membrane behavior of membrane and shell structures.

The two types of composite membrane-based bridges presented in this work differ not only in their structural behavior, as previously discussed, but also in their efficiency in material use. As it is well known, efficient use of materials requires achieving not only in-plane or membrane resultants but also a uniform stress distribution throughout the structure. The distribution of stress demands in a generally anisotropic structure can be represented by strength safety factors of the elements in a finite element model of the structure. The strength safety factor of an element is evaluated by the stress index of that element with respect to a specific failure criterion.

However, due to the different structural geometry, loading and material volume used for CMB and CMS bridge systems, their structural response is different even for the same limit state. Therefore, a concept of *relative stress indices* is introduced to evaluate and compare the efficient use of the FRP membrane. Thus, the stress indices of individual elements are normalized by the maximum stress index for the complete structure (clearly applied to each structure separately). Table 7–28 summarizes the distribution of normalizing stress indices defined by the Tsai-Wu failure theory for the FRP membranes of all membrane-based bridges under the service limit state load demands. The *structural* *fraction distributions*, defined as the number of elements within a given relative index range divided by the total number of elements in the structure, for all three bridges with respect to the relative stress indices are compared in Figure 7–35. The average and the standard deviations of the three curves are given in Table 7–29.

Table 7–28 Stress indices distribution of three bridges

CMB		CMS – Model A		CMS – Model B	
Normalized Stress Index	Fraction $\frac{\#EL}{\sum EL}$	Normalized Stress Index	Fraction $\frac{\#EL}{\sum EL}$	Normalized Stress Index	Fraction $\frac{\#EL}{\sum EL}$
0.00%	0.00%	0.00%	0.00%	0.00%	0.00%
6.67%	0.00%	6.25%	26.73%	6.25%	22.16%
13.33%	0.33%	12.50%	28.52%	12.50%	30.73%
20.00%	1.31%	18.75%	20.41%	18.75%	22.47%
26.67%	2.47%	25.00%	10.70%	25.00%	13.69%
33.33%	6.78%	31.25%	5.83%	31.25%	4.27%
40.00%	19.75%	37.50%	2.27%	37.50%	2.97%
46.67%	24.08%	43.75%	1.70%	43.75%	1.77%
53.33%	19.31%	50.00%	1.94%	50.00%	1.14%
60.00%	14.14%	56.25%	1.22%	56.25%	0.31%
66.67%	3.81%	62.50%	0.19%	62.50%	0.09%
73.33%	3.33%	68.75%	0.06%	68.75%	0.03%
80.00%	2.42%	75.00%	0.13%	75.00%	0.06%
86.67%	1.67%	81.25%	0.00%	81.25%	0.00%
93.33%	0.56%	87.50%	0.06%	87.50%	0.06%
100.00%	0.06%	93.75%	0.00%	93.75%	0.19%
	0.00%	100.00%	0.25%	100.00%	0.06%

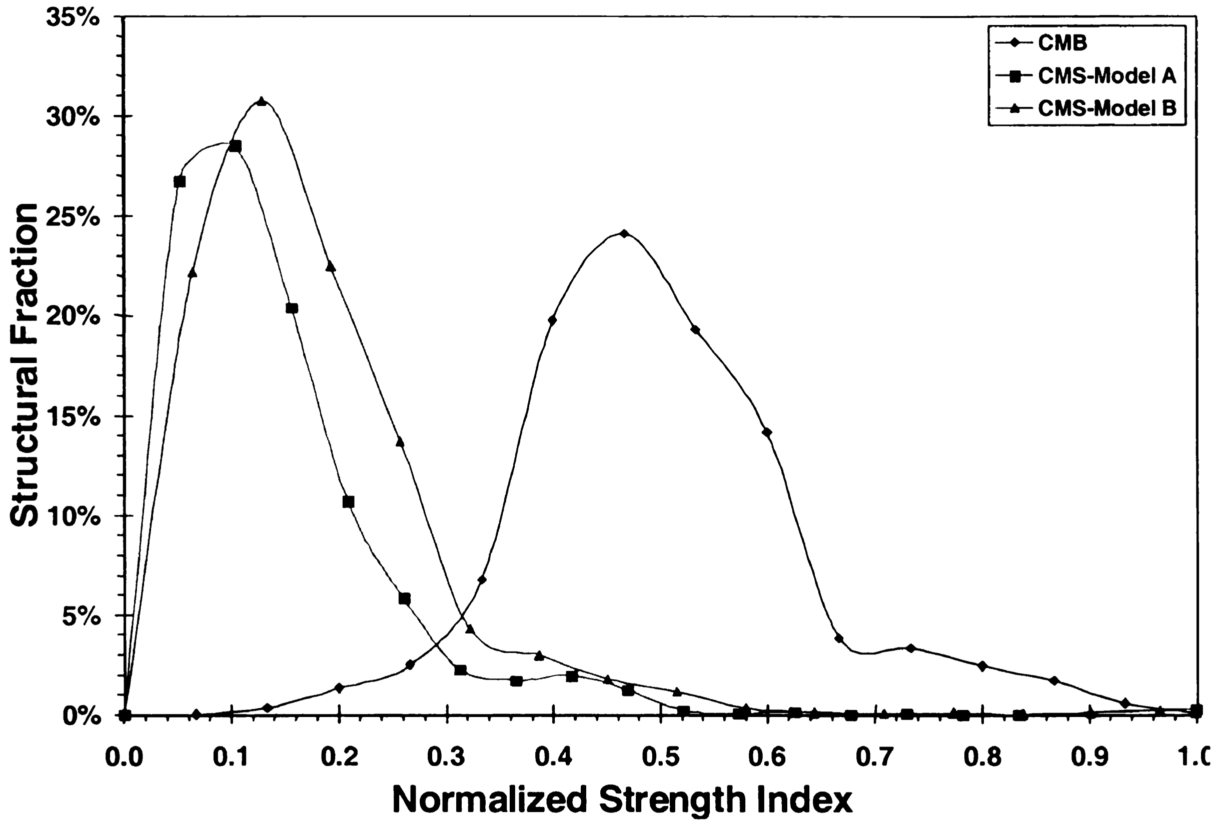

Figure 7–35 Structure material distribution of relative stress index

Table 7–29 Statistics of relative stress index distribution

Relative Stress Index	CMB	CMS – Model A	CMS – Model B
Average	50.07%	14.51%	17.77%
Standard deviation	13.11%	10.43%	11.06%

Evaluation of the data presented in Figure 7–35 and Table 7–29 indicates that a higher average of relative stress index implies a higher average stress level for that structure. Thus, CMS bridges have a higher strength reserve in terms of FRP laminate capacity than CMB bridges of the same structural size and material use when the structures are subjected to an equal loading. On the other hand, a smaller standard deviation of the stress index distribution indicates a large portion of the FRP membrane is located within a smaller range of the average stress index. From this point of view, CMS bridges have a better structural performance of uniform stress distribution than CMB bridges. Therefore, it can be concluded that CMS bridges utilize the FRP material more efficiently than CMB bridges.

7.3.2 Discussion of the objective function

As proved in Section 4.1.2, structural stiffness is maximized by achieving in-plane structural response, which is implemented by minimizing the structural strain energy in the integrated shape and laminate optimization approach. On the other hand, structural stiffness can be also improved by adding material. Therefore, structural geometric dimensions and the thickness of the FRP membrane were constrained to limit the use of laminated FRP composites. However, it is difficult to distinguish the individual contribution from structural shape and material quantity towards improved structural stiffness by minimizing the structural strain energy. For example, strain energy can be further decreased with increased FRP materials even though the structural response be already in-plane dominant. This limitation of the objective function could result in an over-designed optimum as shown in the post optimality analyses for CMB bridges (Table 7–12 and Table 7–14). The results from Section 7.1.4 showed that the stress indices of the optimal CMB bridges were far below the allowable stress levels for all limit states. An over-bound constraint on the FRP membrane thickness is the most possible reason. Therefore, an integrated optimization employing a narrow-bound constraint on the membrane thickness was investigated for the optimum design of CMB bridge.

The effort of a narrow bound constraint on the FRP membrane thickness was implemented by evaluating the optimal design for the CMB bridge with the upper bound on thickness reduced from 19.05 mm to 9.525 mm. The newly optimized CMB bridge

(Model D) is summarized in Table 7–30. It can be noted that the FRP membrane for Model D achieved essentially the same optimal geometric shape and the same optimal laminate properties compared to the previously obtained optimum designs (see Table 7–3). Also, it is noted that the FRP membrane thickness still reached the upper bound of the thickness constraint. Due to the reduced thickness (50% reduction) the structural strain energy was almost doubled. However, this increase of the strain energy does not indicate that the in-plane structural behavior was impaired since the FRP membrane still achieved a close optimal geometric shape. In fact, the increase of the strain energy is caused by the increase of in-plane stress resultants due to the thickness reduction. Therefore, strain energy minimization with geometric constraints can not avoid over-designed optimal structures although the structural stiffness is properly improved by achieving membrane response.

Table 7–30 Optimal CMB bridge designs with different membrane thickness constraints

Optimal design	Model A	Model B	Model C	Model D
Strain Energy (N-m)	83.85	83.85	83.85	161.90
$\{w_1, w_2, h_1, w_2, t\}$ (mm)	{1359.0, 2184.4, 984.3, 1219.2, 19.05}	{1365.2, 2184.4, 1022.4, 1219.2, 19.05}	{1352.6, 2222.4, 997.0, 1219.2, 19.05}	{1327.3, 2174.2, 990.6, 1219.2, 9.525}
$\{V_{1A}, V_{3A}, V_{1D}, V_{3D}\}$	{0.81, 0.31, -1, 1}	{0.81, 0.31, -0.8, 0.7}	{0.81, 0.31, 0.75, 1}	{0.81, 0.31, 0.75, 1}

According to the optimization experience obtained above, optimal CMB bridges with an average optimal geometry were investigated to study the structural response with respect to the FRP membrane thickness (Table 7–31). It can be observed that, while the structure remained under in-plane demands, reductions in membrane thickness increased

the structural strain energy while the maximum deflection and stress index approached the prescribed design criteria values, which is also indicative of a more efficient design.

Table 7–31 Structural response with different membrane thickness

Thickness T (mm)	Strain Energy SE (kN-mm)	Deflection D (mm)	Stress Index SI (%)
19.050	84.51	1.692	34.56
15.875	100.33	1.966	41.16
12.700	127.33	2.464	51.13
9.525	165.07	3.226	66.15
6.350	235.12	4.765	95.17

Several alternative objective functions that could seek to maximize structural stiffness and minimize material use were investigated:

- Objective function f_1: Minimize (Strain Energy)×(Thickness)
- Objective function f_2: Minimize (Strain Energy) / (Stress Index)
- Objective function f_3: Minimize (Strain Energy)×(Thickness) / (Stress Index)

The performance of these objective functions evaluated with optimal CMB bridge designs is summarized in Table 7–32 and graphically represented in Figure 7–36. It can be seen that the proposed objective function (f_3 = SE·T/SI) linearly decreases with reduction of the membrane thickness. Conversely, as shown in Table 7–31, the decrease in the membrane thickness leads to stresses and deflections that are closer to the design criteria. Therefore, the objective of maximizing structural stiffness while minimizing the material can be achieved by implementing a function that incorporates minimization of the structural strain energy and the membrane thickness as well as maximization of stress levels.

Table 7–32 Evaluations of alternative objective functions

f_1 = SE·T (kN-mm^2)	f_2 = SE / T (kN-mm)	f_3 = SE·T / SI (kN-mm^2)
1610.0	244.5	4658.5
1592.7	243.8	3869.6
1617.1	249.0	3162.8
1572.3	249.5	2376.9
1493.0	247.1	1568.8

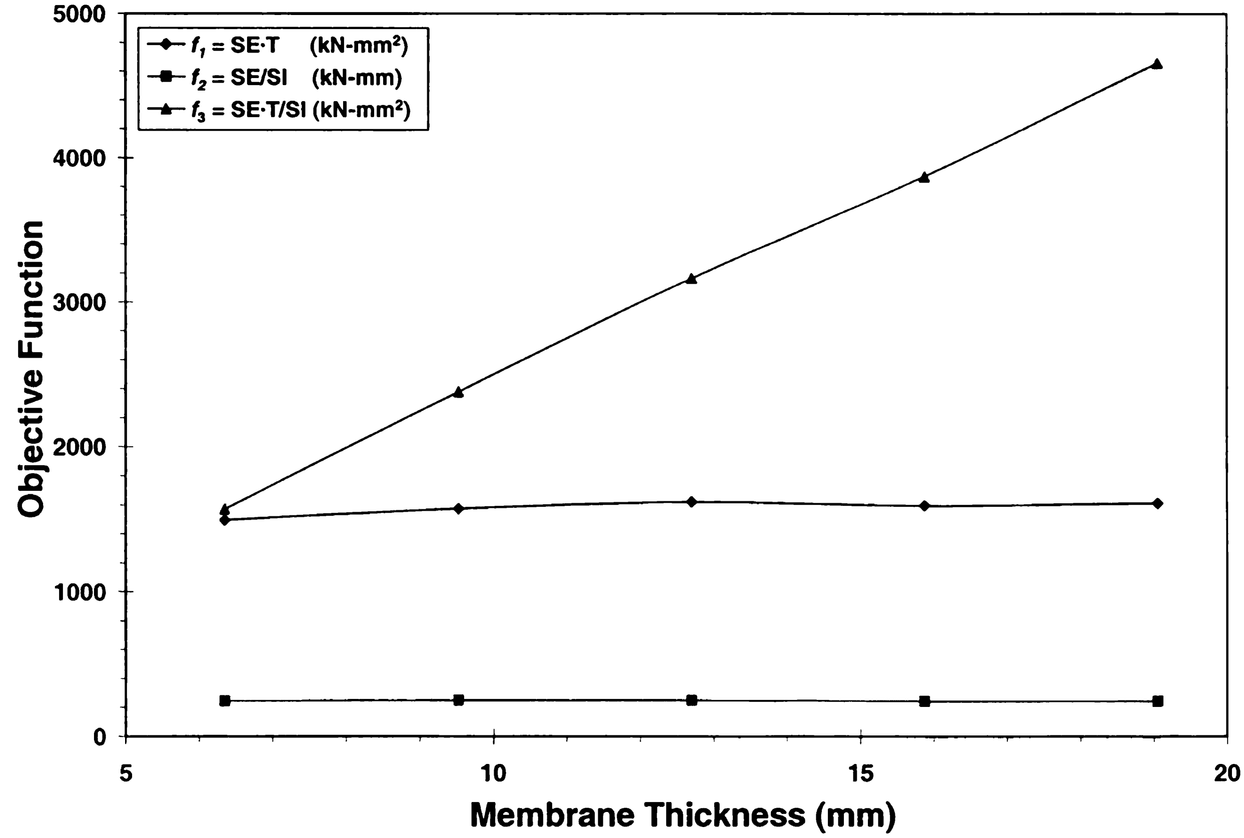

Figure 7–36 Performance of different objective functions for optimal CMB bridge

In addition, the optimum designs for FRP composite membrane-based bridges are currently obtained under an optimization load case taking into account a single loading effect and a single loading pattern. However, as evaluated in the post optimality analyses of both bridges, the structural behavior of the optimum designs can be significantly under non-optimization loading effects and patterns. Therefore, multiple loading effects and loading patterns should be considered simultaneously in a limit state in order to reduce

significant variations in the response of an optimum design. This can be implemented by a general optimization load case in which different loading effects and patterns are combined with different weight factors. For example, the extreme loading effects of maximum torsion, maximum mid-span bending and the normal load effect might be considered with a uniform weight factor of 1/3 in the optimization load case for the optimum design of CMB bridges. Similarly, the optimization load case for CMS bridges might combine the loading patterns of uniform and spaced line loads with a weight factor of 1/2.

Instead of using a general optimization load case, multiple loading effects and patterns can be taken into account by using a multi-objective optimization approach. Multi-objective optimization consists of defining different objective functions assigned with weight factors with respect to their respective loading effects and patterns. The optimum design that compromises among the different loading effects and patterns is obtained by optimizing the multi-objective functions with respect to their own set of constraints.

7.3.3 Selection of the design variables

It should be noted that the structural performance of CMS bridges (Section 7.2) will vary with the position of the pier supports. Therefore, the pier position should be taken into account as one of the geometric design variables in optimizing CMS bridges. However, preliminary optimization efforts revealed that the objective function of minimizing the strain energy varied *discretely* with respect to changes of the pier positions. This resulted in premature optimization solutions at local optimum points.

Thus, the pier positions of CMS bridges were currently fixed at constant locations throughout the optimization process.

Moreover, it should be noted that, for all of the optimization examples presented in this dissertation, the geometric key points that determine the structural shape were selected to achieve a higher computational efficiency. A structural shape is then generated by interpolating the geometric coordinates of the key points. Therefore, the structural shapes that can be obtained are limited by the number of geometric key points and their degrees of freedom. For example, the number of geometric key points selected for shape finding of FRP membranes in the bridge systems can only determine the surfaces high up to a 2^{nd}-order curvature by interpolation techniques. The accuracy of optimal shapes obtained by structural shape optimization for free form finding can be improved by increasing the number of the geometric key points. However, free form finding is achieved at the cost of computational efforts due to the increase of design variables. In addition, general free-forms, although efficient, may not be practically feasible. The determination of the number of design variables therefore requires considering the computational efforts, the accuracy of the optimal shape sought, and the ease of implementation. Thus, in spite of the power provided by these mathematical optimization tools, it is still the design's judgment that dictates the successful design of an efficient structural form.

7.4 Summary

In this chapter, the integrated shape and laminate optimization approach was applied to the design and optimization of two innovative and newly proposed FRP composite membrane-based bridge systems. The characteristic studies for both bridge systems show that the high in-plane stiffness and strength characteristics of FRP laminates are utilized to maximize the performance and efficiency of the bridge systems due to the effectiveness provided by shape resistant membrane structures. Furthermore, based on the observation of over-designed optimal CMB bridges, several alternative objective functions, in addition to the minimization of structural strain energy, were investigated to achieve in-plane structural response with minimum material use. The objective function of minimizing the strain energy and the membrane thickness while maximizing the membrane stress level seems to have the best performance for CMB bridges and is thought to be a viable objective function for maximizing structural stiffness with minimum material use. The use of objective functions that take into account multiple loading effects and patterns were discussed, and the importance behind the selection of geometric design variables was noted to place the current work and its results into context.

References

AASHTO–American Association of State Highway and Transportation Officials (1998). AASHTO LRFD bridge design specifications. Washington, D.C.: The Association.

Azzi, V.D. and Tsai, S.W. (1965). Anisotropic strength of composites. Experimental mechanics: 5, 283-288.

Hibbitt, Karlsson & Sorensen, Inc. (2001). ABAQUS standard user's manual Version 6.2.

Jones, R.M. (1999). Mechanics of composite materials. Philadelphia, PA: Taylor & Francis.

Seible, F., Karbhari, V.M., and Burgueño,R. (1999). Kings Stormwater and I-5/Gilman Bridges. Structural Engineering International: Journal of the International Association for Bridge and Structural Engineering: 9, 4, 250-253.

Tsai, S.W. (1968). Strength theories of filamentary structures. In Fundamental Aspects of Fibeer Reinforced Plastic Composites Schwartz, R.T. and Schwartz H.S. (eds.), 3-11. New York: Wiley Interscience.

Wu, E.M. (1974). Strength and Fracture of composites. In Composite Materials, Broutman, L.J. and Krock, R.H. (eds.) Vol. 5, 191-247. New York: Academic Press.

8 Conclusions and Future Research Needs

8.1 Conclusions

The presented integrated optimization approach offers a procedure for simultaneously finding the optimal shape and optimal laminate design of FRP structures. The integrated approach was investigated by analytical studies on the development of FRP shell structures that combine FRP laminates and shape resistant structures for improved FRP structural designs. The approach provides an efficient tool to determine maximum stiffness designs by optimizing not only the geometry of the membrane or shell but also the material properties and the composite laminate design.

The integrated optimization approach can also serve as an analytical tool to aid the rational implementation of laminated FRP composites in civil infrastructure by developing innovative design concepts. The developed concepts were that of membrane-based FRP composite bridge systems. The bridge systems consist of a shape-and-material optimized laminated FRP membranes that carry the in-plane tensile and shear forces while using a conventional reinforced concrete slab or FRP deck system to provide the live load transfer. The dual-level optimization approach can thus support the analytical studies required for initial development of innovative systems that use FRP composites in their inherent behavioral characteristics for new high-performance structures.

During the efforts of integrated shape and material optimization, it was observed that an over-bounded constraint of material use can lead to an over-designed optimum achieved for maximizing structural stiffness. Several feasible objective functions using combination of the structural strain energy, the membrane thickness, and stresses were investigated. The objective function of minimizing the strain energy and the membrane

thickness while maximizing the membrane stress level seems to have the best performance and is thought to be a viable objective function for maximizing structural stiffness with minimum material use.

The work has provided insight to the concept that FRP laminates can be used with higher efficiency in new structural systems as long as their advantageous properties of directional strength, light weight, and tailored properties are properly considered in the design process.

8.2 Future research needs

8.2.1 About the integrated approach of shape and laminate optimization

As it is well known, shape-resistant structures, such as thin shells subject to compression forces, are sensitive to buckling. While not considered in the presented work, structural buckling performance can be easily included in the proposed integrated optimization procedure. This can be done by two distinct approaches. One is to consider a determined buckling capacity as a constraint in the shape and laminate optimization procedure, thus achieving the optimization objective of maximum stiffness while satisfying the required buckling resistance. Another approach is to search for the maximum buckling capacity along with maximum stiffness in a multi-objective optimization process, where the different design objectives can be weighted to maximize structural performance. Therefore, the presented integrated approach can further evolve into a multi-objective decoupled approach for both shape and laminate optimization of FRP lightweight structures by adding appropriate objectives and constraint functions.

A gradient algorithm is used in the first step of the integrated approach to achieve the objective of maximizing structural stiffness. Due to the expectation of unaffordable computation demands by the large-scale optimizations, the numerical technique of finite difference methods was employed to supply the required gradients information to advance the gradient algorithm. The main disadvantage of calculating gradients by finite difference methods is the uncertainty in the choice of a perturbation step size. A perturbation that is either too large or too small will result in inaccurate gradient evaluations and misguide the search direction of the algorithm. The techniques from analytical methods have a better performance, in terms of robustness and accuracy, to derive gradient information than finite difference methods. However, the differentiation of objective and constraint functions in analytical methods requires the structural stiffness matrix, which will change completely even for small shape changes. This makes gradient derivation computationally costly. Therefore, future research is needed to provide the proposed integrated approach with an efficient and accurate technique for sensitivity analyses.

In the current approach, the shape and laminate optimization processes were decoupled into a two-step procedure, in which laminate designs in the second-step optimization are based on the lamination parameters from the first step. This requires that feasible lamination parameters be obtained during the first-step optimization. Thus, the constrained relationship between the lamination parameters is very important and has to be solved for the first-step optimization. At present, only the constraints between the essential lamination parameters, $\{V_{1A}, V_{3A}, V_{1D}, V_{3D}\}$, required by the current approach were numerically established (with certain assumptions) and applied in the optimization

process. However, this might not be enough for general applications. A competitive approach that can avoid the formulation of explicit constraints and implicitly satisfy the feasibility of laminate designs is to choose fiber orientations as material design variables. For this alternative approach, the integrated optimization has to be implemented with genetic algorithms in which geometric and material design variables are both treated as discrete variables. Although the volume of computations needed for sensitivity analyses can be avoided by using genetic algorithms, the computational effort will probably not be reduced because of the random search approach of genetic algorithms. The formulation of this alternative approach and its computational efficiency can maximize the broad implementation of the developed method.

8.2.2 About applications of the integrated approach

Although not explored in the current research effort, the integrated approach can be applied for the optimum design of different lightweight structures seeking to maximize structural stiffness, such as domes and membrane roof systems. Furthermore, with appropriate formulation of objective and constraint functions, the integrated optimization approach can be employed for many diverse applications. For example, a potential application is vibration tuning of structures. Structures subject to dynamic forces or excitation at their supports might need to be designed to avoid resonance or other negative vibration related problems. By relating the objective function to the fundamental vibration frequency, the integrated approach can yield optimum designs of structures that can avoid vibration problems.

The concept employed in the current approach to consider continuous and discrete design variables separately in a two decoupled procedure can also be applied to other optimization applications, for example, for smart structures made using piezoelectric materials. Piezoelectric materials are the materials that can convert electric energy into mechanical energy and vice versa. They produce an electrical response when mechanically stressed (sensors) and high motion can be obtained when an electric field is applied to them (actuators). Composite structures integrated with piezoelectric sensors and actuators offer potential benefits in a wide range of engineering applications such as vibration suppression and shape control. The development and efficiency of this type of structures rely on optimizing the location of the actuators and sensors that control the behavior of adaptive structures. This type of optimization applications involves continuous design variables of structural geometric shapes and discrete design variables that define the position of actuators and sensors. Therefore, the current integrated approach can be directly applied to investigate this type of optimization problems.

8.2.3 About the engineering and construction of optimal FRP composite structures

It needs to be noted that the fiber orientations of the optimal laminates achieved in the previous optimization examples are based on the local structural coordinates of the finite elements describing the FRP membrane, which vary with the normal of the membrane surface. Therefore, the construction of an FRP membrane with a laminate design in which the layout is specified based on local coordinates requires further study.

In addition, the construction of bridges like those presented in this work requires providing an effective membrane/slab connection to assure composite behavior between the FRP membrane and the concrete slab, or the FRP panel, of the bridge system. Particularly for CMB bridges, shear force resistance is required at the membrane/slab interface under flexural actions. A study on possible forms of shear connectors is thus needed to allow implementation for the developed CMB bridge systems. Finally, post optimality studies on the response of optimal CMS bridges indicated that the distribution of in-plane stresses depends on the form and spacing of diaphragms, which affect the efficiency of load transfer to the FRP membrane. A future study is thus required to investigate geometries and optimal placement of diaphragms for CMS bridges.

MICHIGAN STATE UNIVERSITY LIBRARIES
3 1293 02498 6030